University of Maribor Press

ISSN 1854-0171

ACTA GEOTECHNICA SLOVENICA

2020/2

VOL. 17

ISSN: 1854-0171

ACTA GEOTECHNICA SLOVENICA

Ustanovitelji | Founders

Univerza v Mariboru, Fakulteta za gradbeništvo, prometno inženirstvo in arhitekturo
University of Maribor, Faculty of Civil Engineering, Transportation Engineering and Architecture

Univerza v Ljubljani, Fakulteta za gradbeništvo in geodezijo
University of Ljubljana, Faculty of Civil and Geodetic Engineering

Univerza v Ljubljani, Naravoslovnotehniška fakulteta
University of Ljubljana, Faculty of Natural Sciences and Engineering

Slovensko geotehniško društvo
Slovenian Geotechnical Society

Društvo za podzemne in geotehniške konstrukcije
Society for Underground and Geotechnical Constructions

Izdajatelj | Publisher

Univerza v Mariboru, Fakulteta za gradbeništvo, prometno inženirstvo in arhitekturo
Faculty of Civil Engineering, Transportation Engineering and Architecture

Odgovorni urednik | Editor–in–Chief

Borut Macuh — University of Maribor

Tehnična urednica | Technical Editor

Tamara Bračko — University of Maribor

Uredniki | Co–Editors

Jakob Likar	Geoportal d.o.o.
Janko Logar	University of Ljubljana
Primož Jelušič	University of Maribor
Stanislav Škrabl	University of Maribor
Milivoj Vulić	University of Ljubljana
Bojan Žlender	University of Maribor

Posvetovalni uredniki | Advisory Editors

Heinz Brandl	Vienna University of Technology
Chandrakant. S. Desai	University of Arizona
Bojan Majes	University of Ljubljana
Pedro Seco e Pinto	National Laboratory of Civil Eng.

Lektor | Proof–Reader

Paul McGuiness

Naklada | Circulation

200 izvodov - issues

Cena | Price

25 EUR/letnik - 25 EUR/vol.; (50 EUR for institutions/za institucije)

Tisk | Print

Tiskarna Koštomaj

Revija redno izhaja dvakrat letno. Članki v reviji so recenzirani s strani priznanih mednarodnih strokovnjakov. Baze podatkov v katerih je revija indeksirana: SCIE - Science Citation Index Expanded, JCR – Journal Citation Reports / Science Edition, ICONDA - The international Construction database, GeoRef. Izid publikacije je finančno podprla Javna agencija za raziskovalno dejavnost Republike Slovenije iz naslova razpisa za sofinanciranje domačih periodičnih publikacij.

Založnik | Published by

Univerzitetna založba Univerze v Mariboru	University of Maribor Press
Slomškov trg 15, 2000 Maribor, Slovenija	Slomškov trg 15, 2000 Maribor, Slovenia
e-pošta: zalozba@um.si, http://press.um.si/, http://journals.um.si/	e-mail: zalozba@um.si, http://press.um.si/, http://journals.um.si/

Naslov uredništva | Address

ACTA GEOTECHNICA SLOVENICA
Univerza v Mariboru, Fakulteta za gradbeništvo, prometno inženirstvo in arhitekturo
Smetanova ulica 17, 2000 Maribor, Slovenija
Telefon / Telephone: +386 (0)2 22 94 300
Faks / Fax: +386 (0)2 25 24 179
E-pošta / E-mail: ags@um.si

Spletni naslov | web Address

http://zalozba.um.si/index.php/ags/index

The journal is published twice a year. Papers are peer reviewed by renowned international experts. Indexation data bases of the journal: SCIE - Science Citation Index Expanded, JCR – Journal Citation Reports / Science Edition, ICONDA- The international Construction database, GeoRef. The publication was financially supported by Slovenian Research Agency according to the Tender for co-financing of domestic periodicals.

INVESTIGATION OF SOIL DISPLACEMENTS CAUSED BY THE PRESS-IN PROCESS FOR CLOSE-ENDED MODEL PILES USING AN IMAGING TECHNIQUE

RAZISKAVA PREMIKOV ZEMLJINE, POVZROČENIH Z VTISKANJEM MODELNIH PILOTOV Z ZAPRTO KONICO S POMOČJO SLIKOVNE TEHNIKE

Ye Lu *(corresponding author)*
Shanghai university,
Department of civil engineering
99 Shangda Road, Shanghai 200444, P.R. China
E-mail: ye.lu@shu.edu.cn

Yun Jiang
Shanghai university,
Department of civil engineering
99 Shangda Road, Shanghai 200444, P.R. China

Xiaoyong Wang
Shanghai university,
Department of civil engineering
99 Shangda Road, Shanghai 200444, P.R. China

DOI https://doi.org/10.18690/actageotechslov.17.2.2-15.2020

Keywords

pile press-in, pile model tests, DIC, soil displacements, disturbance layer, image analysis

Ključne besede

vtiskanje pilotov, preizkusi modelnih pilotov, DIC, premiki zemljin, poškodovana plast, analiza slike

Abstract

In recent years, installing piles using the press-in method has gained popularity in urban areas. However, pushing piles into the ground squeezes the surrounding soils and consequently causes a disturbance or even damage to the underground structures and facilities close by. In order to investigate the squeezing effect incurred by press-in piling, a series of model tests were performed. The soil displacement field was captured using a non-contact technique called digital image correlation (DIC), and the horizontal soil stresses were measured by mini pressure cells. Analyses of the soil displacement fields showed that the pile press-in process caused different soil displacement paths at different depths and locations. The development of horizontal soil stresses correlated well with the horizontal and vertical displacements. A thin disturbance layer could be observed along the pile-soil interface and it was about 7.4-11.1 D_{50} in thickness (D_{50}, median particle size). At the end, the soil displacements caused by pushing the model pile with different pile shoes were analyzed and compared, and the analyses showed that a greater shoe angle resulted in greater disturbance to the surrounding soils. However, the influence of the pile shoe angle became less substantial with the increase of the pile penetration depth.

Izvleček

V zadnjih letih je v mestnih območjih postalo priljubljeno vgrajevanje pilotov s t. i. vtiskanjem. Vtiskanje pilotov v tla povzroča stiskanje zemljine ob pilotu in posledično povzroča motnje ali celo poškodbe na bližnjih podzemnih konstrukcijah in objektih. Da bi raziskali učinek stiskanja, ki ga povzročajo vtisnjeni piloti, je bilo izvedenih vrsta modelnih preizkusov. Polje premika zemljine je bilo zajeto z brezkontaktno tehniko, imenovano digitalna korelacija slik (DIC), horizontalne napetosti v zemljini pa so bile merjene z mini tlačnimi celicami. Analize polj pomikov zemljine so pokazale, da je postopek vtiskanja pilotov povzročil različne poti pomikov zemljine na različnih globinah in lokacijah. Razvoj horizontalnih napetosti v zemljini dobro korelira z vodoravnimi in navpičnimi premiki. Na kontaktu med pilotom in zemljino je bilo mogoče opaziti tanko poškodovano plast, ki je bila debela približno 7,4 do 11,1 kratnik D_{50}, pri čemer je D_{50} srednja velikost delcev oz. premer zrna pri 50 % presejka. Na koncu so bili analizirani in primerjani premiki zemljine, povzročeni pri vtiskanju modelnih pilotov z različnimi konicami pilotov, ki so pokazali, da večji naklon konice povzroči večje poškodbe okoliške zemljine. Vpliv naklona konice pilota se manjša s povečanjem globine prodiranja pilota.

1 INTRODUCTION

To avoid excessive settlements, heavy superstructures (e.g., high-rise buildings, bridge piers, liquefied natural gas tanks) are commonly built on pile foundations [1-4]. In recent years, pile-driving activities in the urban environment have raised concerns regarding the effects of ground-borne vibration on adjacent underground pipelines and buildings along with their occupants [5]. The ground-borne vibration due to pile driving will incur distress (e.g., crack) to pipelines and building structures and cause disturbance to residents [6-7]. If the vibration intensity is high enough, it might lead to detrimental effects on structures and buried pipelines, even accompanied by the loss of lives. Therefore, violent construction activities (e.g., pile driving with hammers or vibrators) are rarely permitted in the densely populated, urban areas of China. As both augur cast-in-place (ACIP) piles and press-in piling hardly cause ground-borne vibration, driven piles are gradually being replaced by those two in recent decades. Compared with press-in piles, the construction quality of ACIP piles is difficult to ensure and the construction of ACIP piles could cause pollution to the environment, and hence press-in precast piles are preferable to ACIP piles. Usually, press-in piling induces limited ground-borne vibration on adjacent structures and facilities. Nevertheless, the process of pushing piles (e.g., precast concrete piles, close-ended pipe piles and timber piles) into the ground will squeeze the soils in the proximity. Consequently, the pipelines buried in and the structures resting on the squeezed ground will be adversely affected. Over-squeezed ground might incur serious structural damage to adjacent structures and facilities. Until now, many efforts have been made to investigate the vibration and noise due to pile driving [8-9], while few studies were devoted to investigating the soil displacements caused by press-in piling. Since the soil displacement field is difficult to track in-situ, the relevant studies regarding soil displacement field resulting from press-in piling focused on model tests in the laboratory [10-11]. The model piles used in these researches were fairly small (R = 6.35 mm or 18 mm, and R is pile radius), which caused the influencing zone to develop with less range of scope.

When a pile is pushed into sands, the pile surface interacts with the soils, which consequently form a disturbance layer featuring substantial particle rotations and translations. The rotation and translation of soil particles in the disturbance layer are transitioned to the further region through particle interactions [12-13]. As a result, the disturbance layer is the link between the pile movement and the soil displacements. The thickness of the disturbance layer depends on the characteristics of the pile-soil interface, the soil types, the press-in rate, and etc., and is usually about 5–18 times the particle size [14-15]. Quite a few researchers used interface shear tests to characterize the particle displacements in the disturbance layer [16-19]. However, such a thin layer in the proximity of a pile is difficult to capture during pile driving, and hence limited researches can be found in the literature to characterize the disturbance layer during pile tests.

In this study, a series of pile model tests were designed and performed to investigate the soil displacements caused by the press-in piling process. An imaging technique, digital image correlation (DIC), was applied to track both the global soil displacement field and the soil displacements within the disturbance layer. In addition to the soil displacements, the development of soil stresses was monitored during the pile driving. Finally, the soil stresses were analyzed along with the relevant soil displacements and some conclusions were drawn.

2 PILE MODEL TEST

2.1 Test configuration

The pile model tests were performed in a steel chamber of 1 m × 1 m × 1 m. One side of the steel chamber was replaced with tempered glass to enable the image acquisition. A movable load frame was mounted on the test chamber, and a hydraulic jack was attached to the load frame to carry out the pile loading, see Fig. 1a. The loading capacity was 10 ton and the loading range was 120 mm for the hydraulic jack. The model pile was circular in shape with radius, R, of 25 mm, length, L_o, of 550 mm, and wall thickness, t, of 3 mm, and it was made of aluminum. Three tests using pile shoes with tip angles of 30° (Test JY-1), 90° (Test JY-2), 150° (Test JY-3), and one test without the pile shoe (Test JY-4) were performed in this study, see Table 1. To satisfy the axis-symmetry of the experimental setup, only half of the pile shaft and pile shoe were used, as schematically illustrated in

Table 1. Information of pile press-in model tests.

Test	JY- 1	JY- 2	JY-3	JY- 4
Pile shoe angle (°)	30	90	150	No pile shoe
Calibration of the digital camera (mm/pixel)	0.563	0.575	0.587	0.557
Calibration of the camera module (mm/pixel)	0.015	0.014	0.015	0.013

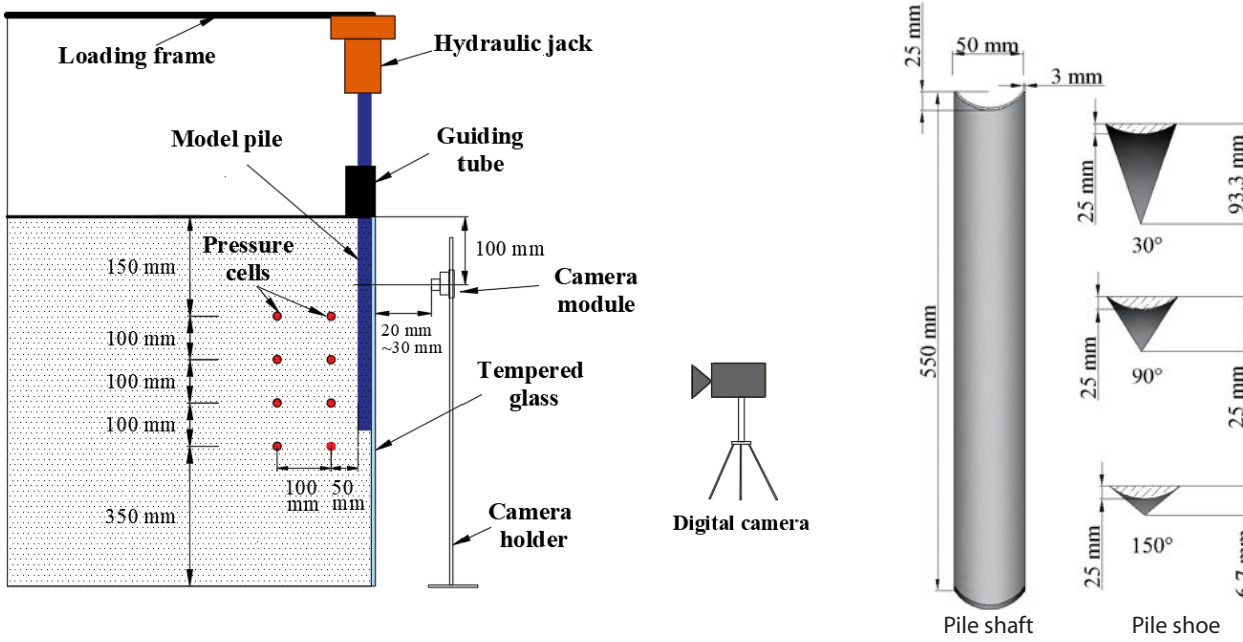

(a) Steel chamber and cameras

(b) Model pile

Figure 1. Schematic view of model test setup.

Fig. 1b. A cushion plate made of aluminum, which could be connected to the hydraulic jack, was attached to the top of the model pile. The model pile was pushed to a final depth of 500 mm below the soil surface by the hydraulic jack. Due to the use of pile shoes, the penetration depth of the pile, H, was calculated using the following formula:

$$H = L + L' \quad (1)$$

$$L' = \Delta V/A \quad (2)$$

where L represents the buried length of the pile shaft; L' is the converted length of the pile shoe; ΔV is the volume of the pile shoe; A is the sectional area of the pile shaft.

A steel pipe was fixed to the chamber by bolts and served as a guiding tube for the pile press-in. To monitor the development of the lateral soil stresses due to pile penetration, a total of 8 mini pressure cells were instrumented in the sands about 50 mm and 150 mm away from the pile surface at four depths of 150 mm, 250 mm, 350 mm, and 450 mm. The mini pressure cell was 11 mm in diameter and 4.2 mm in thickness, and its measuring capacity was 500 kPa with an accuracy of 0.5 %. Signals from the mini pressure cells were collected using a 16-channel GWI Instrument I555 Data Acquisition Unit, and the data were acquired at 100 Hz frequency.

2.2 Preparation of the testing material

The material used in the test was naturally dried fine sand. According to the sieve analysis results, the sands were classified as poorly graded, with D_{50} = 0.27 mm, C_u = 1.94, and C_c = 0.89. The maximum and minimum void ratios of the test sands were 0.893 and 0.571, respectively.

To achieve a fairly uniform density and ensure the repeatability of the tests, a standardized procedure was used – sands were compacted into four layers of predetermined thickness in the test chamber. The compaction was completed by a proctor compactor, of which compacting energy can be assured. To verify the prepared density of the sands, a cone penetration test (CPT) was performed using a mini penetrometer. Based on the CPT data, the relative density (D_r) of prepared sands was estimated using the equations proposed by Mayne et al. [20] and plotted in Fig. 2. It can be seen from the figure that the prepared sands were in the loose to medium dense state and the preparation procedure could achieve fairly good repeatability.

2.3 Image acquisition

Two cameras were used to acquire the images of both the full-field and local soil displacements caused by the

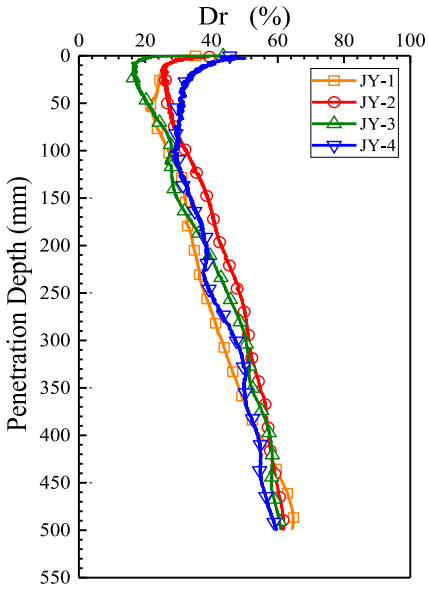

Figure 2. Relative density of prepared sands calculated from CPT data.

press-in procedure. Images of the full-field soil displacements were taken using a commercial digital camera with an 18.0-megapixel hybrid CMOS AF sensor. It was positioned outside the test chamber and recorded soil deformation through the tempered glass. In order to mitigate the impact of the natural light on the image quality, two photoflood lamps were positioned along with the camera to illuminate the tempered glass from different angles, as shown in Fig. 3. During the pile press-in process, videos were continuously recorded

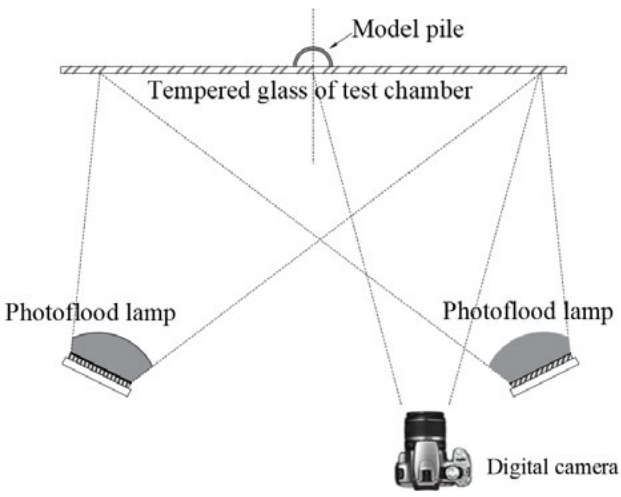

Figure 3. Full-field image-acquisition system for soil displacements during pile press-in process.

with frame rate of 24 fps (frames per second) and a frame size of 1920 × 1088 pixels. For a given digital camera, the number of pixels its electronics can capture is set, and thus increasing the image resolution means a smaller region of view is covered. Considering the fact that the pile press-in usually caused symmetrical displacements to the pile axis, the digital camera only captured the images of the right half of the test chamber in order to balance between the coverage area and the image resolution.

When a pile is pushed into the ground, soil displacements are caused by penetration of the pile tip, expelling of the soils, and shearing at the pile-soil interface. Shearing on the pile-soil interface causes the soil particles in contact with the pile surface to translate and rotate, and consequently trigger the transition of stresses and displacements outwards. To record the images of soil displacements at the pile-soil interface during the model test, a 2.0-megapixel camera module was installed close to the glass surface, which was designated for local images, as shown in Fig. 1a. The camera module was connected to a laptop using a two-meter-long USB cable. Real-time videos were recorded with frame rate of 24 fps and a frame size of 1920 × 1088 pixels.

Since the position of the camera was not fixed and the focal length of the camera was adjusted to different values for each test, the image resolution was calibrated before the pile press-in started. The calibration was made by attaching a graduated scale to the tempered glass and taking pictures using the cameras. The pictures were then inputted into MATLAB and calibrated using the MATPIV toolbox developed by Sveen [21]. Two measures were taken to ensure the accuracy of the calibration. First, at least two calibration results were obtained for each test and the average value was designated as calibration coefficients. Second, if the difference between the calibration coefficients of different experiments was greater than 10%, the camera was re-positioned and the calibration was performed again. After the calibration was made, the press-in test was carried out. The calibration coefficients of four tests are shown in Table 1. For the pile press-in test JY-2, in which pile shoe angle was 90°, image resolutions were 0.575 mm/pixel for the digital camera and 0.014 mm/pixel for the camera module. Since a frame size of 1920 × 1088 pixels was used for the full-field image acquisition, each full-field image covered a region of 1104 × 625.6 mm^2, which enabled the observation of soil displacements up to 17R distant from the model pile during the pile penetration to 500 mm below the soil surface. On the other hand, each local image covered a region of 26.88 × 15.23 mm^2, which contained approximately 750 sand grains.

2.4 Digital image correlation

Digital image correlation (DIC) is an optical-based technique that can detect the deformation of an object without direct contact. A digital image is composed of arrays of pixels and each pixel reflects a grey-scale number representing the brightness. By finding the maximum of the correlation array between the intensity of the pixel subsets on corresponding images, deformations or displacements of objects can be measured. Since this technique is relatively easy to use and implement, it has been applied to many fields of engineering, including geotechnical laboratory and model tests [22-26].

In this paper, a series of pictures taken in the process of pile press-in were processed using the following logic in MATLAB. The standard correlation function for image matching is:

$$C = \frac{\Sigma[f(i,j) - g(i+\Delta x, j+\Delta y)]^2}{\Sigma f^2(i,j)} \quad (3)$$

The intensity values within each subset can be described as an intensity function, $f(i, j)$. If the object being photographed deforms or moves and a second image is taken, the intensity function of the corresponding subset in the second image is $g(i+\Delta x, j+\Delta y)$. The displacements Δx and Δy can be described as functions of i and j. The DIC algorithm assumes trial functions for Δx and Δy and attempts to minimize the error of the correlation coefficient C to find the best trial displacement functions. Once the displacement field functions are known, differentiation can be used to determine the strain fields within the subset. This process is then repeated for all the subsets of the image, allowing the construction of contour plots of both displacements and strains.

When performing DIC, whether the computed displacement field can reflect the investigated deformation depends not only on the image quality, but also on the pixel subset. As noted by Rechenmacher [27], pixel subset sizes used in the analyses have to be large enough to encompass a unique gray-level pattern (to avail a unique mathematical pattern for matching), but also small enough to limit subsets to only affine straining over a deformation increment (an assumption in the DIC matching algorithm). For full-field image acquisition of which the image resolution was 0.557-0.587 mm/pixel, a subset size of 12 × 12 pixels was selected for the correlation. For local images of which the image resolution was 0.013-0.015 mm/pixel, a subset size of 24 × 24 pixels was selected. As a result, the DIC based on full-field images targeted at displacements occurred within a region, while DIC based on local images would yield particle-wise displacements. Since the press-in process of the model pile was recorded as video files, images were extracted at designated time intervals and imported into MATLAB for the displacement computation.

3 ANALYSES ON TESTING RESULTS

3.1 Full-field displacements

Since all the tests featured similar soil displacement patterns but different displacement magnitudes, the testing results from JY-2 (pile shoe angle of 90°) would be introduced in detail here. Based on DIC, the contour maps of the soil displacements in the horizontal direction and vertical direction can be plotted. Fig. 4 shows the accumulated horizontal soil displacements caused by the pile penetration to depths of 6*R* (150 mm),

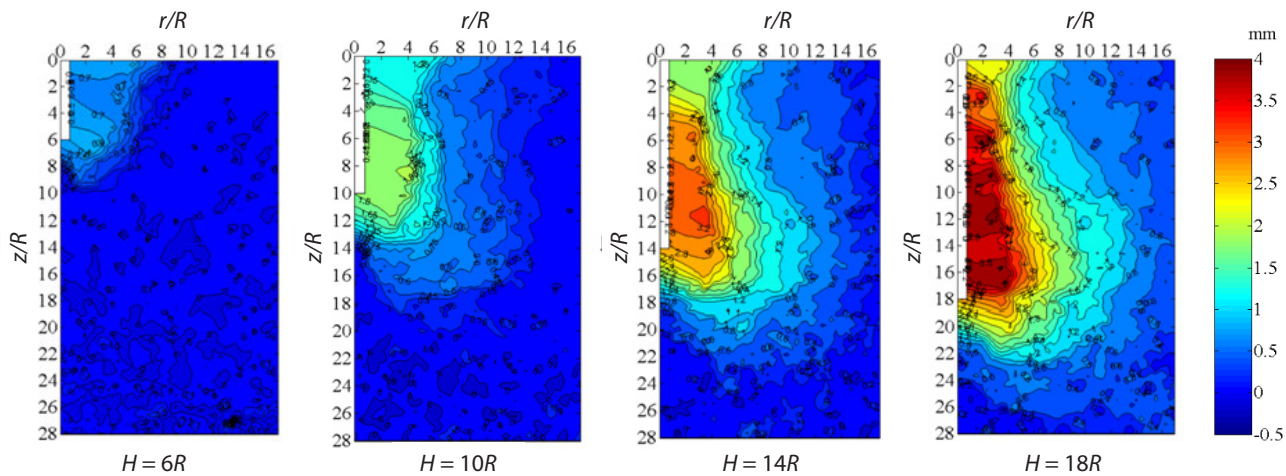

Figure 4. Contour maps of accumulated horizontal soil displacements.

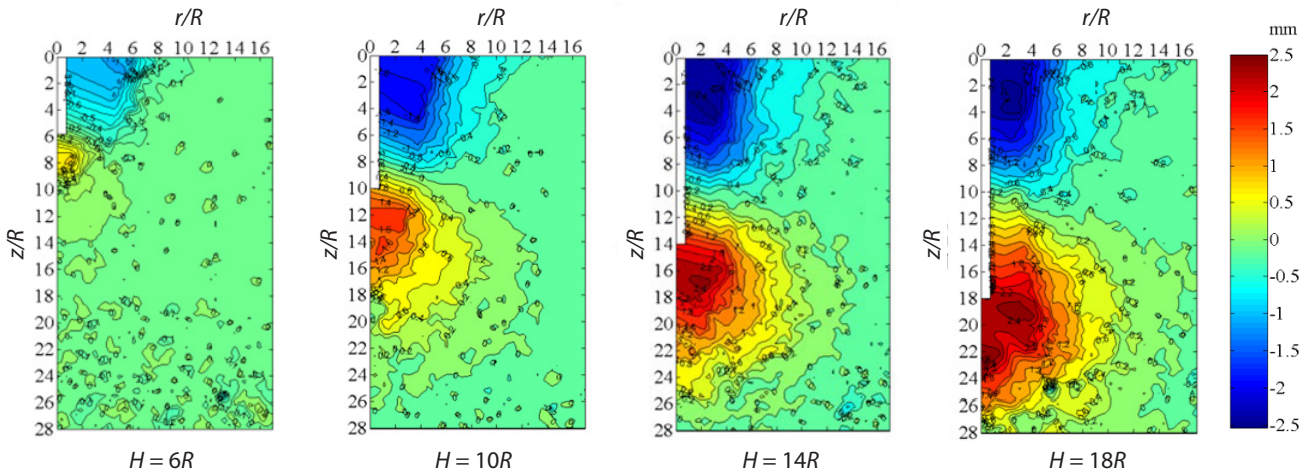

Figure 5. Contour maps of accumulated vertical soil displacements.

10*R* (250 mm), 14*R* (350 mm) and 18*R* (450 mm). The accumulated displacements were calculated using two images, one of which was recorded when $H = 0$, and another one was recorded at the designated depth. H is the pile penetration depth and calculated using Eq. 1. In Fig. 4, r is the horizontal distance from the pile axis, and z is the vertical distance away from soil surface. Both r and z are normalized by the radius of the pile cross-section, R. It is obvious that with the advancement of the close-ended model pile, soils were continuously expelled in the radial direction. When the pile was pushed to a depth of 6*R*, the lateral soil displacement at 9*R* away from pile tip was about 0.2 mm, while it increased to 1.5 mm when the pile was pushed to the depth of 18*R*. That means the influence zone caused by the pile penetration extended with the increase of the penetration depth. In addition, the contour maps indicated pile press-in incurred a lateral soil displacement field that could extend up to 0.5*H* deep beneath the pile tip.

Fig. 5 presents the contour maps of the accumulated vertical soil displacements at pile penetration depths of 6*R*, 10*R*, 14*R* and 18*R*. The positive values indicate downward displacements, while the negative values indicate upward displacements. Generally, the soils under the pile tip were pushed downward so that the maximum downward soil movements always occurred right beneath the pile tip. The vertical soil displacements along the pile shaft could be classified into two zones, one of which was subjected to the influence of the pile tip and the soil movements were downward. The rest of soils along the pile shaft underwent upward movements, which suggested that ground upheaval should have occurred. The demarcation line between the upward and

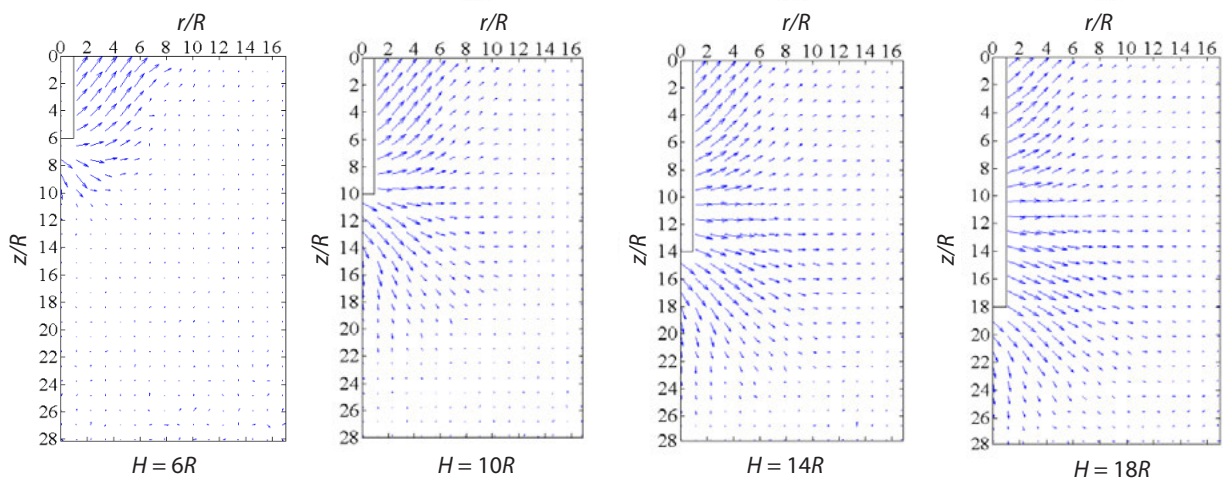

Figure 6. Vector map of soil displacement caused by pile penetration.

downward movement zones (i.e., the contour line with a value of '0') was tilted, and its location gradually shifted upwards relative to the pile shaft. Overall, the contours of the vertical soil displacements were similar to those observed by Lehane and Gill [9] during a penetrometer installation process in transparent soils. On the basis of the horizontal and vertical displacements, the total soil displacements were synthesized and plotted in Fig. 6. In the figure, each vector represents the displacement occurred within a region of about 28 × 28 mm^2. The vector maps showed clearly the upward and downward trends of the soil displacements.

The contours of the accumulated vertical soil displacements showed that the soil layer along the pile shaft could be classified into a downward zone and an upward zone, and the demarcation line between the two zones shifted upwards as the pile was pushed deeper. To clarify the mechanism behind the phenomenon, images were retrieved for every pile penetration of 10 mm to perform the DIC calculation. The calculation results were referred to as 'instantaneous' displacements, since the recorded time interval was much shorter than the accumulated displacements. Fig. 7 presents the instantaneous vertical soil displacements at two different penetration depths. These contours show clearly that the instantaneous push of the pile always incurred downward displacements below the pile tip and upward displacements along the pile shaft. That means the demarcation line lay right below the pile tip and its location was barely affected by the pile penetration depth. However, the scope of both the downward and upward displacement zones was suppressed as H increased. The phenomenon, observed for accumulated vertical displacements, that the demarcation line shifted up relative to the pile shaft with the increase of the pile penetration depth should be ascribed to the accumulation of downward displacements below the pile tip.

3.2 Relations between the soil displacements and stresses

It has been widely recognized for a long time that the stresses developed in soils were closely related to the soil displacements. Therefore, 8 mini pressure cells were instrumented in the soils to monitor the development of horizontal stresses caused by the pile press-in. The displacement information at the locations where the mini pressure cells were instrumented was extracted from the DIC calculation, and can be summarized in the following steps: (1) one image was retrieved for every 10-mm advancement of the pile, and finally 45 images were extracted for H = 450 mm; (2) DIC was done for every two images, and a series of displacement arrays were calculated; (3) displacement data at selected

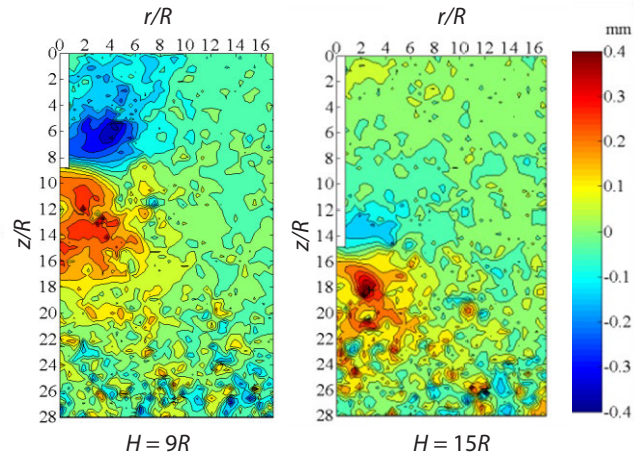

Figure 7. Instantaneous vertical soil displacements caused by pile penetration of 10 mm.

locations were retrieved. As mentioned previously, the subset size for DIC calculation was 12 × 12 pixels, which means each data point represented displacements of a 6.9 × 6.9 mm^2 region.

Fig. 8 presents the horizontal stress increment, $\Delta\sigma_h$, and the corresponding horizontal displacement, u_x, at 3R and 7R distances from the pile axis. It should be noted that the horizontal stress increments were relative to the original at-rest state, and the accumulated displacements data were calculated since the start of the pile press-in at the ground surface. At 3R distance, $\Delta\sigma_h$ measured by the pressure cell started to increase when the pile tip advanced to 4-7R distance above the burial depth of the pressure cell. As the pile tip approached the pressure cells, $\Delta\sigma_h$ reached the maximum. After the pile passed the burial depth of the relevant pressure cell, the magnitude of $\Delta\sigma_h$ decreased gradually. It is obvious that the measured horizontal stress increment peaked before the pile reached the burial depth of the corresponding pressure cell. Such a phenomenon could be denoted as an 'advance' effect and was consistent with the observations of Jardine and Zhu [10]. In general, the horizontal soil displacements correlated well with the soil stresses. The soil displacements increased with the increase of the soil stresses and tended to stabilize when the soil stresses decreased.

Fig. 9 presents $\Delta\sigma_h$ and the corresponding vertical displacements, u_y, at 3R and 7R distances from the pile. For the vertical displacements, a positive value represents a downward motion, while a negative value represents an upward motion. Generally, the soils at the measuring points moved downwards first and later moved upwards in the pile press-in process, which correlated with the contour maps in Fig. 5. It can be seen from the figure that the accumulative vertical displacements almost reached stable values when the lateral stresses decreased to the

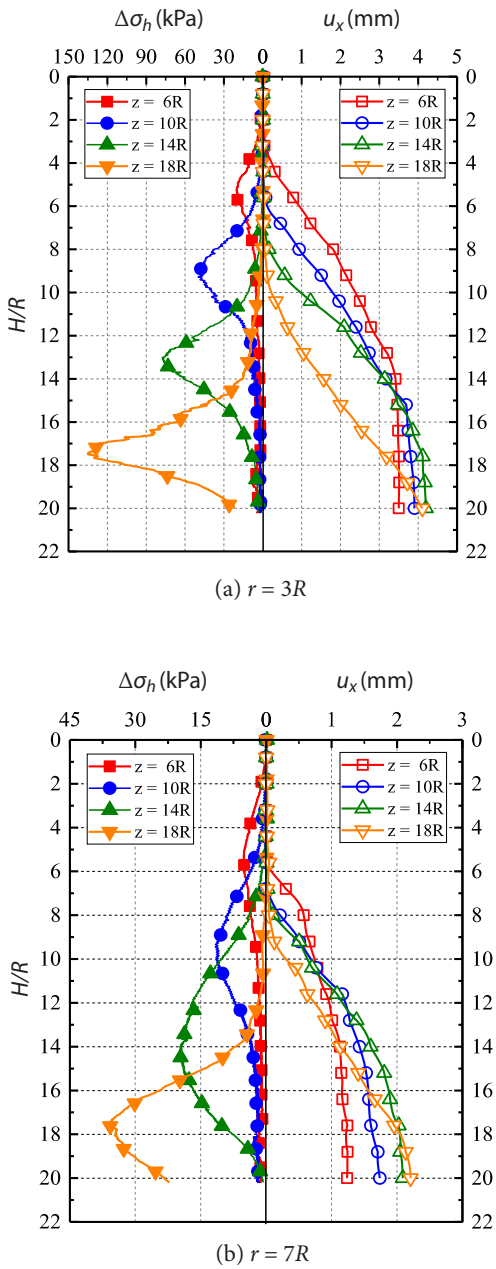

(a) $r = 3R$

(b) $r = 7R$

Figure 8. Horizontal stress increment in the soil and corresponding accumulative horizontal soil displacements.

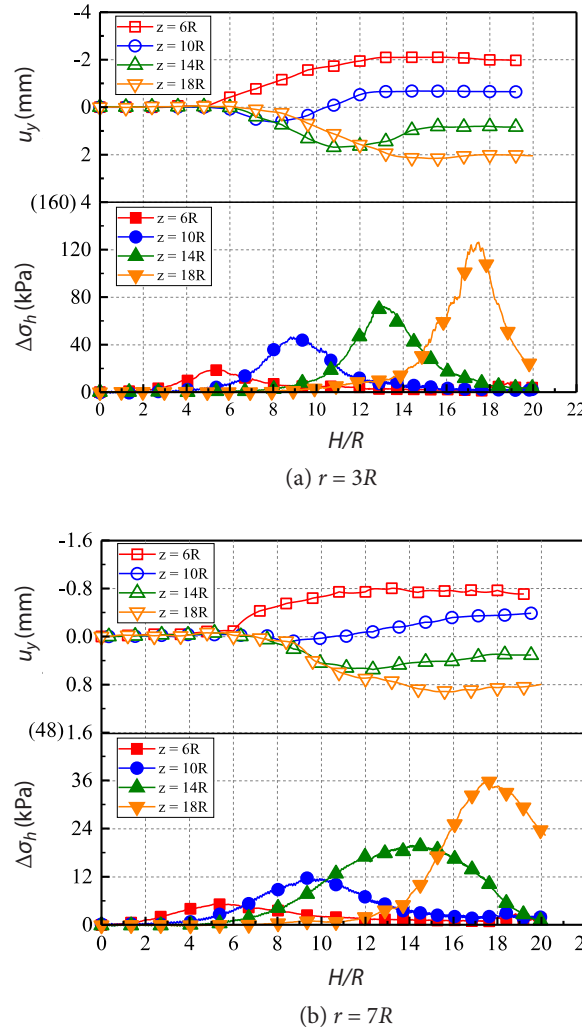

(a) $r = 3R$

(b) $r = 7R$

Figure 9. Horizontal stress increment and corresponding accumulative vertical soil displacements.

original at-rest state. Comparing the stress increment and the vertical displacement, it is found that the $\Delta\sigma_h$ at the corresponding position almost reached the peak value when the soil displacements transitioned from downward movements to upward movements.

Since $\Delta\sigma_h$ was relevant to both the horizontal and vertical displacements, displacement trajectories at different depths at $3R$ and $7R$ distances from pile axis were plotted in Fig. 10. The maximum stress increments were also marked at the relevant displacement points in the figure. For the vertical displacement, positive values represent downward movements and negative values represent upward movements. It can be observed from Fig. 10 that $\Delta\sigma_h$ increased as the soils were pushed outwards and downwards. The stresses reached peak values right after the soil displacements at corresponding positions transitioned from the downward movement to upward movement. Then, the horizontal soil stresses decreased to at-rest stresses until the soils could not be squeezed any more (i.e., the soil displacements ceased). Generally, the soil at different depths underwent downward movements followed by upward movements. However, soils at shallower depths underwent much less downward movements and more upward movements than the soils at greater depth, which could be ascribed to that greater vertical soil stresses suppressed upheaval tendency at greater depth.

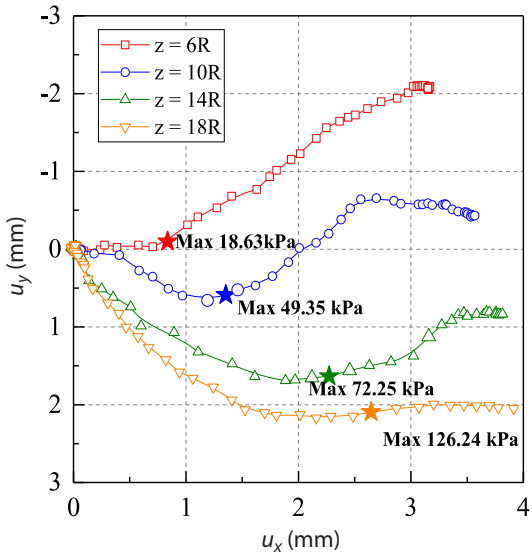

(a) $r = 3R$

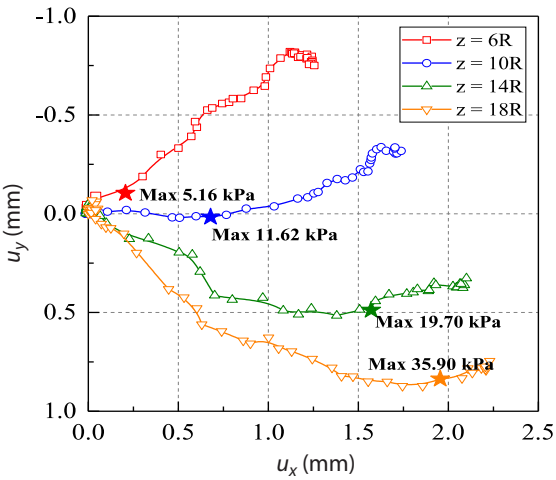

(b) $r = 7R$

Figure 10. Displacement trajectories of the measuring points 3*R* and 7*R*.

3.3 Soil displacement at the pile-soil interface

For the full-field displacement analyses, soil displacements in the proximity of the pile-soil interface were sacrificed due to the image resolution and the dimensions of the field that needed to be covered by each image. Therefore, an extra external camera module was installed to capture the local soil displacements at the pile-soil interface during the pile press-in process. The calibrated image resolution for each test can be found in Table 1. The camera module (see Fig. 1a) was positioned to capture images of the soil displacement at the pile-soil interface 100 mm below the soil surface.

To perform the DIC calculation on the local images, the time when the pile shoe just passed the observation

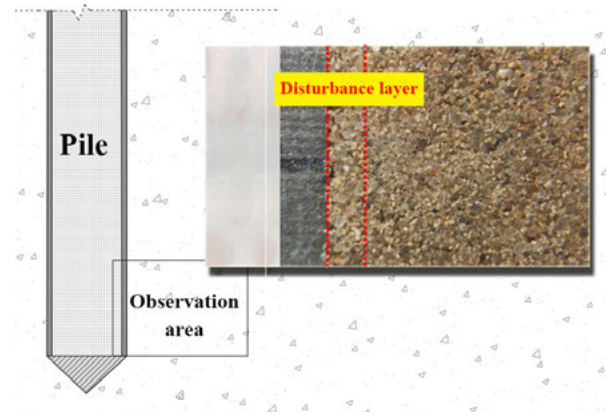

Figure 11. Illustration of the reference point for local image correlation.

area (i.e., the disturbance layer fully developed in the observation area) was designated as the reference point, see Fig. 11. Then images were recorded whenever the pile was pushed by 2 mm, and every two images were calculated by the DIC. Fig. 12 shows the contour maps of the horizontal and vertical soil displacements when the pile shoe was pushed 2 mm below the observation area for test JY-2, and the positive number represents the right or downward motions. Generally, the horizontal soil displacements were quite homogeneous within the

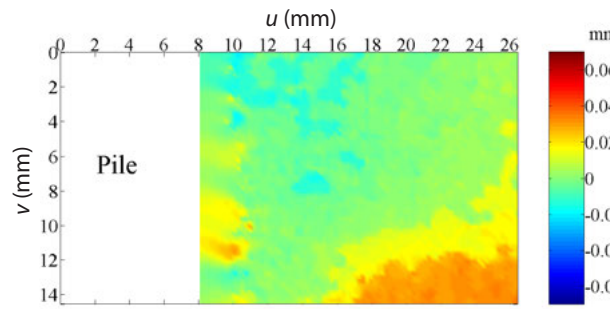

(a) Horizontal soil displacements

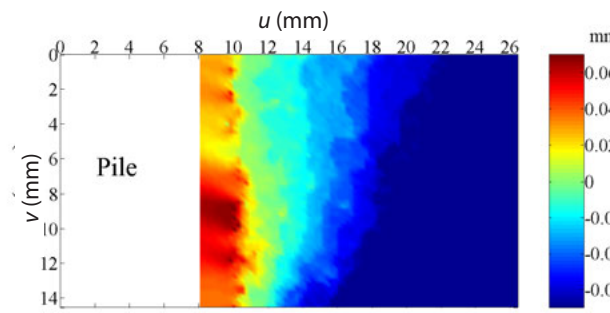

(b) Vertical soil displacements

Figure 12. Contour maps of soil displacements when pile tip was pushed 2 mm below the observation area.

observation area, with magnitudes less than ±0.02 mm. Meanwhile, the soils in close proximity (within 2 mm region) of the pile interface underwent downward displacements, and the downward displacements gradually transitioned to upward displacements as the distance from the pile interface increased. The total soil displacements were synthesized and plotted in Fig. 13. It can be seen that the observation area was dominated by the vertical movements and could be classified into three zones accordingly. Zone I was the dist urbance layer and

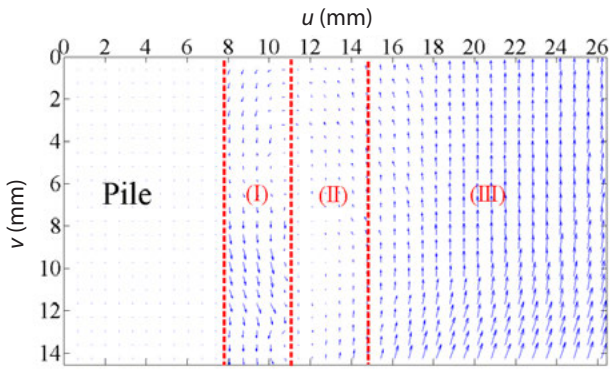

(a) Pile pushed by 2 mm

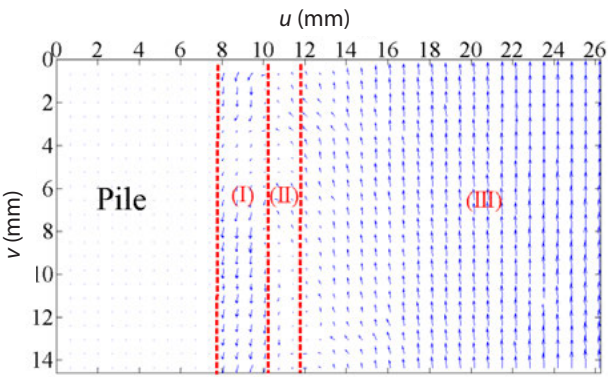

(b) Pile pushed by 10 mm

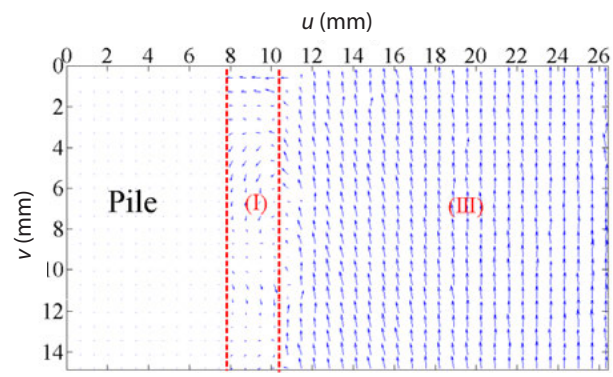

(c) Pile pushed by 24 mm

Figure 13. Vector maps of soil displacement caused by pile penetration for test JY-2.

2-3 mm (7.4-11.1 D_{50}, D_{50} is the median particle size) in thickness, which correlated well with those findings in the literature. The soils within zone I basically moved downwards, while the soils in zone III generally moved upwards. Between zones I and III, there was a transition zone (zone II) which was 3-4 mm in thickness. The soils in zone II hardly moved. The displacements occurring in zone III were consistent with the displacements observed in the full-field image (Fig. 5), while the displacements in zone I and zone II could not be reflected in the full-field image, which indicated that the installation of the camera module was effective in characterizing the disturbance layer. As the pile was continuously pushed by 24 mm after the reference time point, zone II gradually diminished. The vertical displacements of the soils in zone I (at the pile-soil interface) decreased, and the sands in zone III continued to move upwards.

To better analyze the displacement of the disturbance layer, the average vertical displacement of zone I was calculated for every 2 mm of pile advancement. Fig. 14 shows the vertical displacements of the disturbance layer at different times after the pile shoe passed the observation area. It can be seen that with continuous pushing of the pile, the vertical displacement of the disturbance layer quickly peaked after 2 mm of pile pushing and then decreased to zero after 18 mm of pile pushing.

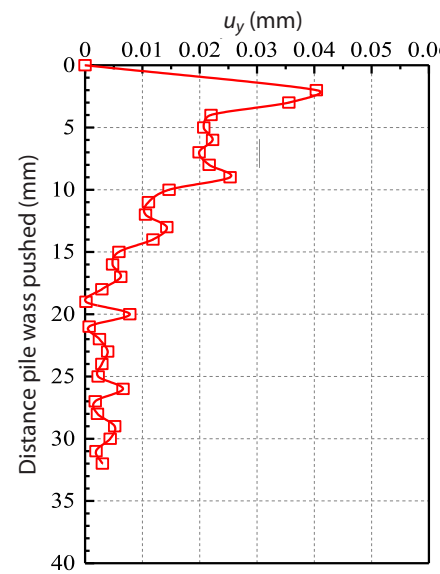

Figure 14. Vertical downward displacements of the disturbance layer during pile press-in.

3.4 Analysis of different pile shoes

In this study, the influence of different pile-shoe angles on the soil displacements was investigated. Overall, the influencing range of each pile shoe reached more than

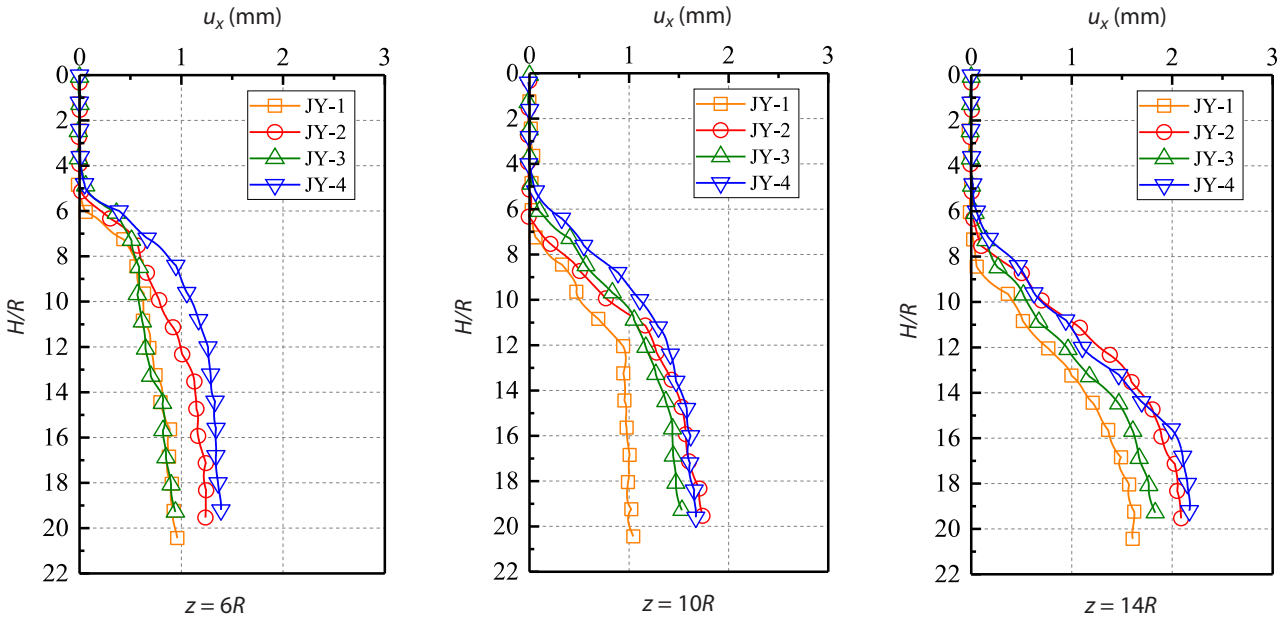

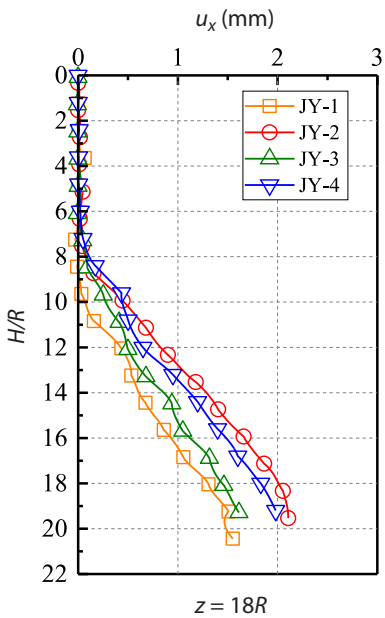

Figure 15. Accumulative horizontal displacement at 7*R* distance from the pile axis for different pile shoe angles.

13*R* distance away from the pile axis. Fig. 15 shows the development of cumulative horizontal displacements 7*R* distance away from the pile axes at depths of 6R, 10*R*, 14*R*, and 18*R* for different pile-shoe angles. In general, a larger shoe angle caused greater horizontal displacements. The pile with no shoe (JY-4) caused the greatest horizontal displacements while the pile with 30° pile shoe (JY-1) induced the smallest horizontal displacements. It is worth noting that the horizontal displacements caused by the 90° pile shoe (JY-2) were larger than the 150° pile shoe (JY-3), which was contrary to expectations. Such a phenomenon can be explained by the higher relative density achieved during the preparation of sands in the test JY-2 than that in the test JY-3.

Fig 16 presents the cumulative vertical displacement at 7R distance from the pile axis. Like the test results of JY-2 (Fig. 9), with the penetration of the pile, the soil usually underwent downward displacements and then upward displacements. Usually, a greater shoe angle induced greater vertical displacements. However, in the deep soil, the vertical displacements did not vary significantly with shoe angles, which indicated that the influence of different pile shoes on the vertical displacement was gradually reduced in the deep soil.

4 SUMMARY AND CONCLUSIONS

In this study, a series of pile model tests were performed to investigate the influence of the press-in process on soil displacements. The half pile was adopted in the model test so that digital images of soils could be captured continuously during the pile pushing through a tempered glass on one side of the test chamber. The DIC technique was applied to the digital images to calculate both the full-field and local soil displacements. Comprehensive analyses of the soil displacements were performed, and the following conclusions could be reached:

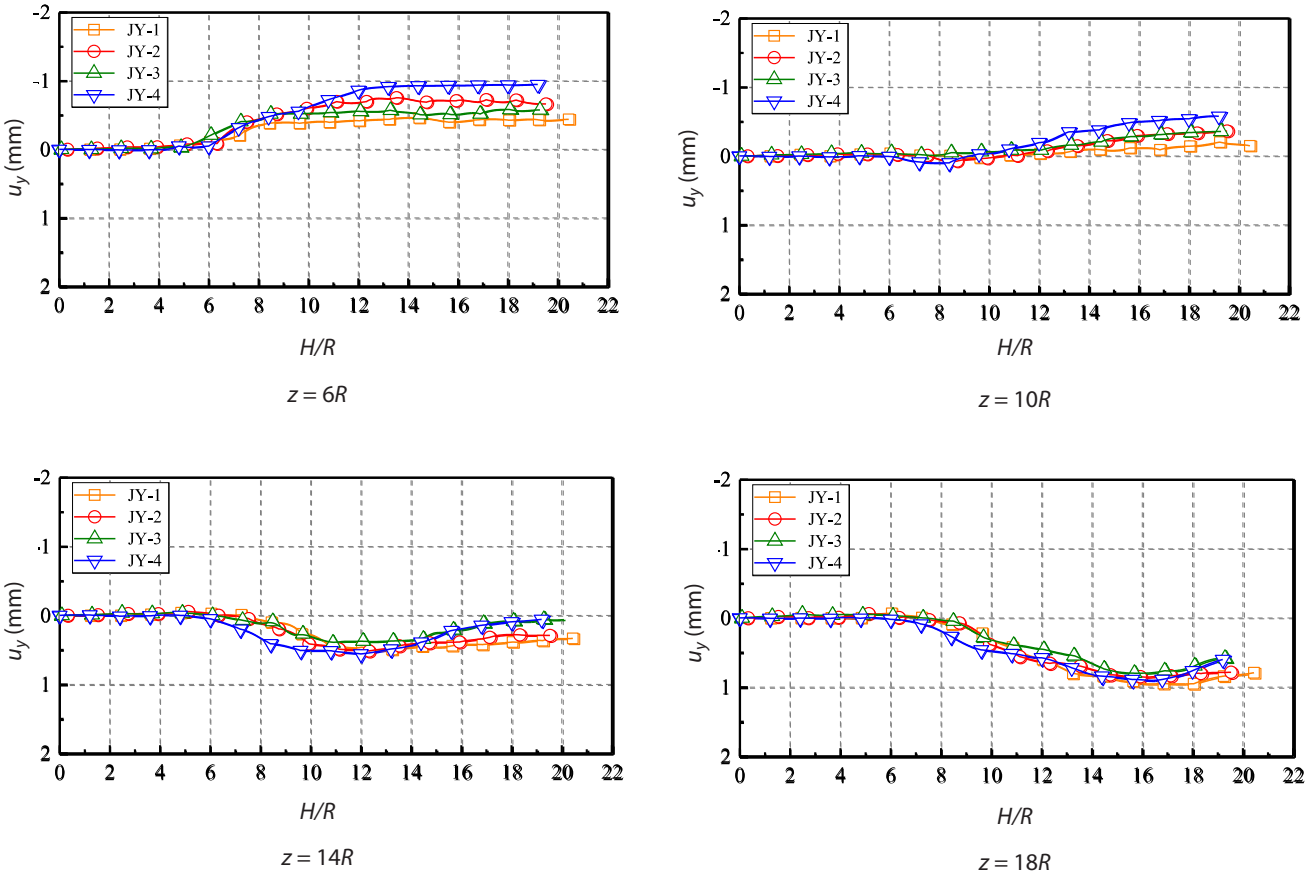

Figure 16. Accumulative vertical displacement at 7*R* distance from the pile axis for different pile shoe angles.

(1) The digital image correlation technique is a non--contact technique that can be used to capture soil displacements in a model test. Compared with traditional displacement sensors, many more points in the displacement field could be sampled and analyzed. In this study, one digital camera and one camera module were used to capture the images of the full-field displacements and the displacements in the disturbance layer, respectively. The setting of those two cameras provided good opportunities to investigate the soil displacements caused by the pile press-in for multiple scales. To complete all the image analyses in the current study, a DIC calculation program based on MATLAB was compiled. Compared with commercial DIC systems, the compiled program could yield more comprehensive data processing, compute horizontal and vertical displacements for any time and any positions, and generate both contour plots and vector diagrams.

(2) The development of the horizontal soil stresses correlated well with the horizontal and vertical displacements. Both soil displacements and soil stresses experienced an 'advance' effect during the pile press--in, i.e., the soil displacement and soil stress at one designated point peaked before the pile tip passed the point. However, the 'advance' effect became less obvious with greater pile penetration.

(3) Analyses on local soil displacements showed that the disturbance layer on the pile-soil interface was about 2-3 mm (7.4-11.1 D_{50}) in thickness, which correlated well with those findings in the literature. The disturbance layer mainly featured downward vertical displacements. However, the magnitude of the vertical displacements decreased with the advancement of the pile.

(4) A pile shoe with a greater angle resulted in a greater disturbance to the soil. Therefore, pushing the pile with no pile shoe caused the greatest impact, while a 30° pile shoe had the least effect on the surrounding soils. The influence of the pile shoe angle became less substantial when the pile penetration depth increased.

REFERENCES

[1] Tan, Y., Lin, G. 2013. Full-scale testing of open-ended steel pipe piles in thick varved clayey silt deposits along the Delaware River in New Jersey. Journal of Geotechnical and Geoenvironmental Engineering 139(3), doi: 518-524. 10.1061/(asce) gt.1943-5606.0000777

[2] Tan, Y., Lin, G. 2014. Comprehensive load test on prestressed concrete piles in alluvial clay and marl in Savannah, Georgia. Journal of Performance of Constructed Facilities 28(1), 178-190. doi: 10.1061/(asce)cf.1943-5509.0000305

[3] Gurbuz, A., Paikowsky, S.G. 2016. New simple approach to prediction of axial settlement of single piles under design load. Journal of Bridge Engineering 21(10), 04016067. doi: 10.1061/(asce) be.1943-5592.0000939

[4] Song, Y., Yang, J., Xiang, H., Zhou, B. 2019. Bearing capacity of a single pile in saturated and drained clay. Acta Geotechnica Slovenica 10(1), 70-78. doi: 10.18690/actageotechslov.16.1.70-78.2019

[5] Tan ,Y., Lan, H. 2012. Vibration effects attributable to driving of PHC pipe piles. Journal of Performance of Constructed Facilities 26(5), 679-690. doi: 10.1061/(asce)cf.1943-5509.0000278

[6] Attewell, P.B, Farmer, I.W. 1973. Attenuation of ground vibration from pile driving. Ground Engineering 6(4), 26-29.

[7] Athanasopoulos, G.A., Pelekis, P.C. 2000. Ground vibrations from sheetpile driving in urban environment: measurements, analysis and effects on buildings and occupants. Soil Dynamics and Earthquake Engineering 19(5), 371-387. doi: 10.1016/s0267-7261(00)00008-7

[8] White, D.J., Finlay, T., Bolton, M.D., Bearss G. 2002. Press-in piling: ground vibration and noise during pile installation. Proceedings of the International Deep Foundations Congress. Orlando, USA, pp. 363-371. doi: 10.1061/40601(256)26

[9] Rockhill, D.J., Bolton, M.D., White, D.J. 2003. Ground-borne vibrations due to press-in piling operations. Proceedings of BGA International Conference on Foundations: Innovations, Observations, Design and Practice. London, UK, pp. 743-751.

[10] Lehane, B., Gill, D. 2004. Displacement fields induced by penetrometer installation in an artificial soil. International Journal of Physical Modelling in Geotechnics 1(1), 25-36. doi: 10.1680/ijpmg.2004.040103

[11] Jardine, R.J., Zhu, B.T., Foray, P., Yang, Z. 2013. Measurement of stresses around closed-ended displacement piles in sand. Géotechnique 63(1), 1-17. doi: 10.1680/geot.9.p.137

[12] Wang, L.B., Frost, J.D., Lai, J.S. 2004. Three-dimensional digital representation of granular material microstructure from X-ray tomography imaging. Journal of Computing in Civil Engineering 18(1), 28-35. doi: 10.1061/(asce)0887-3801(2004)18:1(28)

[13] Martinez, A., Frost, J.D. 2016. Particle-scale effects on global axial and torsional interface shear behaviour. International Journal of Numerical and Analytical Methods in Geomechanics 41(3), 400-421. doi: 10.1002/nag.2564

[14] Dejong, J.T., White, D.J., Randolph, M.F. 2006. Microscale observation and modelling of soil-structure interface behaviour using particle image velocimetry. Soils and Foundations 46(1), 15-28. doi: 10.3208/sandf.46.15

[15] Zhang, G., Liang, D., Zhang, J.M. 2006. Image analysis measurement of soil particle movement during a soil-structure interface test. Computers and Geotechnics 33(4-5), 248-259. doi: 10.1016/j.compgeo.2006.05.003

[16] Frost, J.D., Han, J. 1999. Behavior of interfaces between fiber-reinforced polymers and sands. Journal of Geotechnical and Geoenvironmental Engineering 125 (8), 633-640. doi: 10.1061/(asce)1090-0241(1999)125:8(633)

[17] Edil, T., Bosscher, P., Sundberg, A. 2006. Soil-Structure interface shear transfer behavior. Geotechnical Special Publication 156, 528-543. doi: 10.1061/40870(216)35

[18] Guler, M., Edil, T.B., Bosscher, P.J. 1999. Measurement of particle movement in granular soils using image analysis. Journal of Computing in Civil Engineering 13(2), 116-122. doi: 10.1061/(asce)0887-3801(1999)13:2(116)

[19] Hu, L., Pu, J. 2004. Testing and modeling of soil-structure interface. Journal of Geotechnical and Geoenvironmental Engineering 130(8), 851-860. doi: 10.1061/(asce)1090-0241(2004)130:8(851)

[20] Mayne, P.W., Christopher, B.R., DeJong, J. 2001. Manual on subsurface investigations. National Highway Institute, Publication No. FHWA NHI-01-031.

[21] Sveen, J.K. 2004. An introduction to MatPIV v. 1.6.1. eprint series, Dept. of Math. University of Oslo, Mechanics and Applied Mathematics No. 2.

[22] Evans, T.M. 2005. Microscale physical and numerical investigations of shear banding in granular soils. Ph.D. Thesis, Georgia Institute of Technology, Atlanta.

[23] Hall, S.A., Bornert, M., Desrues, J., Pannier, Y., Lenoir, N., Viggiani, G., Besuelle, P. 2010. Discrete and continuum analysis of localized deformation in sand using X-ray μCT and volumetric digital

image correlation. Geotéchnique 60(5), 315-322. doi: 10.1680/geot.2010.60.5.315
[24] Alshibli, K.A., Jarrar, M.F., Druckrey, A.M., Al-Raoush, R.I. 2016. Influence of particle morphology on a 3D kinematic behavior and strain localization of sheared sand. Journal of Geotechnical and Geoenvironmental Engineering 143(2), 04016097-1-25. doi: 10.1061/(asce)gt.1943-5606.0001601
[25] Chu, T.C., Ranson, W.F., Sutton, M.A., Peters, W.H. 1985. Application of Digital-Image-Correlation techniques to experimental mechanics. Experimental Mechanics 25(3), 232-244. doi: 10.1007/bf02325092
[26] Yates, J.R., Zanganeh, M., Tai, Y.H. 2010. Quantifying crack tip displacement fields with DIC. Engineering Fracture Mechanics 75(11), 2063-2076. doi: 10.1016/j.engfracmech.2010.03.025
[27] Rechenmacher, A.L. 2005. Grain-scale processes governing shear band initiation and evolution in sands. Journal of the Mechanics and Physics of Solids 54(1), 22-45. doi: 10.1016/j.jmps.2005.08.009

NUMERICAL ESTIMATION OF THE ONE-DIMENSIONAL CONSOLIDATION BEHAVIOR OF CLAY

NUMERIČNA OCENA OBNAŠANJA GLINE PRI ENODIMENZIONALNI KONSOLIDACIJI

Firdevs Uysal *(corresponding author)*
Nigde Omer Halisdemir university,
Department of civil engineering
51240, Nigde, Turkey
E-mail: firdevsuysal@ohu.edu.tr

Osman Sivrikaya
Karadeniz technical university,
Department of civil engineering
61080, Trabzon, Turkey
E-mail: osivrikaya@ktu.edu.tr

DOI https://doi.org/10.18690/actageotechslov.17.2.16-25.2020

Keywords

one-dimensional consolidation test, clay, excess pore-water pressure, deformation, side friction, numerical analysis

Ključne besede

enodimenzionalni konsolidacijski preizkus, glina, presežni porni vodni tlak, deformacija, bočno trenje, numerična analiza

Abstract

The consolidation behavior of clayey soils is traditionally evaluated in the laboratory using the one-dimensional consolidometer test. A new oedometer cell design with a ring of 60 mm in height, 75 mm in diameter was made to measure the excess pore-water pressure at the undrained base of the specimen and the friction between the soil and the ring, and to determine the ε – log p curve. This study deals with numerical modeling of the one-dimensional consolidation test and comparing the data obtained from the experimental study with the data from the modeling. In the modeling, the Soft Soil and Soft Soil Creep models were used for the clay proposed in this study. The results show, as a general trend, that the data from the numerical modeling are compatible with those from the experimental study.

Izvleček

Konsolidacijsko obnašanje glinenih zemljin se tradicionalno ocenjuje v laboratoriju z uporabo enodimenzionalnega konsolidacijskega preizkusa. Izdelana je bila nova zasnova celice edometra z obročem višine 60 mm in premerom 75 mm za merjenje presežnega pornega vodnega tlaka na nedrenirani osnovi preizkušanca in trenja med zemljino in obročem ter za določitev krivulje ε – log p. Študija zajema numerično modeliranje enodimenzionalnega konsolidacijskega preizkusa in primerjavo podatkov iz eksperimentalne študije s podatki iz modeliranja. Pri modeliranju sta bila za glino v tej študiji uporabljena modela »Soft Soil« in »Soft Soil Creep«. Rezultati kažejo kot splošen trend, da so podatki numeričnega modeliranja primerljivi s podatki iz eksperimentalne študije.

1 INTRODUCTION

The consolidation of soft clayey soils is a complex and relevant process in soil-consolidation testing that simulates the load conditions, the dissipation of excess pore-water pressure and the amount of compression under vertical loads. Geotechnical engineers must be careful about estimating the amount of consolidation settlement. Terzaghi [1] established the first theory of consolidation. Considering the lack of Terzaghi's theory, several authors studied the consolidation process for theoretical, numerical and centrifuge studies ([2], [3], [4], [5], [6], [7], [8], [9], [10], [11], [12]). Time-dependent consolidation models were developed to model creep, firstly by Taylor [13]. Mesri and Choi [14]

developed a finite-difference model that accounts for the time-dependent loading, secondary compression and changing material properties. Duncan et al. [15] developed a program to predict the rate of settlement during the primary consolidation, after which secondary compression is added to the calculated settlement. Perrone [16] offered the elasto-viscoplastic finite--element model that can simulate the consolidation and creep of layered soils. The model uses an incremental and small-strain approach to model the time-dependent stress-strain relationships, and the effect of strain rate on the pre-consolidation stress observed in the laboratory and in the field. Gonzalez [17] conducted an extensive experimental program to study the behavior during a constant rate of strain (CRS) consolidation. The tests were scrutinized using a numerical simulation based on a rigorous solution that accounts for the initial transient effects. Kimoto et al. [18] studied the effects of strain rates and the destructuration on the consolidation process numerically. The model was developed based on the overstress type elasto-viscoplastic model. Jeeravipoolvarn et al. [19] compared the experimental long-term consolidation data to a one-dimensional finite-element model. Sorbino et al. [20] performed a numerical procedure for selecting and calibrating different analytical models of the soil parameters based on the best fit between a controlled oedometer test and the results of a numerical simulation of the test. Pu et al. [21] presented a numerical model for one-dimensional, large-strain consolidation under conditions of a constant rate of strain loading. Fox et al. [22] developed a numerical model for one-the dimensional, large-strain consolidation of layered soils. The results indicate an excellent agreement with analytical and numerical solutions.

To know the effect of the height of the clay specimen on the stress-strain relationship is so important that the difference between the behavior of the thick clay stratum and thin clay stratum is understood. However, the major problem of friction over a high laboratory specimen that represents the field in the laboratory comes across. Therefore, the friction between the ring and the specimen is required to obtain acceptable and accurate results. It is crucial to interpret the data obtained from the high laboratory specimen without considering the amount of friction [23]. The specimen thickness plays an important role in the creep or secondary compression for clays of high plasticity and peats under laboratory conditions ([24], [25], [26]). In addition, this observation has been confirmed by Kabbaj et al. [27] in the field. Yin and Graham [28] recently examined the influence of the thickness on total settlements, the dissipation of pore pressures, the strain and the stress. The size of the test specimen can vary the data obtained from a consolidation test. The effect of side friction between the specimen and containing ring increases with the height-to-diameter (*H/D*) ratio, so this value should not be too large. Therefore, the British Standard specifies a *H/D* ratio of between 1/3 and 1/4. A fixed-ring type of oedometer cell with a test specimen 75 mm diameter and 20 mm high is typical of that which is commercially available in Britain for routine testing in accordance with the BS. However, ASTM D 2435-03 [29] requires a minimum *H/D* ratio of 1/2.5, and a specimen not less than 50 mm in diameter and 12.5 mm thick ([29]).

There are limited studies on the friction between the consolidometer ring and the clay specimen to understand the stress-strain behavior in the consolidometer in the literature ([30], [31], [32]). Berre and Iversen [32] designed special apparatus to reduce the side friction and drew the conclusion that the side friction between the sample and ring was very low. The frictional loss was found to depend on the material of the consolidometer ring and the surface smoothness ([30], [31]). Olson [33] stated that Taylor [34] examined friction in a simple but useful concept. The details about Taylor's theory exist in the literature ([23]). Brumund et al. [35] and Burmister [36] also suggested that friction might be much larger during rebound than during the initial compression. Taylor [34] reported values of friction ratio (*F*, %) in the range 5–10 % for undisturbed and remolded Boston Blue clay. Leonards and Girault [37] measured the force needed to support the consolidation ring and obtained values of *F* (%) for normally consolidated clay of 18 % for steel rings, 11 % for rings lined with tetrafluoroethylene, and 7 % for tetrafluoroethylene coated with molybdenum disulfide grease. They found a tendency for *F* (%) to increase slightly with time. Burland and Roscoe [38] placed a load cell in the consolidation rings and measured the base stress directly. They reported values of *F* (%) approaching zero for height/diameter (*D/H*) ratios close to 2.5 and for ungreased brass tubes. The use of silicone grease initially reduced the friction greatly, but after a period of time, the friction began to increase. However, values of *F* (%) of less than, or equal to, 12 % were reported even for apparently tall samples when greased rings were used. They found much higher levels of friction during unloading ([23]).

The goal of this study was to make a numerical model of the one-dimensional consolidation test and to compare the data obtained from the experimental study with those from the numerical modeling of a finite-element software package called PLAXIS. The responsive performance of the finite-element model in predicting the time-dependent behavior of one-dimensional consolidation test is presented.

2 LABORATORY INVESTIGATION

2.1 Materials

Bothkennar soft clay was used for the tests where consistency-limit tests were carried out on the soil samples in accordance with BS1377 [39]. Index tests on the two samples used for slurry were approximately the liquid limits (w_L) of 85 %, plastic limits (w_P) of 40 %, and natural moisture contents (w_n) of 70 %. The specific gravity (G_s) of Bothkennar clay for the one-dimensional consolidation tests was assumed as 2.70, based on studies in the literature ([40], [41], [42]). The soil can be classified as inorganic clay with very high plasticity (CH) ([43], [44], [23]).

2.2 Specimen, testing and new design of oedometer cell

The sample was reconstituted at a water content of 1.7 times the liquid limit by mixing it to make a slurry. After the slurry was poured into the tube, the tube was gently tapped from the outside using a small laboratory hand vibrator. Again, the vacuum was reconnected to draw the entrapped air from the sample in the tube. As a result, the sample was assumed to be fully saturated. After the completion of the de-airing period, removing the air from a sample to make the sample fully saturated, a 75-mm-diameter stainless-steel tube, attached to the consolidation ring, was assembled and transferred onto the loading frame. The axial consolidation stress was then applied under one-dimensional conditions and kept constant with the aid of a regulated air-pressure supply by means of a pneumatic piston. The vertical consolidation pressure was applied with an increase in the effective pressure from 6.25 kPa to 800 kPa. Two-way drainages were applied and the soil slurry was allowed to consolidate for 24 h. While extruding the sample from the tube into the ring, extreme care was taken to prevent any sample disturbance ([43], [44], [23]).

A fixed-ring-type consolidometer was used for the test in which the ring was made of highly polished stainless steel. The side friction between the specimen and the ring was minimized by applying a thin layer of silicon grease inside the ring. The test was conducted on specimens 75 mm in diameter and 60 mm in height ([43]). For this specimen, one-way drainage through the top porous stone was allowed during the test. A load cell and pore pressure transducers were used to measure the applied load and the induced pore pressures respectively. In addition, a displacement transducer was used to measure the axial deformation. A special oedometer cell was designed to measure the pore pressure at the undrained base of

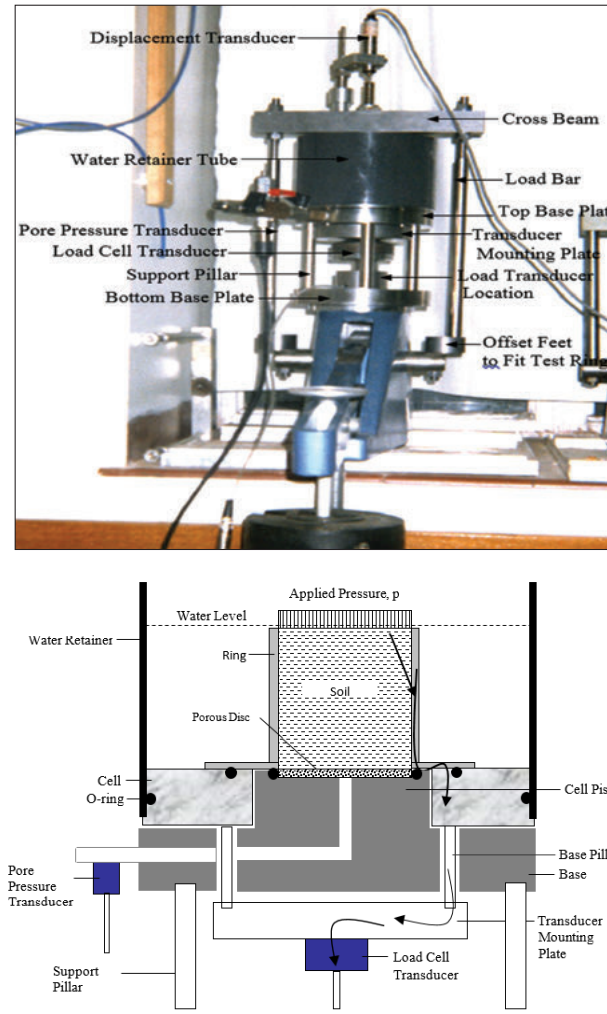

Figure 1. Special design of oedometer with measuring friction ([23]).

the specimen and the friction between the ring and the specimen side in the consolidation tests (Fig. 1).

The friction load is transferred to the load cell by means of the ring, the base pillar and the transducer mounting plate (Fig. 1). In addition, the pore pressure on the bottom of the specimen was measured by means of the pore-pressure transducer mounted on the edge of the cell base (Fig. 1). The compression of the specimens was determined with displacement transducers. The friction between the specimen and the ring was measured in a specially designed apparatus using a load cell. The settlement and the stress were read from the computer by means of the transducers connected to a data logger (ADU). Incremental loading (IL) consolidation tests were conducted on reconstituted specimens with the table model consolidation test apparatus (Fig. 1). A 24-h loading time increment with a load increment ratio of 1.0 was adopted for the test BS 1377 [45] ([43], [44], [23]).

The applied vertical load (P) was known for each increment and the load (T) transmitted to the ring, which is directly related to the side friction, was monitored by a load cell mounted on the bottom base plate. The friction load is transferred to the load cell by means of the ring, the base pillar and the transducer mounting plate in experimental studies, as shown in Figure 2. The friction stress (τ) and friction ratio (F, %) were calculated by means of Eq. (1) and Eq. (2), respectively.

$$\tau = p - q = \frac{T}{\pi DH} \qquad (1)$$

$$F(\%) = \frac{\tau}{p} \qquad (2)$$

where p is the stress applied to the top of the specimen, q is the stress occurring on the bottom of the specimen, D is the diameter of the ring and H is the height of the ring.

3 NUMERICAL MODEL

In this study, the one-dimensional consolidation behavior of clay was simulated involving the vertical displacement with elapsed time, deformation with consolidation pressure, pore-water pressure with elapsed time and friction with elapsed time and consolidation pressure.

A numerical model was developed to simulate and further analyze the one-dimensional consolidation test under laboratory conditions. The finite-element software PLAXIS 2D is used in the analysis. The cell in the oedometer test was considered in an axisymmetric model to represent the one-dimensional consolidation test. The model had a diameter (D) of 75 mm and a height (H) of 60 mm. The mesh was formed by 15-noded elements with a "fine" global coarseness. Drainage boundaries were applied to be at the ground surface and the lateral boundaries were closed. A hydrostatic pore pressure was generated from a groundwater table level at the ground surface. The manual of the PLAXIS 2D offers two types of analyses to model a one-dimensional compression test. The first analysis models drained conditions to show the logarithmic stress-strain relationship and the logarithmic time-settlement behavior for the long term. The second analysis also models the undrained conditions and the consolidation. It is stated that the second type of analyses gives more realistic results ([46]). Two types of analyses are used for the validation against experimental data simulating the consolidation tests in this study. An external load p is applied as a plastic calculation and then the consolidation analyses are performed to one day in the undrained analysis. The modeling has thirty calculation stages as plastic and consolidation phases ([46]).

Creep is a very important problem for time-dependent settlements ([47], [48], [49]). Two constitutive soil models, the Soft Soil Model (SS-M) and Soft Soil Creep model (SSC-M), which are commonly employed in the PLAXIS program for clays, were used to model the soil in this study. SS-M is based on modified Cam-Clay model that includes the stress-dependent stiffness by using the Mohr–Coulomb criterion for the primary compression of near normally consolidated soils ([46]). SSC-M is an extension SS-M and the standard creep model in PLAXIS to account for the creep. The model has an elastic-viscoplastic formulation that incorporates the creep time-dependent state variable to estimate the viscoplastic deformation ([50]). In the model, the creep strain rate is defined as a function of time. The parameters of the SS-M (λ^*, κ^*, c, ϕ, ψ) coincide with the SSC-M. However, SS-M does not include the time and the modified creep index (μ^*). PLAXIS allows both undrained and drained analyses for SS-M and SSC-M. In this study, the drained SS-M and the undrained SSC-M analyses were conducted. Table 1 presents the clay parameters needed to perform an analysis in PLAXIS 2D for the SS-M and SSC-M models. These parameters are selected from the literature ([40], [41], [51], [52]). The vertical pre-consolidation stress is fixed at 30 kPa.

PLAXIS models the soil-structure interaction by using zero-thickness elements between the soil-structure interactions. However, some numerical approaches use continuum elements instead of zero-thickness elements to model the soil and the structural components ([53]). Interface elements are used to assess the investigation of the interface friction between the clay and the steel ring in this paper. The ring was considered as a rigid soil

Table 1. Soil properties used in modeling.

	SS-M	SSC-M
γ_{unsat} (kN/m^3)	18	18
γ_{sat} (kN/m^3)	20	20
k_x (m/day)	1.86x10^{-4}	1.86x10^{-4}
k_y (m/day)	1.44x10^{-4}	1.44x10^{-4}
c (kN/m^2)	5	5
ϕ	35	35
ψ	0	0
λ^*	0.08	0.08
κ^*	0.018	0.018
R_{inter}	0.5	0.5
POP (kPa)	30	30
μ^*	-	0.01
c_k	0.7	0.7

element. The rigid soil was computed with linear elastic using an elastic modulus of 30 GPa, a Poisson's ratio of 0.30 and a unit weight of 24 kN/m^3. The interface elements are controlled by the strength-reduction factor (R_{inter}). The R_{inter} models the roughness of the interaction and reduces the interface friction. The interface is affected by the internal friction angle, cohesion, dilatancy angle, shear modulus, Poisson's ratio, and oedometer modulus ([46]). In this case, R_{inter} is chosen as rigid, 1.0 and the value cannot be less than 0.01. Since R_{inter} cannot be measured in a simple way, it is recommended that interface ([54]). The strength-reduction factor, R_{inter} = 0.5 is chosen in this study. Fig. 2 shows the FE model and the mesh in PLAXIS.

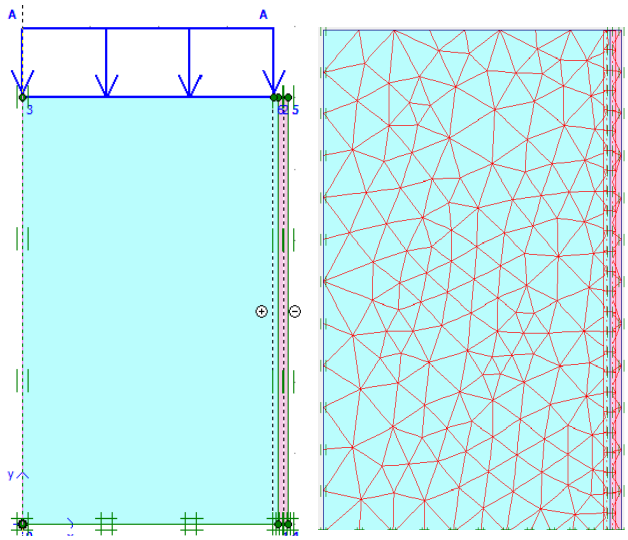

(a) Loading stage (b) Mesh generation

Figure 2. Modeling of one-dimensional consolidation test.

4 RESULTS AND DISCUSSION

As a result of the experimental study, the data measured from the tests were obtained for the variation between the vertical strain and the effective stress at the top (p) of the specimen with friction and the bottom (q) of the specimen without friction, and between the friction stress, the friction ratio, and the effective stress and the excess pore-water pressure with an elapsed time ([23]).

In this study, the compression curve was investigated in terms of the drained Soft Soil Model (SS-M) and the undrained Soft Soil Creep model (SSC-M). Fig. 3 shows the variation of the deformation with the consolidation pressure based on the laboratory tests SS-M and SSC-M. The Drained Soft Soil Model (SS-M) and the undrained Soft Soil Creep model (SSC-M) analyses were validated against the experimental data. Simulations of the tests confirm that the compression curves obtained from the SS-M and SSC-M are compatible with that from the laboratory tests. They almost match in the normal consolidation curve; however, there is a small distinction in the over-consolidation curve (Fig. 3). The results show that SSC-M has no large differences compared to the SS-M, in general. The similarity between the vertical strain predicted by the SS-M and SSC-M models would indicate that creep does not influence the settlement under the current experimental conditions. It is considered that the reason why both models give the same result is that the experimental system does not provide an effective time

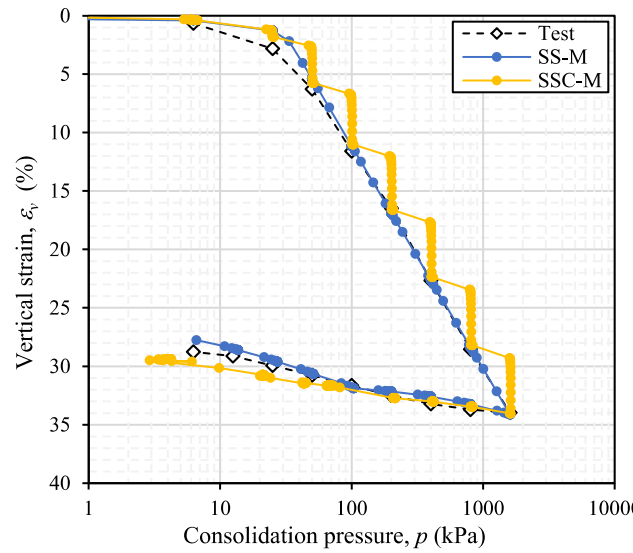

Figure 3. Measured and modeled vertical strain (ε_v).

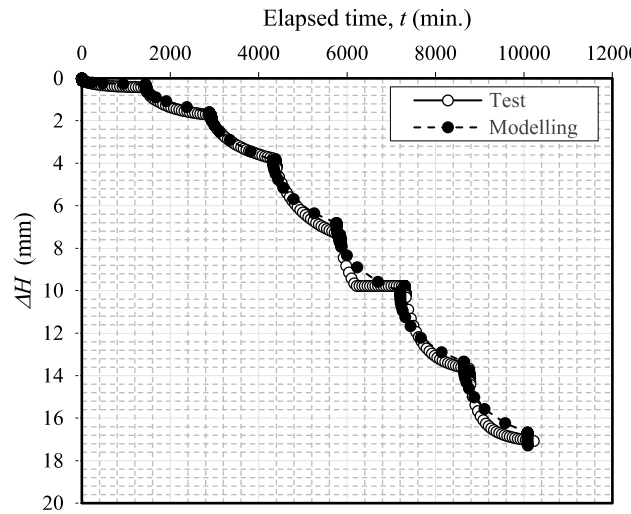

Figure 4. Measured and modeled vertical displacement (ΔH) with elapsed time (t).

for creep. However, in the rest of the study the SSC-M is used for modeling due to it including all the soft clay properties, such as creep effects. For each loading stage, the settlement of the clay samples is measured and modeled based on the SSC-M with an elapsed time and they present the same trend and close behavior (Fig. 4). The modeling represents the SSC-M in Figs. 4-8.

The excess pore-water pressure (u_b) on the bottom of the specimen was measured with the elapsed time from the tests and it is estimated from the numerical analyses. The variation of the excess pore-water pressure is examined using a numerical approach based on the SSC-M and the comparisons of the test data with the SSC-M data are made for all the load steps. Fig. 5 shows the distributions of the excess pore-water pressure for four load increments. They present similar trends and close results (Fig. 5). It is also observed that the differences between the pore-water pressures measured and modeled increase when the stress is increased. It is considered that the difference between the test data and the modeling data has occurred since the consolidation cell is not a closed system.

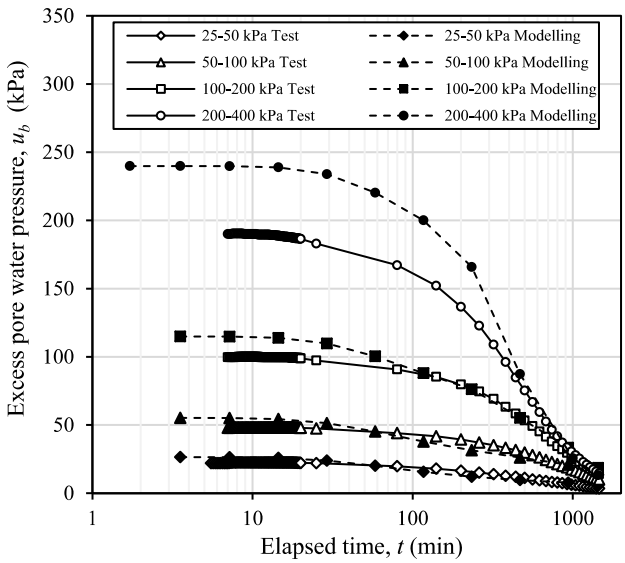

Figure 5. Measured and modeled excess pore-pressure (u_b) distributions with elapsed time (t).

The comparison is made between the friction (τ) with the elapsed time measured from the test and that calculated by the modeling (Fig. 6). The side friction ratio did not remain constant and slightly increased with time for each pressure. Up to about 100 min., the side friction sharply increased, then slightly increased at a decreasing rate, assumed to be constant. The side friction results obtained from the tests and the modeling are presented in Table 2. The measured friction and the calculated friction by modeling appear to be the same pattern, and to be consistent with each other, as shown in Fig. 6. Despite these small differences, it is clear that the friction measured from the test is consistent with those calculated from the modeling approach.

Table 2. Data obtained from tests and modeling.

p (kPa)	Tests		Modelling	
	Vertical strain ε_v (%)	Friction stress τ (kPa)	Vertical strain ε_v (%)	Friction Stress τ (kPa)
0	0.00	0.00	0.00	0.00
6.25	0.65	3.33	0.40	2.56
25	2.82	5.99	1.87	5.85
50	6.27	9.98	5.75	6.16
100	11.59	16.96	9.89	13.16
200	16.48	26.28	15.47	21.09
400	22.66	43.24	21.22	40.35
800	28.54	83.84	28.17	82.42

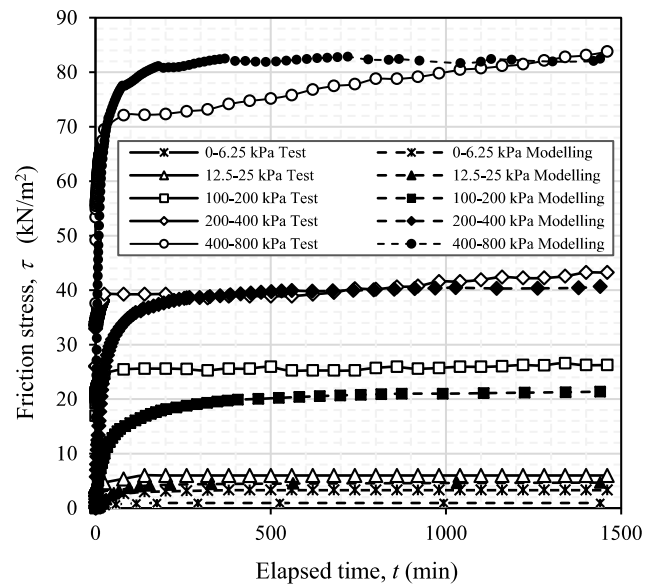

Figure 6. Measured and modeled friction stresses (τ).

Fig. 7 shows the side friction ratio (F, %) at the specimen with time after the application of each applied pressure. The measured friction ratio (F, %) and the calculated friction ratio using the modeling approach appear to be the same pattern and to be consistent with each other. As can be seen clearly from Fig. 7, there is a tendency for F (%) to decrease when the applied pressure increases. Despite these small differences, it seems clear that the friction ratio measured from the test is consistent with

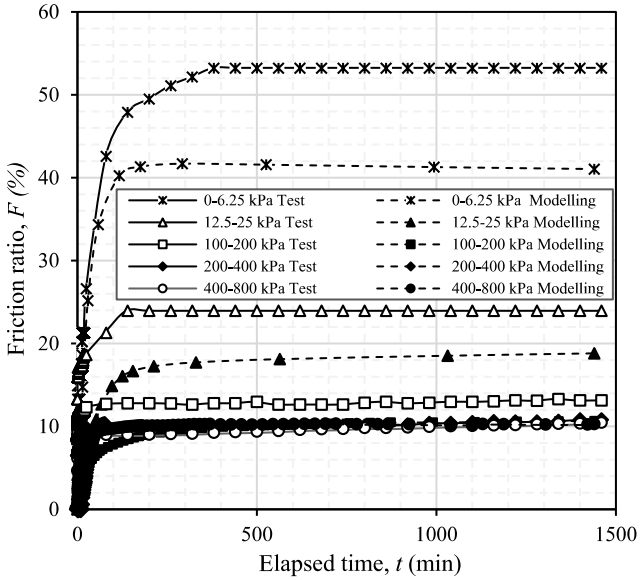

Figure 7. Measured and modeled friction-stress ratios.

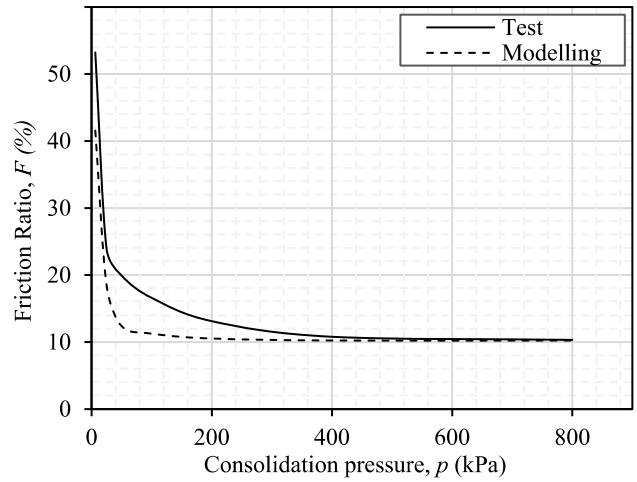

Figure 8. Comparison of F (%) determined from the test and modeling with pressure.

those calculated from the modeling approach. The effects of side friction are markedly less noticeable at high pressures, in particular (Fig. 6). However, the side friction ratio is clearly present to a considerable extent at low pressures (Fig. 7, Table 3).

The values of F (%) were in the range 10 to 16 % for the tests and in the range 10 to 11 % for the modeling for normally consolidated, reconstituted clay, and in the range 20 to 53 % for the tests and in the range 12 to 42 % for the modeling for the over-consolidated reconstituted clay for a highly polished, stainless-steel ring of D = 75 mm and H = 60 mm with a thin layer of silicon grease. The values of F (%) obtained from the modelling for normally consolidated soils are all in very narrow range (10-11%). The values of F (%) found in the current study are compatible with the data from the literature ([37], [23]).

The test and modeling results, as given in Table 3, indicate that the side friction ratio depends on the level

Table 3. Data from tests and modeling for the friction ratio.

p (kPa)	F % (Test)	F % (Modelling)
6.25	53.22	41.57
25	23.95	18.52
50	19.95	12.40
100	16.63	11.26
200	13.14	10.54
400	10.81	10.24
800	10.35	10.25

of the applied vertical consolidation pressure on the specimen. As the consolidation pressure on the top of the specimen was increased, the amount of side friction ratio decreased (Fig. 8). The friction ratio was found to be most significant at low stresses, where the clay was still over-consolidated.

5 CONCLUSIONS

In this study the data were collected from a special oedometer cell design that was used to measure the pore pressure at the undrained base of the specimen and the friction between the ring and the specimen. A one-dimensional consolidation test under laboratory conditions was examined in terms of the numerical method and the data obtained from the modeling were compared with the test data. As a result of this study, the following results were concluded:

- The compression curves obtained from SS-M and SSC-M were found to be consistent and compatible with that from the laboratory tests, and they almost match.

- The excess pore-water pressures (u_b) with an elapsed time (t) determined from the SSC-M display similar trends and close results with that from the test. The differences between the test data and the modeling data in terms of the excess pore-water pressure distribution were considered, since the consolidation cell is not a closed system.

- The side friction (τ) did not remain constant and increased slightly with the elapsed time at a decrea-

sing rate based on the test and modeling results. The amount of the side friction depends on the level of the applied vertical consolidation pressure on the specimen. When the consolidation pressure on the top of the specimen was increased, the amount of side friction increased.

– While the friction ratio (F, %) was the most significant at low stresses, where the clay was still over--consolidated, it was low at high stresses where the clay was normally consolidated. Despite the small differences, it appears clear that the friction determined from the modeling is consistent with those measured from the test. The values of F (%) obtained from modeling were found to be compatible with those in the literature.

REFERENCES

[1] Terzaghi, K. 1943. Theory of consolidation., Wiley Online Library, 265–296.

[2] Cryer, C.W. 1963. A comparison of the three-dimensional consolidation theories of Biot and Terzaghi. Quarterly Journal of Mechanics and Applied Mathematics 16, 4, 401–412. https://doi.org/10.1093/qjmam/16.4.401

[3] McVay, M., Townsend, F., Bloomquist, D. 1986. Quiescent consolidation of phosphatic waste clays. Journal of Geotechnical Engineering 112, 11, 1033-1049. doi: 10.1061/(ASCE)0733-9410(1986)112:11(1033)

[4] Moo-Young, H., Myers, T., Tardy, B., Ledbetter, R., Vanadit-Ellis, W., Kim, T.H. 2003. Centrifuge simulation of the consolidation characteristics of capped marine sediment beds. Engineering Geology 70, 3-4, 249–258. doi: 10.1016/S0013-7952(03)00093-0

[5] Lee, J. 2007. Experimental and numerical investigation of consolidation-induced solute transport, Ph.D. Dissertation, Ohio State Univ., Columbus, Ohio.

[6] Mei, G.X., Lok, T.M.H., Xia, J. and Wu, S.S. 2014. One-dimensional consolidation with asymmetrical exponential drainage boundary. Geomechanics and Engineering 6, 1, 47-63. doi: 10.12989/gae.2014.6.1.047

[7] Pu, H., Fox, P.J. 2014. Consolidation-induced solute transport for constant rate of strain. I: Model development and simulation results. Journal of Geotechnical and Geoenvironmental Engineering 141, 4, 04014127. https://doi.org/10.1061/(ASCE)GT.1943-5606.0001171

[8] Li, J., Wang, H. 2014. Analytical solutions for one-dimensional consolidation in unsaturated soils considering the non-Darcy law of water flow. Acta geotechnica Slovenica, 11, 1 , 51-60.

[9] Le, T.M., Fatahi, B., Disfani, M., Khabbaz, H. 2015. Analyzing consolidation data to obtain elastic viscoplastic parameters of clay. Geomechanics and Engineering 8, 4, 559–594. doi: 10.12989/gae.2015.8.4.559

[10] Le, T.M. 2015. Analysing consolidation data to optimise elastic visco-plastic model parameters for soft clay. Ph.D. Dissertation, University of Technology, Sydney.

[11] Jalali-Milani1a, S., Asghari-Kaljahi, E., Barzegari, G., Hajialilue-Bonab, M. 2017. Consolidation deformation of Baghmisheh marls of Tabriz, Iran. Geomechanics and Engineering, 12, 4, 561-577. doi: 10.12989/gae.2017.12.4.561

[12] Olek, B. S. 2018. Consolidation analysis of clayey soils using analytical tools. Acta Geotechnica Slovenica, 2018, 2, 58-73. doi: 10.18690/actageotechslov.15.2.58-73.2018

[13] Taylor, D.W., Merchant, W. 1940. A theory of clay consolidation accounting for secondary compression. Journal of Mathematics and Physics 19, 3, 167-185. https://doi.org/10.1002/sapm1940191167

[14] Mesri, G., Choi, Y.K. 1985. Settlement analysis of embankments on soft clays. Journal of Geotechnical Engineering 4, 441 , 441–464. https://doi.org/10.1061/(ASCE)0733-9410(1985)111:4(441)

[15] Duncan, J.M., Smith, R.W., Brandon, T.L., Wong, K.S. 1988. Consol Version 2.0, A Computer Program For 1-D Consolidation Analysis of Layered Soil Masses, The Charles E. Via, Jr. department of Civil Engineering, 104 Patton Hall, Virginia Polytechnic Institute and State University, Blacksburg, VA, 24061.

[16] Perrone, V.J. 1998. One dimensional computer analysis of simultaneous consolidation and creep of clay. Ph.D. Dissertation, Virginia Polytechnic Institute and State Univ., Blacksburg, VA.

[17] Gonzalez, J.H. 2000. Experimental and Theoretical Investigation of Constant Rate of Strain Consolidation. MSc Thesis, Massachusetts Institute of Technology.

[18] Kimoto, S., Oka, F., Higo, Y. 2004. Strain localization analysis of elasto-viscoplastic soil considering structural degradation. Computer Methods in Applied Mechanics and Engineering 193, 27-29, 2845-2866. doi: 10.1016/j.cma.2003.09.017

[19] Jeeravipoolvarn, S., Scott, J.D., Chalaturnyk, R.J., Shaw, W., Wang, N. 2008. Sedimentation and consolidation of in-line thickened fine tailings. In Proceedings of 1st International Oil Sands Tailings

Conference 209-223.
[20] Sorbino, G., Calvello, M., Cuomo, S. 2008. Inverse analysis of suction controlled oedometer tests. In Proceedings of the international conference on numerical computation in geotechnical engineering 123-129.
[21] Pu, H.F., Fox, P.J., Liu, Y. 2013. Model for large strain consolidation under constant rate of strain. International Journal for Numerical and Analytical Methods in Geomechanics 37, 11, 1574–1590. https://doi.org/10.1002/nag.2100
[22] Fox, P.J., Pu, H.P., James, D.B. 2014. CS3: Large strain consolidation model for layered soils. Journal of Geotechnical and Geoenvironmental Engineering 140, 8, 04014041. doi: 10.1061/(ASCE) GT.1943-5606.0001128
[23] Sivrikaya, O., Togrol, E. 2006. Measurement of Side Friction between Specimen and Consolidation Ring with Newly Designed Oedometer Cell. Geotechnical Testing Journal, 29, 1, 1-7. doi: 10.1520/GTJ12513
[24] Barden, L. 1968. Primary and secondary consolidation of clay and peat. Geotechnique, 18, 1-24. doi: 10.1680/geot.1968.18.1.1
[25] Imai, G. 1989. A unified theory of one-dimensional consolidation with creep. Proceedings 12th International Conference on Soil Mechanics and Foundation Engineering, 1, 57-60.
[26] Imai, G., Tang, Y.X. 1992. A constitutive equation of one-dimensional consolidation derived from inter-connected tests. Soils and Foundations, 32, 2, 83-96. https://doi.org/10.3208/sandf1972.32.2_83
[27] Kabbaj, M., Tavenas, F., Leroueil, S. 1988. In situ and laboratory stress-strain relationships. Geotechnique, 38, 1, 83-100. https://doi.org/10.1680/geot.1989.39.2.361
[28] Yin, J.H., Graham, J. 1996. Elastic visco-plastic modelling of one-dimensional consolidation. Geotechnique 46, 46, 515-527.
[29] ASTM Standard D-2435 2003 Test Methods for One-Dimensional Consolidation Properties of Soils Using Incremental Loading, Annual Book of ASTM Standards, Vol. 04.08, ASTM International,West Conshohocken, PA.
[30] Hansbo, S. 1960. Consolidation of clay, with special reference to influence of vertical sand drains. Swedish Geotechnical Institute Proc. No. 18 Stockholm.
[31] Kallstenius, T. 1963. Studies on clay samples taken with standard piston sampler. Swedish Geotechnical Institute Proceedings No. 21 Stockholm.
[32] Berre, T., Iversen, K. 1972. Oedometer tests with different specimen heights on a clay exhibiting large secondary compression. Geotechnique, 22, 1, 53-70. https://doi.org/10.1680/geot.1972.22.1.53
[33] Olson, R.E. 1986. State of the Art: Consolidation Testing, Consolidation of Soils. Testing and Evaluation, ASTM STP 892, 7-70.
[34] Taylor, D.W. 1942. Research on consolidation of clays. 82, Massachusetts Institute of Technology.
[35] Brumund, W.F., Jonas, E., Ladd, C.C. 1976. Estimation of Consolidation Settlement. Special Report 163, Transportation Research Board, 4-12.
[36] Burmister, D.M. 1960. Papers on Soils-1959 Meetings. ASTM STP 254, American Society for Testing and Materials, Philadelphia, 88-105.
[37] Leonards, G.A., Girault, O. 1961. A study of one-dimensional consolidation test. Fifth Int. Conf. on Soil Mechanics and Foundation Engineering, 1, 213-218.
[38] Burland, J. B., Roscoe K. H. 1969. Local strains and pore pressures in a normally consolidated clay layer during one-dimensional consolidation. Geotechnique 19, 3, 335-356. https://doi.org/10.1680/geot.1969.19.3.335
[39] BS 1377 1990. British Standard Methods of Test for Soils for Civil Engineering Purposes, Part 2: Classification Tests.
[40] Nash, D.F.T., Powell, J.J.M., Lloyd, I.M. 1992. Initial investigations of the soft clay test site at Bothkennar. Geotechnique 42, 2, 163-181.
[41] Hight, D.W., Paul, M.A., Barras, B. F., Powell, J. J. M., Nash, D.F. T., Smith, P.R., Edwards, D. H. 2003. The characterisation of the Bothkennar clay. Characterisation & Engineering Properties of Natural Soils. 1, 543-597.
[42] McGinty, K. 2006. The stress-strain behaviour of Bothkennar clay. Doctoral Thesis, University of Glasgow, England.
[43] Sivrikaya, O. 1997. Behavior of soft Bothkennar clay under one-dimensional compression. Msc Thesis, Department of Civil Engineering, University of Bristol, England.
[44] Sivrikaya, O. 2001. Effects of thickness of clay layer on cα. Proceedings of the 15th Int. Conf. on Soil Mechanics and Geotechnical Engineering, 275-278, Istanbul, Turkey.
[45] BS 1377 1990. British Standard Methods of Test for Soils for Civil Engineering Purposes, Part 5: Compressibility, permeability and durability tests.
[46] Brinkgreve, R.B.J., Vermeer, P.A. 1998. Finite element code for soil and rock analysis. PLAXIS 7.0 manual, Balkema.
[47] Bjerrum, L. 1967. 7th rankine lecture: Enginnering geology of Norwegian normally-consolidated marine clays as related to settlements of buildings. Geotechnique, 17, 1, 81-118. doi: 10.1680/geot.1967.17.283

[48] Garlanger, J.E. 1972. The consolidation of soils exhibiting creep under constant effective stress. Geotechnique, 22, 1, 71-78.
[49] Jostad, H.P., Palmieri, F., Andresen, L. and Boylan, N. 2018. Numerical prediction and back-calculation of time-dependent behaviour of Ballina test embankment. Computers and Geotechnics 93, 123-132. doi: 10.1016/j.compgeo.2017.05.026
[50] Yuan, Y., Whittle, A.J. 2013. Examination on time-dependent soil models in one dimensional consolidation. Constitutive Modeling of Geomaterials, 159–166. doi: 10.1007/978-3-642-32814-5_18
[51] Nash, D.F.T., Sills, G.C., Davison, L.R. 1992. One-dimensional consolidation testing of soft clay from Bothkennar. Geotechnique, 42, 2, 241-256. https://doi.org/10.1680/geot.1992.42.2.241
[52] Leroueil, S., Lerat, P., Hight, D.W., Powell, J.J.M. 1992. Hydraulic conductivity of a recent estuarine silty clay at Bothkennar Scotland. Géotechnique, 42, 2, 275–288. doi: 10.1680/geot.1992.42.2.275
[53] Damians, I.P., Yub, Y., Lloret, A., Bathurst, R.J., Josa, A. 2015. Equivalent interface properties to model soil-facing interactions with zero-thickness and continuum element methodologies. Fundamentals to Applications in Geotechnics, 1065-1072. doi: 10.3233/978-1-61499-603-3-1065
[54] Carlstedt, E. 2008. Soil-Structure Interaction for Bridges with Backwalls, FE Analysis Using PLAXIS. TRITA-BKN MSc thesis, ISSN1103-4297, ISRN KTN/BKN/Ex—270—SE, Sweden.

EFFECT OF GRAIN SIZE DISTRIBUTION ON THE MAXIMUM AND MINIMUM VOID RATIOS OF GRANULAR SOILS

VPLIV PORAZDELITVE VELIKOSTI ZRN NA NAJVEČJI IN NAJNIŽJI KOLIČNIK POR V GROBOZRNATIH ZEMLJINAH

Jose Duque *(corresponding author)*
University de la Costa
Barranquilla, Colombia
E-mail: jochedf@hotmail.com

William Mario Fuentes Lacouture
Findeter
Bogotá, Colombia
E-mail: fuenteslacouture1@gmail.com

Jorge Andres Barros Ayala
University de la Costa
Barranquilla, Colombia
E-mail: jbarros8@cuc.edu.co

DOI https://doi.org/10.18690/actageotechslov.17.2.26-33.2020

Keywords

grain size distribution, granular soils, relative density, maximum void ratio, minimum void ratio

Ključne besede

porazdelitev velikosti zrn, grobozrnata zemljina, gostotno stanje, največji količnik por, najmanjši količnik por

Abstract

The maximum and minimum void ratios define the loosest and densest conditions of a granular soil. Correlations with some granulometric properties of soil are of interest for practical applications, but the experimental procedure to determine these variables can be time consuming. In this work the influence of the grain size distribution on the maximum and minimum void ratios is investigated. Twenty different granular soils with varying grain size distributions were prepared and tested. The experimental results, together with a compilation of 56 additional results reported in the literature, are statistically analysed. The analysis is conducted to examine the influence of some granulometric properties (D_{10}, D_{30} and D_{60}) on the maximum and minimum void ratios. As a result, some correlations considering the aforementioned variables are proposed. Subsequently, it is shown that the proposed correlations have better agreement with the experimental data than other proposals reported in the literature. The paper ends with some concluding remarks.

Izvleček

Najvišji in najmanjši količnik por določata meji med najrahlejšim in najgostejšim gostotnim stanjem grobozrnate zemljine. Korelacije z nekaterimi granulometrijskimi lastnostmi zemljin so zanimive za praktično uporabo, vendar je preizkusni postopek za določanje teh spremenljivk lahko dolgotrajen. V tem delu je raziskan vpliv porazdelitve velikosti zrn na največji in najmanjši količnik por. Pripravljenih in preizkušenih je bilo dvajset različnih grobozrnatih zemljin z različno porazdelitvijo velikosti zrn. Eksperimentalni rezultati teh preizkusov so bili, skupaj s 56 dodatnimi rezultati iz literature, statistično analizirani. Z analizo se je proučeval vpliv nekaterih granulometrijskih lastnosti (D_{10}, D_{30} in D_{60}) na največji in najmanjši količnik por. Kot rezultat analize so predlagane nekatere korelacije, ki upoštevajo zgoraj omenjene spremenljivke. Kasneje se je pokazalo, da se predlagane korelacije bolje ujemajo z eksperimentalnimi podatki kot drugi predlogi, navedeni v literaturi. Prispevek se konča z nekaj zaključnimi pripombami.

1 INTRODUCTION

In this work the influence of the grain size distribution of granular soils on their maximum and minimum void ratios is investigated. Hereafter, the maximum and minimum void ratios, denoted by e_{max} and e_{min}, are collectively referred to as the characteristic void ratios. The literature has shown that these characteristic void ratios depend mainly on some physical properties of the grains, such as sphericity S (cf. eccentricity or platiness) [1, 2, 3, 4], roundness R (cf. angularity) [5, 6, 7], smoothness S_m (cf. roughness) [8, 9, 10] and the grain size distribution [11, 12, 13, 14, 15, 16]. Even though the characteristic void ratios depend on all the aforementioned properties, only the grain size distribution is commonly measured in engineering practice. Therefore, authors aiming to provide useful correlations, usually interrelate the characteristic void ratios with some grain-size-distribution properties, such as the grain size diameters D_{10}, D_{30}, D_{50}, and, D_{60}, and/or some other related variables, such as the uniformity and curvature coefficients, denoted by C_u and C_c [17, 18, 19]. A summary of some reported correlations for the characteristic void ratios using the index and physical properties of the grains is presented in Table 1.

Some modern techniques based on new theoretical approaches such as the random-close-packing theory [25] are also found in the literature. Such methodologies consist of mapping the 3D packing of grain particles, idealized as spheres, onto 1D rods. The technique aims to estimate the combinations of the rods that generates the densest and the loosest packing states of the soil. However, such calculations can be complicated for ordinary engineering practice. In this article, empirical correlations relating the characteristic void ratios with some grain-size-distribution properties are proposed. Twenty different granular samples with varying grain size distributions were prepared and tested. In addition, 56 different samples reported in the literature are also considered. For all the samples, the grain size parameters D_{10}, D_{30}, D_{50}, D_{60}, C_u and C_c were collected and their influence on the characteristic void ratios was analysed. Some correlations for the characteristic void ratios considering the mentioned variables are proposed. A comparison between the prediction capabilities of the proposed correlations and some previous existing correlations is made. To that end, some additional equations are derived using the mathematical structures of the correlations proposed in previous studies and the collected database in this study. The results indicate that the mathematical structure of the proposed correlations offers better accuracy than the ones proposed in some previous investigations.

2 EXPERIMENTAL PROCEDURE

One of the main limitations of most existing correlations (see, e.g., [20-24]) between the grain size diameters, or some other related variables, and the characteristic void ratios is the fact that they are based solely on a single independent variable (e.g., D_{50}, C_u). Hence, in the case of materials having completely different granulometric distributions, but same parameters D_{50} or C_u, the equations would predict the same characteristic void ratios, which is unrealistic. To analyse this limitation, 20 samples of sands and gravels with different grain size distributions were created, see Figure 1. The test material was collected from the construction site of the new "Barranquilla – Cartagena" highway in Colombia. The material has almost no fines content, a subangular

Table 1. Correlations between maximum and minimum void ratios of granular materials and some index and physical properties of the grains.

Reference	Type of soil	Model	Units	Statistical indicator
[20]	Granular soils	$e_{max} = 0.6042 D_{50}^{-0.304}$ $e_{min} = 0.3346 D_{50}^{-0.491}$	D_{50} in mm	$R^2 = 0.76$ $R^2 = 0.85$
[21]	Clean sands	$e_{max} - e_{min} = 0.23 + 0.06/D_{50}$	D_{50} in mm	-
[22]	Granular soils	$e_{max} = -0.076\ln(C_u)+0.83$ $e_{min} = -0.101\ln(C_u)+0.56$	Dimensionless	$R^2 = 0.64$ $R^2 = 0.90$
[23]	Granular soils	$e_{max} \approx 1.62 e_{min}$	Dimensionless	-
[5]	Granular soils	$e_{max} = 1.30 - 0.62(R)$ $e_{min} = 0.80 - 0.34(R)$	Dimensionless	$R^2 = 0.81$ $R^2 = 0.58$
[6]	Uniform sands	$e_{max} = 0.642(R)^{-0.354}$	Dimensionless	-
[7]	Granular soils	$e_{max} = 0.072 + 1.53 e_{min}$	Dimensionless	$R^2 = 0.93$
[24]	Granular soils	$e_{max} = 0.554 + 0.154(R)^{-1}$ $e_{min} = 0.359 + 0.082(R)^{-1}$	Dimensionless	-

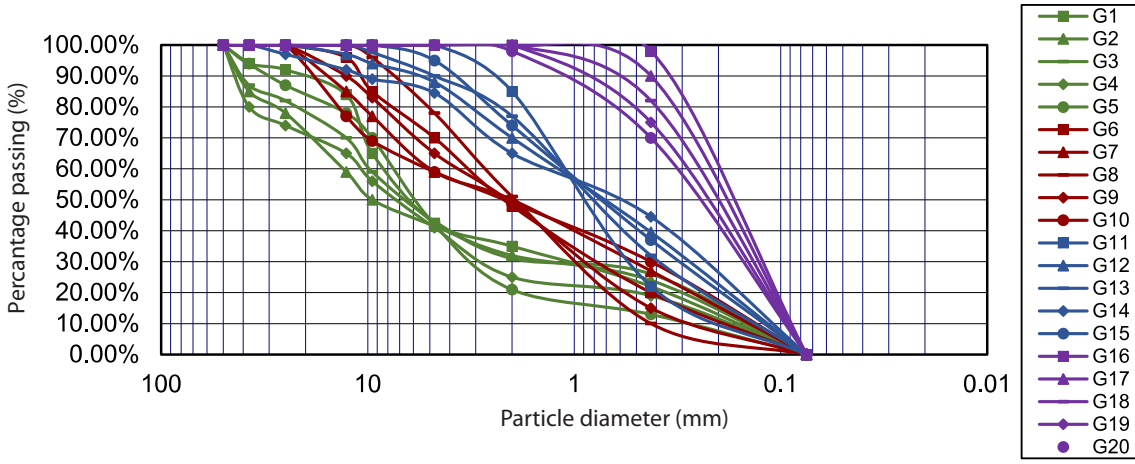

Figure 1. Grain size distribution from the performed experiments.

grain shape, and is mainly composed of quartz [26]. The samples are summarized in four different groups:

- Group 1: samples G1-G5, presenting a mean grain size between D_{50} = [6-9.5] mm.
- Group 2: samples G6-G10, presenting a mean grain size between D_{50} = [2-2.2] mm.
- Group 3: samples G11-G15, presenting a mean grain size between D_{50} = [0.6-0.9] mm.
- Group 4: samples G16-G20, presenting a mean grain size between D_{50} = [0.17-0.25] mm.

The minimum and maximum void ratios were determined according to the procedures given by the ASTM test designations D4253 and D4254, respectively. The particle size distribution (gradation) of each sample was determined using sieve analysis using the method described in ASTM D6913. The samples were classified as GW, SW and SP according to the Unified Soil Classification System (USCS) and as A-1-a, A-1-b and A-3 according to the American Association of State Highway and Transportation Officials (AASHTO) classification system.

A summary of the experimental results of the tested samples (G1-G20, see Figure 1) together with 56 extra experimental results from 13 different studies is presented in Table 2. The results show that each group of curves has similar values of D_{50}, and presents values of the characteristic void ratios that are not similar to each other. For that reason, the proposed correlations described in Section 3 include more independent variables to account for the granulometric variability of the materials.

3 CORRELATION EQUATIONS

In this section the statistical analysis of the database presented in Table 2 is described. The proposed mathematical structure of the correlations for the maximum and minimum void ratios has a potential form and uses the parameters D_{10}, D_{30} and D_{60} in millimetres as independent variables, as shown in Eqs. (1) and (2):

$$e_{max} = k_1 D_{10}^{k_2} D_{30}^{k_3} D_{60}^{k_4} \qquad (1)$$

$$e_{min} = k_5 D_{10}^{k_6} D_{30}^{k_7} D_{60}^{k_8} \qquad (2)$$

For the calibration of the k_i constants, Eqs. (1) and (2) are linearized as follows:

$$\ln(e_{max}) = \ln(k_1) + k_2 \ln(D_{10}) + k_3 \ln(D_{30}) + k_4 \ln(D_{60}) \quad (3)$$

$$\ln(e_{min}) = \ln(k_5) + k_6 \ln(D_{10}) + k_7 \ln(D_{30}) + k_8 \ln(D_{60}) \quad (4)$$

Subsequently, a linear-regression analysis is performed using the Statgraphics software to determine the constants of each equation. The results of the regression analyses are presented in Table 3 and suggest that the model accurately predicts the experimental results with coefficients of determination (R^2) of 0.75 and 0.65. Additionally, all the parameters are statistically significant using a statistical significance of 0.01.

Replacing the results of the regression analyses presented in Table 3 on Eqs. (1) and (2), the correlation equations can be rewritten as presented in Eqs. (5) and (6):

$$e_{max} = 0.657 D_{10}^{-0.180} D_{30}^{0.263} D_{60}^{-0.277} \qquad (5)$$

$$e_{min} = 0.365 D_{10}^{-0.322} D_{30}^{0.353} D_{60}^{-0.323} \qquad (6)$$

Table 2. Database of minimum and maximum void ratios of granular materials from this study and other studies available in the literature.

	D_{10} (mm)	D_{30} (mm)	D_{50} (mm)	D_{60} (mm)	C_u (-)	C_c (-)	e_{max} (-)	e_{min} (-)	Reference
G1	0.150	1.000	6.900	8.500	56.67	0.78	0.601	0.393	
G2	0.180	2.000	10.000	14.000	77.78	1.59	0.584	0.406	
G3	0.150	2.000	7.000	10.000	66.67	2.67	0.630	0.412	
G4	0.200	3.000	7.800	11.000	55.00	4.09	0.587	0.410	
G5	0.300	2.200	6.000	7.600	25.33	2.12	0.612	0.398	
G6	0.190	0.800	2.200	3.200	16.84	1.05	0.524	0.388	
G7	0.150	0.540	2.000	5.000	33.33	0.39	0.543	0.409	
G8	0.450	1.000	1.950	2.900	6.44	0.77	0.588	0.406	
G9	0.290	0.900	2.100	3.900	13.45	0.72	0.548	0.402	
G10	0.140	0.420	2.100	5.100	36.43	0.25	0.564	0.352	
G11	0.220	0.600	0.900	1.200	5.45	1.36	0.716	0.472	Present study
G12	0.120	0.300	0.750	1.300	10.83	0.58	0.693	0.469	
G13	0.150	0.410	0.850	1.150	7.67	0.97	0.701	0.492	
G14	0.110	0.240	0.670	1.600	14.55	0.33	0.678	0.495	
G15	0.130	0.340	0.800	1.200	9.23	0.74	0.688	0.485	
G16	0.090	0.130	0.180	0.200	2.22	0.94	0.943	0.682	
G17	0.090	0.140	0.190	0.220	2.44	0.99	0.940	0.666	
G18	0.092	0.140	0.200	0.250	2.72	0.85	0.930	0.660	
G19	0.095	0.160	0.220	0.290	3.05	0.93	0.967	0.654	
G20	0.098	0.170	0.250	0.310	3.16	0.95	0.990	0.679	
G21	0.130	0.190	0.202	0.210	1.62	1.32	0.805	0.550	[27]
G22	0.088	0.120	0.163	0.180	2.05	0.91	0.865	0.580	
G23	0.120	0.220	0.340	0.400	3.33	1.01	0.966	0.584	[28]
G24	0.250	0.500	1.130	1.200	4.80	0.83	0.567	0.334	
G25	0.120	0.150	0.160	0.180	1.50	1.04	0.992	0.679	
G26	0.190	0.280	0.350	0.380	2.00	1.09	0.930	0.630	[29]
G27	0.290	0.470	0.550	0.600	2.07	1.27	0.874	0.577	
G28	0.160	0.280	0.520	0.680	4.25	0.72	0.691	0.422	
G29	0.210	0.460	0.660	0.810	3.86	1.24	0.620	0.380	[30]
G30	0.320	0.800	2.000	3.640	11.38	0.55	0.470	0.250	
G31	0.200	0.310	0.390	0.410	2.05	1.17	0.740	0.680	[31]
G32	0.345	0.484	0.700	0.790	2.29	0.86	0.791	0.504	
G33	0.329	0.421	0.580	0.700	2.13	0.77	0.775	0.512	
G34	0.325	0.405	0.550	0.680	2.09	0.74	0.771	0.510	
G35	0.286	0.363	0.375	0.440	1.54	1.05	0.888	0.597	
G36	0.292	0.355	0.365	0.420	1.44	1.03	0.906	0.619	
G37	0.335	0.427	0.540	0.610	1.82	0.89	0.890	0.577	
G38	0.544	0.570	0.750	0.810	1.49	0.74	0.703	0.389	
G39	0.200	0.324	0.350	0.410	2.05	1.28	0.766	0.484	
G40	0.335	0.423	0.580	0.650	1.94	0.82	0.841	0.555	
G41	0.226	0.308	0.360	0.400	1.77	1.05	0.844	0.552	
G42	0.236	0.308	0.350	0.390	1.65	1.03	0.827	0.577	
G43	0.251	0.336	0.380	0.420	1.67	1.07	0.803	0.544	
G44	0.224	0.273	0.350	0.390	1.74	0.85	0.801	0.544	
G45	0.310	0.401	0.600	0.700	2.26	0.74	0.732	0.483	
G46	0.200	0.320	0.380	0.410	2.05	1.25	0.761	0.516	
G47	0.242	0.327	0.350	0.390	1.61	1.13	0.842	0.569	
G48	0.217	0.325	0.350	0.390	1.80	1.25	0.853	0.566	
G49	0.200	0.300	0.340	0.370	1.85	1.22	0.919	0.633	
G50	0.224	0.292	0.340	0.360	1.61	1.06	0.919	0.625	
G51	0.242	0.337	0.360	0.400	1.65	1.17	0.857	0.562	[20]
G52	0.248	0.317	0.350	0.390	1.57	1.04	0.861	0.567	
G53	0.220	0.300	0.360	0.390	1.77	1.05	0.729	0.457	
G54	0.245	0.337	0.390	0.460	1.88	1.01	0.710	0.468	
G55	0.230	0.289	0.360	0.400	1.74	0.91	0.757	0.512	
G56	0.190	0.290	0.350	0.390	2.05	1.13	0.843	0.542	
G57	0.248	0.359	1.400	2.000	8.06	0.26	0.480	0.268	
G58	0.199	0.259	0.590	0.650	3.27	0.52	0.578	0.356	
G59	0.440	0.689	1.000	2.000	4.55	0.54	0.583	0.278	
G60	0.270	0.382	0.780	1.200	4.44	0.45	0.545	0.315	
G61	0.410	0.914	1.400	2.000	4.88	1.02	0.548	0.292	
G62	0.297	0.395	0.410	0.890	3.00	0.59	0.551	0.346	
G63	0.342	0.541	1.250	1.900	5.56	0.45	0.492	0.261	
G64	0.388	0.875	1.200	1.700	4.38	1.16	0.590	0.302	
G65	0.300	0.484	1.100	1.500	5.00	0.52	0.524	0.288	
G66	0.410	0.970	1.300	1.500	3.66	1.53	0.621	0.331	
G67	0.382	0.967	1.300	1.450	3.80	1.69	0.621	0.335	
G68	0.350	0.840	1.250	1.400	4.00	1.44	0.618	0.341	
G69	0.319	0.681	1.100	1.400	4.39	1.04	0.607	0.330	
G70	0.227	0.300	0.390	0.450	1.98	0.88	0.770	0.490	[32]
G71	0.120	0.180	0.210	0.235	1.96	1.15	0.850	0.540	[33]
G72	0.070	0.300	0.500	0.700	10.00	1.84	0.704	0.536	[34]
G73	0.350	0.550	0.770	0.820	2.34	1.05	0.844	0.519	[35]
G74	0.130	0.290	0.480	0.600	4.62	1.08	0.791	0.461	
G75	0.090	0.140	0.145	0.150	1.67	1.45	1.054	0.677	[36]
G76	0.130	0.150	0.167	0.180	1.38	0.96	0.930	0.581	[37]

Table 3. Database of minimum and maximum void ratios of granular materials from this study and other studies available in the literature.

Parameter	Coefficient	Typical error	t-statistic	P-value	Lower 95%	Upper 95%	R^2
$\mathrm{Ln}(k_1)$	-0.420	0.041	-10.161	1.5×10^{-15}	-0.503	-0.338	0.75
k_2	-0.180	0.038	-4.787	8.7×10^{-6}	-0.255	-0.105	
k_3	0.263	0.052	5.035	3.4×10^{-6}	0.159	0.367	
k_4	-0.277	0.029	-9.575	1.8×10^{-14}	-0.335	-0.220	
$\mathrm{Ln}\ (k_5)$	-1.007	0.063	-15.884	3.1×10^{-25}	-1.134	-0.881	0.65
k_6	-0.322	0.058	-5.596	3.7×10^{-7}	-0.438	-0.208	
k_7	0.353	0.080	4.409	3.6×10^{-5}	0.193	0.512	
k_8	-0.323	0.044	-7.272	3.5×10^{-10}	-0.412	-0.235	

Table 4. Descriptive statistics of the samples implemented in the statistical analyses.

	D_{10} (mm)	D_{30} (mm)	D_{50} (mm)	D_{60} (mm)	C_u (-)	C_c (-)	e_{max} (-)	e_{min} (-)
Minimum value	0.07	0.12	0.14	0.15	1.38	0.25	0.470	0.250
Maximum value	0.57	3.0	10.0	14.0	77.78	4.09	1.054	0.682
Range	0.50	2.88	9.86	13.85	76.39	3.84	0.584	0.432
Mean	0.23	0.52	1.15	1.61	8.11	1.04	0.739	0.482
Standard deviation	0.10	0.49	1.82	2.58	14.87	0.53	0.15	0.12
Coefficient of variation (%)	44.0	94.6	158.9	160.2	183.3	50.9	20.0	24.8
Number of samples (-)	76	76	76	76	76	76	76	76

Table 5. Developed equations using mathematical structures from previous studies.

Model	Equation number	Equation form by	Units	Statistical indicator
$e_{max} = 0.6729 D_{50}^{-0.166}$	(7)	[20]	D_{50} in mm	$R^2 = 0.59$
$e_{min} = 0.4291 D_{50}^{-0.189}$	(8)			$R^2 = 0.46$
$e_{max} = -0.094\ln(C_u) + 0.868$	(9)	[22]	Dimensionless	$R^2 = 0.42$
$e_{min} = -0.061\ln(C_u) + 0.566$	(10)			$R^2 = 0.27$

Table 4 presents a summary of the descriptive statistics of each of the variables considered for the development of the equations. Note that the proposed equations are only valid for granular soils with the parameters D_{10}, D_{30} and D_{60} within the ranges (maximum and minimum values) presented in Table 4.

For comparison purposes, some equations were also derived from the same database relating the grain-size--distribution parameters D_{50} and C_u and using the mathematical structure of previous studies, e.g., [20, 22]. The results of this analysis are summarized in Table 5. The comparison between the measured and predicted characteristic void ratios, using the proposed correlations and the equations from Table 5, is presented in Figure 2 and Figure 3. The results show that the proposed correlations provide better agreement with the experimental data, as well as higher coefficients of determination, than the equations with previously reported mathematical structures, see Table 6. In addition, the graphs include the 95% confidence interval for the estimated characteristic void ratios, which shows that few points lie outside the intervals for the predictions with equations (7) and (9), but not for the prediction with the proposed equation (5).

Table 6. Comparison of the errors obtained in the predictions.

Variable	Equation	R^2	MAE	RMSE
e_{max}	(5)	0.75	0.062	0.074
	(7)	0.59	0.073	0.088
	(9)	0.42	0.093	0.112
e_{min}	(6)	0.65	0.060	0.069
	(8)	0.46	0.069	0.080
	(10)	0.27	0.082	0.102

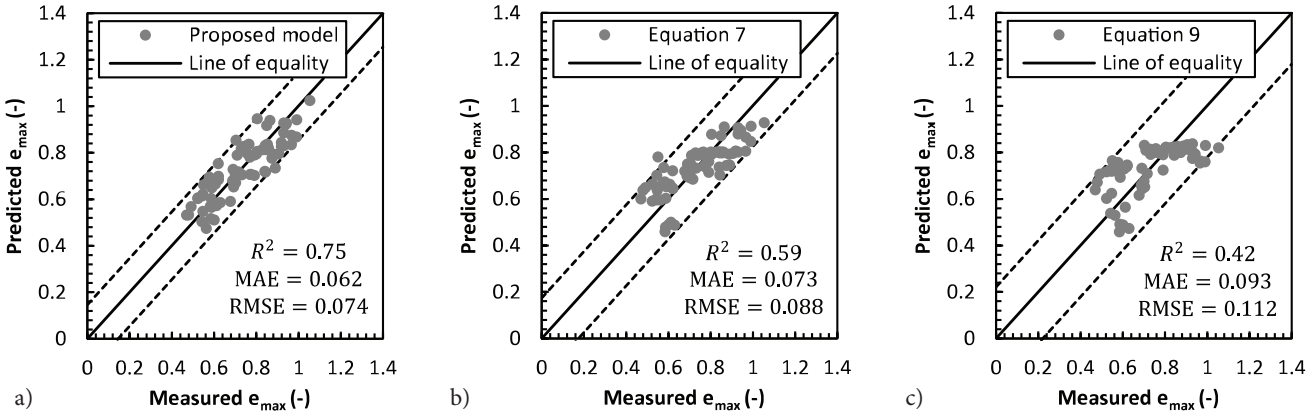

Figure 2. Measured and predicted e_{max} with: a) proposed equation (5), b) equation (7), c) equation (9).

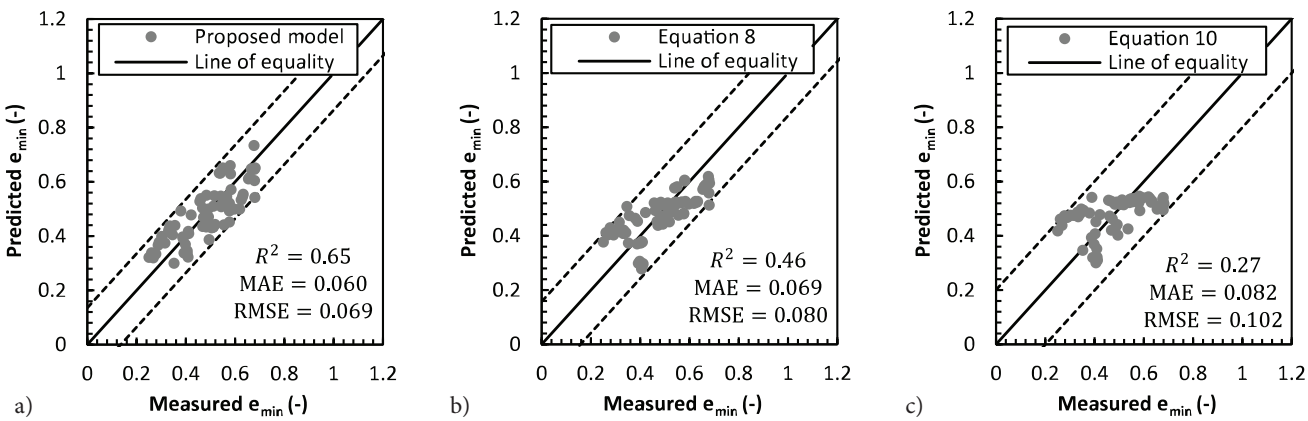

Figure 3. Measured and predicted e_{min} with: a) proposed equation (6), b) equation (8), c) equation (10).

The statistical variables root-mean-square error (RMSE) and mean-absolute error (MAE) were considered to evaluate the errors between predicted and measured results. In line with the above findings, the errors obtained in the predictions using the proposed equations are lower than the ones using the equations developed with previously reported mathematical structures.

Based on the database presented in Table 2, a correlation to relate the maximum and minimum void ratios is now proposed. The correlation is presented in Eq. (11) and plotted on Figure 4. The results indicate that the proposed correlation accurately predicts the experimental results with a coefficient of determination (R^2) equal to 0.85. The form and magnitude of Eq. (11) is similar to the one proposed by [7, 23].

$$e_{max} = 1.52 e_{min} \qquad (11)$$

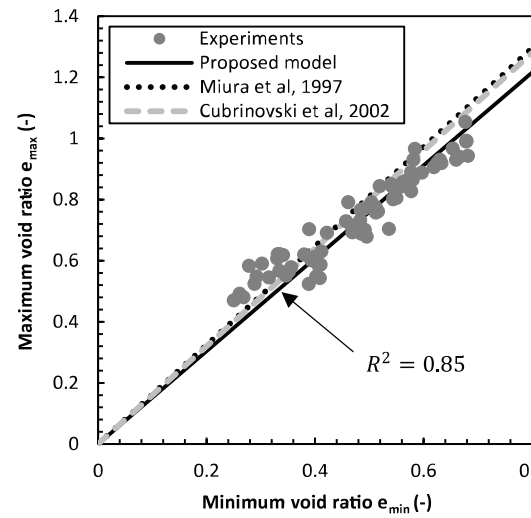

Figure 4. Relation between maximum and minimum void ratios. The proposed correlation and the ones reported by [7, 23] are indicated.

4 FINAL REMARKS

In this work, correlations for the maximum and minimum void ratios, depending on some grain-size--distribution properties were proposed. To that end, the experimental results of 76 samples on granular materials compiled from 13 different studies were considered. The principal findings of this work can be summarized as follows:

- Previous works presented correlations between the soil-grain-size distribution and the maximum and minimum void ratios based solely on a single independent variable. However, the granulometric variability of granular soils, and therefore its influence on the values of the characteristic void ratios, are not properly captured when only one variable is considered on the correlations. For that reason, the proposed equations incorporate three common grain size diameters, D_{10}, D_{30} and D_{60}, to account for the granulometric variability of the soil.

- The proposed correlations accurately predict the developed experimental database and have higher coefficients of determination than the equations that only depend on D_{50} or C_u, as proposed in some previous studies, see Table 6.

- A correlation between the maximum and minimum void ratios of granular soils ($e_{max} = 1.52e_{min}$) was proposed.

- The proposed correlations are valid for granular soils with the parameters D_{10}, D_{30} and D_{60} within the ranges (maximum and minimum values) presented in Table 4, and with a fines content of less than 10 %.

REFERENCES

[1] Miura, K., Maeda, K., Furukawa, M., Toki, S. 1998. Mechanical characteristics of sands with different primary properties. Soils and Foundations 38(4), 159-172. https://doi.org/10.3208/sandf.38.4_159

[2] Dyskin, A., Estrin, Y., Kanel, A., Pasternak, E. 2001. Toughening by fragmentation—How topology helps. Advanced Engineering Materials 3(1), 885-888. https://doi.org/10.1002/1527-2648(200111)3:11<885::AID-ADEM885>3.0.CO;2-P

[3] Nakata, Y., Kato, Y., Hyodo, M., Hyde, A., Murata, H. 2001. One-dimensional compression behaviour of uniformly graded sand related to single particle crushing strength. Soils and Foundations 41(2), 39-51. https://doi.org/10.3208/sandf.41.2_39

[4] Guimaraes, M. 2002. Crushed stone fines and ion removal from clay slurries—Fundamental studies. Georgia Institute of Technology: Ph.D. Thesis.

[5] Cho, G., Dodds, J., Santamarina, C. 2006. Particle shape effects on packing density, Stiffness, and Strength: Natural and Crushed Sands. Journal of Geotechnical and Geoenvironmental Engineering 132(5), 591-602. https://doi.org/10.1061/(ASCE)1090-0241(2006)132:5(591)

[6] Shimboe, S., Moreto, N. 1995. A new classification for sand liquefaction. 1st International Conference of Earthquake Geotechnical Engineering, Tokyo, pp. 315-320.

[7] Cubrinovski, M., Ishihara, K. 2002. Maximum and minimum void ratio characteristics of sands. Soils and Foundations 42(6), 65-78. https://doi.org/10.3208/sandf.42.6_65.

[8] Norris, G. 1980. Shape and surface roughness effects on maximum and minimum void ratios of sand. Proceedings of the Eighteenth Annual Engineering Geology and Soils Engineering Symposium. Idaho, pp. 187-197.

[9] Edil, T., Krizek, R., Zelasko, J. 1975. Effect of grain characteristics on packing of quartziferous sands. Proceedings of the Istanbul Conference on Soil Mechanics and Foundation Engineering. pp. 46-54.

[10] Panayiotopoulos, K. 1989. Packing of Sands - A Review. Soil & Tillage Research 13(2), 101-121. https://doi.org/10.1016/0167-1987(89)90085-8

[11] Yang, Z. 2013. Study of the minimum void ratio for soils with a range of grain-size distributions. University of Massachusetts Amherst: Master Thesis.

[12] Holtz, R., Kovacs, W. 1981. An Introduction to Geotechnical Engineering. Prentice Hall, Englewood Cliffs, New Jersey.

[13] Lade, P., Liggio, C., Yamamuro, J. 1998. Effects of nonplastic fines on minimum and maximum void ratios of sand. Geotechnical Testing Journal 21(4), 336-347. https://doi.org/10.1520/GTJ11373J

[14] Das, B., Sivakugan, N., Atalar, C. 2012. Maximum and minimum void ratios and median grain size of granular soils: their importance and correlations with material properties. 3rd International Conference on New Developments in Soil Mechanics and Geotechnical Engineering, pp. 37-54.

[15] Youd, T. 1973. Factors controlling maximum and minimum densities of sands. Evaluation of Relative Density and Its Role in Geotechnical Projects Involving Cohesionless soils, ASTM, STP 523, 98-112. https://doi.org/10.1520/STP37866S

[16] Zheng, J. Hryciw, R. 2016. Index Void Ratios of Sands from Their Intrinsic Properties. Journal of Geotechnical and Geoenvironmental Engineering 142(12), 06016019-1-10. https://doi.org/10.1061/(ASCE)GT.1943-5606.0001575

[17] Åberg, B. 1992. Void ratio of noncohesive soils and similar materials. Journal of Geotechnical Engineering 118(9), 1315-1334. https://doi.org/10.1061/(ASCE)0733-9410(1992)118:9(1315)

[18] Patra, C., Sivakugan, N., Das, B., Rout, S. 2010. Correlations for relative density of clean sand with median grain size and compaction energy. International Journal of Geotechnical Engineering 4(2), 195-203. https://doi.org/10.3328/IJGE.2010.04.02.195-203

[19] Riquelme, J., Dorador, L. 2014. Metodología para determinar densidades máxima y mínima en suelos granulares gruesos a partir de ensayos de laboratorio de escala reducida. VII congreso chileno de ingeniería geotécnica, pp. 1-11.

[20] Patra, C., Sivakugan, N., Das, B. 2010. Relative density and mean grain-size correlations from laboratory compaction tests on granular soil. International Journal of Geotechnical Engineering 4(1), 55-62. https://doi.org/10.3328/IJGE.2010.04.01.55-62

[21] Cubrinovski, M., Ishihara, K. 1999. Empirical correlations between SPT N-values and relative density of sandy soils. Soils and Foundations 39(5), 61-71. https://doi.org/10.3208/sandf.39.5_61

[22] Alvarado, R. 2010. Análisis experimental de las metodologías de curvas homotéticas y corte en la evaluación de propiedades geotécnicas de suelos gruesos. Universidad de Chile: Master Thesis.

[23] Miura, K., Maeda, K., Furukawa, M., Toki, S. 1997. Physical characteristics of sands with different primary properties. Soils and Foundations 37(3), 53-64. https://doi.org/10.3208/sandf.37.3_53

[24] Santamarina, J., Cho, G. 2004. Soil behaviour: the role of particle shape. Advances in geotechnical engineering: The Skempton conference, pp. 604-617.

[25] Shen, C. Liu, S. Xu, S. Wang, L. 2019. Rapid estimation of maximum and minimum void ratios of granular soils. Acta Geotechnica 14(4), 991–1001. https://doi.org/10.1007/s11440-018-0714-x

[26] Moreno, N. 2014. Zonificación geotecnica de los suelos en Barranquilla. Twelfth LACCEI Latin American and Caribbean Conference for Engineering and Technology, pp 1-9.

[27] Salgado, R., Bandini, P., Karim, A. 2000. Shear strength and stiffness of silty sand. Journal of Geotechnical and Geoenvironmental Engineering 126(5), 451-462. https://doi.org/10.1061/(ASCE)1090-0241(2000)126:5(451)

[28] Kokusho, T. 2000. Correlation of pore-pressure B-value with P-wave velocity and poisson's ratio for imperfectply satured sand or gravel. Soils and Foundations 40(4), 95-102. https://doi.org/10.3208/sandf.40.4_95

[29] Wichtmann, T. 2005. Explicit accumulation model for non-cohesive soils under cyclic loading, Ruhr-Universität Bochum: PhD Thesis, pp. 1-288.

[30] Simoni, A., Houlsby, G. 2006. The Direct Shear Strength and Dilatancy of Sand–gravel Mixtures. Geotechnical and geological engineering 24(3), 523-549. https://doi.org/10.1007/s10706-004-5832-6

[31] Bandini, P., Salthiskumar, S. 2009. Effects of silt content and void ratio on the saturated hydraulic conductivity and compressibility of sand-silt mixtures. Journal of Geotechnical and Geoenvironmental Engineering 135(12), 1976-1980. https://doi.org/10.1061/(ASCE)GT.1943-5606.0000177

[32] Arab, A., Sadek, M. Belkhatir, M., Shahrour, I. 2014. Monotonic Preloading Effect on the Liquefaction Resistance of Chlef Silty Sand: a Laboratory Study. Arabian Journal for Science and Engineering 39(2), 685-694. https://doi.org/10.1007/s13369-013-0700-4

[33] Bablu, K., Maheshwari, B. 2013. Effects of silt content on dynamic properties of solani sand. Seventh International Conference on Case Histories in Geotechnical Engineering, pp. 1-7.

[34] Mahmoudi, Y., Cherif, T., Belkhatir, M., Arab, A., Schanz, T. 2014. Influence of the equivalent intergranular void ratio on shear strength of sand-silt mixtures. Colloque International: Caractérisation et Modélisation des Matériaux et Structures, pp. 1-18.

[35] Bensoula, M., Missoum, H., Bendani, K. 2015. Critical undrained shear strength of loose-medium sand-silt mixtures under monotonic loadings. Journal of Theoretical and Applied Mechanics 53(2), 331-344. https://doi.org/10.15632/jtam-pl.53.2.331.

[36] Fuentes, W., Gil, M., Duque, J. 2019. Dynamic simulation of the sudden stettlement of a mine waste dump under earthquake loading. International Journal of Mining, Reclamation and Environment 33(6), 425-443. https://doi.org/10.1080/17480930.2018.1483703

[37] Pham, H., Van-Impe, P., Van-Impe, W., Mengé, P., Cnudde, V., Haegeman, W. 2017. Effects of particle characteristics on the shear strength of calcareous sand. Acta Geotechnica Slovenica 14(2), 76-89.

DETERMINING THE PILE BEARING CAPACITY USE OF PDA TEST RESULTS AND NEURAL NETWORKS

DOLOČANJE NOSILNOSTI PILOTOV Z UPORABO REZULTATOV PDA PREIZKUSOV IN NEVRONSKIH MREŽ

Saeed Ghaffarpour Jahromi *(corresponding author)*
Shahid Rajaee teacher training university,
Department of civil engineering
Tehran, Iran
E-mail: saeed_ghf@sru.ac.ir

Mohammad Sharafuddin
Pouyandegan Danesh institution of higher education,
Geotechnical engineering
Chalus, Iran

DOI https://doi.org/10.18690/actageotechslov.17.2.34-45.2020

Keywords

pile, bearing capacity, PDA data, artificial neural network, sensitivity analysis

Ključne besede

pilot, nosilnost, PDA podatki, umetna nevronska mreža, analiza občutljivosti

Abstract

The dynamic loading or PDA test is one of the on-site experiments to estimate the bearing capacity of a pile. This test is based on the wave-propagation theory and can provide a good estimate of the bearing capacity of a pile as well as an assessment of the health of the pile. In this research, using the results of 100 dynamic loading tests carried out with different piles and projects, three types of artificial neural network (ANN) have been used to estimate the load. Initially, the perceptron multi-layer neural network was one of the most used neural networks. Subsequently, the neuro-fuzzy network is used in a combination of neuro-fuzzy networks and, at the end of the radial-based neural network, a successful network was used for non-linear problems. Between the different models of the neural network used by researchers, the multi-layered perceptron network has a better performance. However, other networks used have also proven successful. Finally, different models of the neural networks were compared and the network that has the best performance was identified in both phases. The models based on neural networks, unlike conventional behavioral models, do not explain how the input parameters affect the output. In this research, by analyzing the sensitivity to the optimal structure of the introduced models in each step, we have tried to partly answer this question. Also, the extraction

Izvleček

Dinamični obremenitveni ali PDA preizkus je eden od terenskih preizkusov za oceno nosilnosti pilotov. Ta preizkus temelji na teoriji širjenja valov in lahko zagotovi dobro oceno nosilnosti pilota ter oceno stanja izvedenega pilota. V predstavljeni raziskavi so na podlagi rezultatov 100 preizkusov dinamične obremenitve, izvedenih na različnimi pilotih in projektih, za oceno obremenitve bile uporabljene tri vrste umetnih nevronskih mrež (ANN). Sprva je bila uporabljena večslojna nevronska mreža perceptron, ki je ena najpogosteje uporabljenih nevronskih mrež. Nato se je uporabilo nevro-mehko omrežje kot kombinacija nevro-mehkih omrežji in konca radialne nevronske mreže. Slednje kombinirano omrežje se je uspešno uporabilo za nelinearne probleme. Med različnimi modeli nevronske mreže, ki jih uporabljajo raziskovalci, daje večplastna mreža perceptron najboljše rezultate. Vendar so se tudi druga uporabljena omrežja izkazala za uspešna. Na koncu so primerjani različni modeli nevronskih mrež ter ugotovljena tista, ki ima najboljše rezultate v obeh fazah. Modeli, ki temeljijo na nevronskih mrežah, za razliko od običajnih vedenjskih modelov ne pojasnijo, kako vhodni parametri vplivajo na izhodne vrednosti. V tej raziskavi so z analizo občutljivosti na optimalno strukturo uvedenih modelov v vsakem koraku poskušali delno odgovoriti na to vprašanje.

and presentation of the relations governing a neural network model to the user is more reliable in the use of such models, which facilitates the application of such models in engineering works. In this research, four first indicators were used to evaluate and compare the models and structures.

Tudi pridobivanje in predstavitev odnosov, ki urejajo model nevronske mreže, je uporabniku bolj zanesljivo pri uporabi takšnih modelov, kar olajša uporabo takšnih modelov v inženirskih problemih. V tej raziskavi so bili za oceno in primerjavo modelov in struktur uporabljeni prvi štirje kazalniki.

1 INTRODUCTION

Structures consist of several components that are important for the lower and the most part of the other components. The piles are among the components that are responsible for connecting the structure and transferring the structure's load to the ground. In recent years, due to the heavy use of high-rise structures such as telecommunications and commercial and residential towers, marine structures, bridges and increased forces, as well as for the transfer of loads from the pavement to the hard layers, the use of deep pile foundations in projects, various development projects, especially coastal and offshore structures, have increased considerably and are often an integral part of the project. The lack of proper soil load in loose soils to construct various structures has inevitably led to the use of different types of piers (pile), and the main concern in this regard is to reach the required load capacity in these structures. Static and dynamic tests are the only way to ensure that the bearings are in the pile. Having sufficient information about the behavior and performance of the pile, including the bearing capacity of the pile, is very important, especially since the loads are often a kind of dynamic load, including earthquakes, winds, and sea waves. There are various methods, including empirical, analytical and in-situ tests, to estimate the pile bearing's bearing capacity. A proper estimation of the deep bearing capacity in construction projects, and in particular the design of offshore platforms, is of particular importance and a significant contribution to the safety and security of such structures is realized. The recognition and understanding of the behavior of a candle under dynamic loads is a significant contribution to ensuring that the lack of accurate information and the use of empirical relationships lead to the use of high reliability coefficients, results in high costs, which involves the use of a statistical method and the optimization of data using artificial intelligence, such as a genetic algorithm can play an effective role in predicting and estimating the bearing capacity of a candle under a dynamic load.

Recent advances in the design of deep foundations indicate that a candle is not required to maintain the general foundation stability and is also used as a dimming element. The design and implementation of deep foundations are often performed in a series of candles of equal length and diameter, symmetrical, which facilitates the installation and implementation of the pile, as well as the simplicity of the methods for analyzing and designing candles of the same length and diameter [1].The most famous method for analyzing this group of candles is the method of the coefficient of interaction introduced by Paulus in 1968 and the analytical method introduced by Randolph and Worth in 1979 [2]. Similarly, in the transfer method, which was proposed by various researchers, the interaction between the frictional strength of the wall and the pile bearing load is considered separately, and it is also considered necessary for the application of it to assume equal and uniform lengths [3 and 4]. Under these conditions, even with the change in the geometry and the location of the pile, a pile of the same length and diameter in terms of the degree of hardness of the group (load ratio to the summit of the pile group) and differential warhead meeting (difference between the maximum and minimum seals) have the best performance and performance will not be possible. Many improvements in numerical optimization were made in recent years and are widely used in various civil-engineering sciences, such as transportation, bridge design and the design of various structures and deep foundation optimization. A recent example is the use of depth-optimized optimization by Kim et al. (2002), which attempted to optimize the carrying capacity of a pile-type warhead by changing the geometric characteristics of the group, such as the thickness of the cap, the cross-section and the position of the piles [5]. Bilvikius et al. (2011) tried to optimize a pile group connected by interconnected beams for the location of the piles [6]. In this research, a genetic algorithm and an optimization algorithm were used locally and randomly. Since the optimization of the location of the spray locus has both local and non-local optimal points, in order to achieve the optimal overall condition in the pile group, the genetic algorithm showed the best-possible performance among the mentioned algorithms. Momeni et al. (2014) tried to combine the genetic algorithm with the artificial neural network and predicted the carrying capacity of prefabricated concrete piles. In this research, data from the PDA test data were used on 50 candles samples. The input variables include the geometric properties of the pile (section and length), the hammer's weight and the

height of the fall, and the objective function is the capacity of the compressive bearing load of the pile. After optimization it became known that the hammer weight and the geometric characteristics of the piles had the most effect on the results of the sensitivity testing [7]. Manifestations et al. (2014), using multi-layer artificial neural network (MLP), attempted to predict the load capacity of sandstone-based pile-type piles. In the study, open-ended metal tube tubes were used. The length and diameter of the pile, the modulus of elasticity and the internal friction angle of the soil were defined as the input and bearing capacity of the pile as the output. In this study, it was determined that the neural network is very efficient in predicting the results. Also, according to the sensitivity analysis, it was determined that the soil's soil friction angle, soil elastic modulus, pile diameter and candle length had the highest effect on the bearing capacity of the piles [8]. Although the use of different lengths of candles is not common in practice, the use of this theory in the design of deep foundations of large projects has a history in which they aim to enhance the performance of the candle group by changing the geometry of the piles [9]. Chavo et al. tried to use optimization to minimize the difference in the meeting of the flap group with a flexible cap and also to minimize the power difference in the rigid pile group. The results showed that in the same type of pile with a flexible cap, the central pylons had higher concentrations than the periphery of the group, while with a rigid cap, less force was transmitted through the middle pile due to the interaction of the pile and the soil. The differential meeting and the difference in the contribution of the piles to the group can be reduced by using a longer cylinder in the center [10]. The researcher and his colleagues also found that the group's candles should have an uneven length [11].

Many deep-seated optimization researches are based on the so-called slope-reduction methods, which have limited variables and must be differentiated in mathematical relationships. In these methods, the discontinuous variables are not applicable. In this paper, an automatic optimization method based on a genetic algorithm is introduced to optimize the bearing capacity of a deep foundation. Since the variables in this category of engineering issues are diverse and discontinuous, the use of genetic algorithms in the optimization can be useful. Another field method in estimating the bearing capacity of a pile is to evaluate the impact of the hammer with a hammer. In most analytical and empirical methods, the prediction of the load-bearing capacity based on experience is verified using the static loading test of a candle [12]. Although the static loading test has many abilities, it has several disadvantages, including being non-economic and time consuming. Another approach that has been developed in recent decades to evaluate analytical and empirical methods in the pivot bearing capacity of the pile can be referred to as the dynamic testing of a pile or PDA. These relationships have many disadvantages, such as failure to simulate the impact. In the meantime, high-strain testing (HSDPT) by combining the wave equation method has shown good performance in predicting the bearing capacity of a candle [13, 14].

Kordjezi and Pooyanejad [15] used a machine-learning method called the support vector machine (SVM) to predict the ultimate bearing capacity of piles under the influence of an axial load. Maizir and Kassin [16] used the collected data from approximately 300 projects in Indonesia and Malaysia for the training and testing of artificial neural networks to predict the axial bearing capacity of the slamming piles for the various pile characteristics and the results of the slamming pile data analysis (PDA). McVay et al. [17] researched on pile/shaft design using an artificial neural network using the genetic algorithm method (genetic programming) using Florida data and information based on the bearing capacity of the piles (the wall and tip resistance of the pile), the internal friction angle (ϕ) and the extraction SPT number of the boreholes.

Although much research has been done on the bearing capacity of piles, there is a serious lack of candle bearing capacity. In this research, by selecting two types of used piles in the construction of offshore and offshore marine platforms, including tubular metal piles and pre-made concrete piles, the axial load-bearing capacity of the pile was assessed by modeling in Plaxis 2D finite-element software under harmonic load in a layer of soil. The pile driving analyzer (PDA) data from a case study of a project was compared. The results of more than 100 numerical analyzes were optimized using a genetic algorithm, which resulted in an estimation of the relationship but with high accuracy in the axial load-bearing capacity of the pile by separating the concrete and metal piles. This relationship has the least amount of mean square error (MSE) compared to the input data. One of the most important innovations of this paper is the use of PDA test results to predict the pile bearing capacity. In this study, comparing different methods of assessing the capacity of a candle bearing indicates the fact that most empirical methods provide a much larger load capacity than other methods.

2 BEARING CAPACITY OF PILE

There are several methods for estimating the axial load of a pile, which include analytical methods, pile knuckle-based methods, on-site testing methods, dynamic wave

propagation (PDA) techniques, and static loading of the pile. Each of these methods has limitations and sometimes does not require precision. Analytical methods are the simplest method based on the physical and mechanical properties of the soil and the geometry of the pile, i.e., the length, diameter and section of the pile in the axial bearing of the pile (compression and tensile strength), by various researchers, such as Vasic, Meyerhof, and Costello, have been developed. Costello and his colleagues examined twenty-four piles for the piles' bearing capacity in sandy soil in accordance with equation (1):

$$Q_{ult} = q' N_q^* A_p + \sum p \, \Delta l (k \sigma_{v'} tan\delta) \qquad (1)$$

In this regard, the geometric properties of the pile, such as the section, diameter and length of the pile, as well as the mechanical properties of the soil, such as adhesion, internal friction of the soil and specific gravity, are effective in the estimation of the bearing capacity. This relationship is strongly influenced by the mechanical properties of the soil, and inadequate soil specification can affect the estimation of the load capacity [18].

Researchers and geotechnical operators have always been concerned about the costly and time-consuming process of static loading, and the precise, cheap and fast replacement of it. From the beginning of the history of candles, there is the idea that static bearing could be determined on the basis of the behavior of the candles during a knock, but before the 1950s there was no scientific theorizing. In the 1950s, based on the theory of longitudinal wave propagation in a candle, a numerical solution was proposed for modeling the behavior of a hammer, a candle and a soil, which has since been recognized as the analysis of wave-wave equation (WEAP). The propagation of a longitudinal wave in a candle with the aim of calculating the bearing capacity of a candle as a type of loading method ultimately led to the introduction of a dynamic analysis of the pile or the PDA method. A PDA test also suggests high strain dynamical testing (HSDPT) [14].

One of the famous methods for determining the bearing of a candle is Hayley's relationship, based on the amount of penetration and the impact of a candle under hammer blows, which has been evaluated by various researchers. Precedent and the factor using Haley's relationship theory and some experiments in Iran, evaluated the sensitivity of this method to different soil parameters [19]. Also, Kahanian et al. (2006) examined the accuracy of the PDA test in comparison with the results of dynamic and static loading tests in a Bandar Abbas project and a 150,000-ton quay of the Imam Khomeini port, which had a relatively limited technical background and support for consultants and contractors active in the field of marine and inland offshore piles is in the dynamic loading test [20].

Another study by Hosininya et al. (2006) described the dynamics of the PDA and its results in controlling the activity of piling, health checking and determining the load capacity [21]. Fakharian and Hosseinzadeh Attar (2010) examined the results of static compression loading and the results of a dynamic pilot experiment (PDA) on a few pile piles that were implemented in a project at the port of Mahshahr. The results of this study showed that there is a good agreement between the final static bearing capacity obtained from the candle dynamics experiment with what the static loading pressure test is proposing. Of course, the condition of this consistency is the correct test, especially the pile dynamics experiment, which requires a lot of experience and expertise. In this study, the evaluation of static and dynamic piles' tests was reported in a large industrial project with an optimization approach, a case study in Mahshahr's special economic zone [22]. Fakhariyan and Hosseinzadeh, in another study (2011), evaluated the use of the PDA test data in carrying steel tubes executed at the Chabahar port pier [23]. Nejadqomi and his colleague (2013) compared the actual data of the seven pile metal castable in the South Pars region, which were tested by the PDA, with the results of the knock-out relationships. The purpose of this study was to find the most suitable coupling relationship for estimating the bearing capacity of the piles in that area, which could be very promising. [24]. An investigation of the above research shows that there is still uncertainty in the analysis and design of the pile using the PDA method. In this regard, it is necessary to evaluate and analyze the sensitivity of various parameters, which is used in this study using the neural network method.

3 DATABASE

In this research, the results of 100 PDA experiments that were carried out in various piles and projects were used by Raumar Research Institute Consulting Engineers. These results were from projects in the south of the country at the Mahshahr petrochemical site and the Assaluyeh area, with the characteristics of its sub layers, as in Table 1. Considering the factors affecting the bearing capacity of the pile, the input variables, including internal friction angle (φ), soil elastic modulus (E), pile diameter (D) and pile length (L), were considered and the bearing capacity of the pile as a parameter output is considered. An example of the input data used in the neural network is presented in Table 2.

Table 1. Geotechnical parameters of hypothetical subsurface layers.

Layer depth	m	0-5	5-15	15-25	>25
Soil type	—	Fine grained (CL, ML)	Fine grained (CL, ML)	Fine grained and somewhat sandy (CL, ML)	Fine grained and somewhat sandy (CL, ML)
Undrained cohesion	kPa	20 ~ 30	30 ~ 40	40 ~ 50	50 ~ 80
Drain cohesion	kPa	5 ~ 10	10 ~ 20	20 ~ 30	40 ~ 50
Undrain internal friction angle	°	2 ~ 4	6 ~ 8	12 ~ 16	22 ~ 25
Drain internal friction angle	°	10 ~ 12	16 ~ 18	20 ~ 24	28 ~ 32
Dry density	g/cm^3	1.55 ~ 1.60	1.60 ~ 1.65	1.70 ~ 1.75	1.80 ~ 1.85
Poisson's ratio	—	0.38 ~ 0.42	0.35 ~ 0.40	0.32~ 0.34	0.30 ~ 0.33
Elastic modules	MPa	5 ~ 8	8 ~ 12	20 ~ 30	40 ~ 60

Table 2. Example of an input database.

Test site	Input variable				Output variable
	Diameter (m)	Length (m)	φ (°)	E (MPa)	Q_{all} (kN)
Mahshahr Petrochemical	0.5	10	33	12	1500
	0.5	10	33	15	1800
	0.5	15	22	18	2000
	0.5	15	22	12	2200
	0.8	20	25	30	2500
	0.8	20	25	35	2700
Pars Petrochemical	0.4	10	28	15	1500
	0.4	10	28	15	1800
	0.4	15	20	18	2000
	0.6	15	20	20	2200
	0.6	20	23	22	2500
	0.6	20	23	25	2700
	1.0	25	28	50	2820

4 IMPLEMENTING NEURAL NETWORK MODELS

In order to use the neural network in the prediction stages of this research, three types of neural networks were used, which include perceptron multi-layer networks, neuro-fuzzy networks and radial-base grid functions. Given the factors affecting the PDA test, as well as the available data from the laboratory and field results performed at the site, the input variables were selected. Of course, the fact that input parameters are obtained from the results of typical geotechnical tests also has a significant role in selecting the input variable. At this stage, networks with four input variables were obtained, which are obtained from the physical and mechanical properties of the soil. These variables are estimated from direct and triangular cutting or standard field penetration testing (SPT). Soil physical properties, as primary indicators, can provide a general view of the status of subsurface layers, the most important of which are specific germination and specific gravity. The soil's mechanical properties also provide an appropriate assessment of the soil behavior, including the internal friction angle, adhesion, and modulus of elasticity.

Also, the results of the standard penetration test (SPT), which is one of the most common on-site experiments to determine the physical and mechanical properties of the soil, can also be used to express the soil properties because the results of this test are available in most geotechnical reports. The soil's elastic modulus derived from the SPT data as input variable is also used. The pump bearing capacity is presented as the only output variable in this modeling. The limits of the input and output parameter changes are presented in Table 3.

Table 3. Range of the variations of input and output parameters.

Range of variation	Input variable				Output variable
	Diameter (m)	Length (m)	φ (°)	E (MPa)	Q_{all} (kN)
Minimum	0.5	10	33	12	1500
Maximum	0.4	10	28	15	1500

5 STRUCTURE OF THE NEURAL NETWORK MODEL

The basic structure of an ANN consists of artificial neurons (similar to biological neurons in the human brain) that are grouped into layers. The most common ANN structure consists of an input layer, one or more hidden layers and an output layer. A modified simple model of an artificial neuron is shown in Figure 1. In this section, the architecture of the used neural networks is described, including multi-layer perceptron, neoprene, and radial basis function. The multilayered lacquered perceptron network is generally composed of three layers of input, hiding, and output. In this research, the multilayered perceptron network (MLP) has four inputs and one output. The number of layers and intermediate neurons are suitably chosen, so that the structure is presented with a hidden layer and two hidden layers, respectively, for both models. Neuro-fusion networks are one of the most widely used neural networks, which have a very high ability to solve non-linear problems. The neo-fossil networks are composed of input layers, fuzzy rules, and output layers that are present in the graphics environment of the Matlab 6 toolbox. In this research, the neo-fuzzy network (NF) is used and the network structure is like the multilayer perceptron network. The grid radial basis function is a special mode of post back transmission network. Each unit in the hidden layer uses a radial base function (like a Gaussian kernel) as the activation function, while the output units use the same function as the activation function [25]. In this research, the grid radial function network (RBF) is used, and the grid structure is similar to the perceptron multi-layer network (Table 4 and 5).

Table 4. MLP network structure evaluation index with two hidden layers having different numbers of neurons.

Num. of hidden Neurons in layer 1	Num. of hidden Neurons in layer 2	R	RMSE	MAE	MAXAE	SDAE	SSE
Validation Subset							
5	5	0.60	0.13	0.098	0.63	0.10	3.91
5	8	0.75	0.12	0.090	0.44	0.086	3.0
8	8	0.89	0.085	0.056	0.48	0.065	1.5
8	11	0.82	0.098	0.075	0.31	0.068	2.0
11	11	0.83	0.10	0.076	0.40	0.084	2.35
11	15	0.93	0.072	0.051	0.27	0.064	1.08
15	15	0.88	0.097	0.065	0.50	0.073	1.95
15	20	0.86	0.083	0.046	0.56	0.077	1.46
20	20	0.94	0.061	0.033	0.37	0.056	0.75
20	25	0.96	0.048	0.033	0.15	0.055	0.48
25	25	0.97	0.046	0.032	0.16	0.056	0.44
Training Subset							
8	8	0.96	0.054	0.037	0.32	0.051	2.65
11	15	0.96	0.060	0.039	0.39	0.045	3.5
15	15	0.98	0.046	0.029	0.30	0.035	2.11
20	20	0.99	0.022	0.007	0.27	0.021	0.48
25	25	0.99	0.029	0.010	0.34	0.024	0.82
Testing Subset							
8	8	0.80	0.099	0.065	0.48	0.085	2.12
11	15	0.88	0.082	0.059	0.27	0.070	1.42
15	15	0.93	0.071	0.049	0.28	0.057	1.11
20	20	0.96	0.055	0.033	0.21	0.045	0.64
25	25	0.95	0.063	0.039	0.27	0.055	0.85

Table 5. Comparison between the optimal structures of the MLP network.

Networks	Num. of neurons		R	RMSE	MAE	MAXAE	SDAE	SSE
Validation Subset								
MLP1-1	15		0.93	0.067	0.050	0.20	0.049	0.99
	20		0.92	0.072	0.055	0.31	0.045	1.1
	30		0.89	0.080	0.055	0.46	0.058	1.4
MLP1-2	20	20	0.94	0.061	0.033	0.37	0.056	0.75
	25	25	0.97	0.046	0.032	0.16	0.056	0.44
Training Subset								
MLP1-1	15		0.97	0.056	0.039	0.38	0.045	3.1
	20	0.96	0.055	0.036	0.36	0.043	3.1	
	30	0.95	0.056	0.037	0.35	0.051	3.2	
MLP1-2	20	20	0.99	0.022	0.007	0.27	0.021	0.48
	25	25	0.99	0.029	0.010	0.34	0.024	0.82
Testing Subset								
MLP1-1	15		0.91	0.079	0.055	0.22	0.056	1.3
	20		0.90	0.080	0.057	0.30	0.057	1.35
	30		0.87	0.081	0.060	0.27	0.059	1.4
MLP1-2	20	20	0.96	0.055	0.033	0.21	0.045	0.64
	25	25	0.95	0.063	0.039	0.27	0.055	0.85

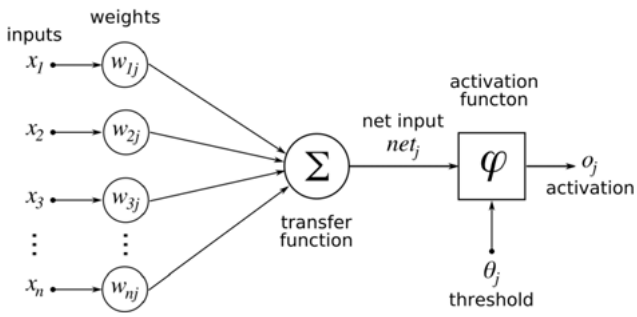

Figure 1. The artificial neuron.

6 EVALUATION INDICATORS OF NEURAL NETWORK MODELS

In order to evaluate the efficiency of the used neural network models, we need indicators that can judge and evaluate the function of the models in comparison with the data set and the empirical results. Therefore, different statistical indices are used to evaluate the models and, finally, to compare their efficiency. These statistical indicators are presented below. The correlation coefficient (R), which defines the relationship between the two variables, x and y, is defined as follows [26]:

$$R = \frac{\Sigma(x\text{-}\bar{x})(y\text{-}\bar{y})}{\sqrt{\Sigma(x\text{-}\bar{x})^2\Sigma(y\text{-}\bar{y})^2}} \qquad (2)$$

In this regard, the means of the variables x and y are the sum of the data. The high values of this coefficient indicate a strong correlation between the variables in the two sets of data, and in contrast to the low correlation coefficient, the weak correlation or non-relationship between the two sets. Smith (1986) proposed the following range for the correlation coefficient between zero and one [27].

$\|R\|\geq 0.8$	Strong correlation
$0.2<\|R\|<0.8$	Existence of correlation
$\|R\|<0.2$	Lack of correlation

In this research, the correlation coefficient was used to evaluate the correlation of the responses obtained from multi-layered network perceptron models. The mean magnitude error (MAE) represents the average error in the desired set. This indicator is expressed with the following equation.

$$MAE = \frac{1}{N}\sum_{i=1}^{N}|E_i| \qquad (3)$$

An average square error (RMSE) represents the mean error value, the difference between the values obtained from the experiments and the models, with the difference being that it focuses on large errors, as expressed below [26].

$$RMSE = \sqrt{\frac{1}{N}\sum_{i=1}^{N}\left(E_i\right)^2} \qquad (4)$$

The maximum magnitude of error (MAXAE) represents the maximum error that occurs in the desired set and is determined as follows:

$$MAXAE = Max(|E_i|) \qquad (5)$$

The total Squared Error (SSE), which represents the sum of the squares of the set error, and is defined as:

$$SSE = \sum_{i=1}^{N} (E_i)^2 \qquad (6)$$

SDAE indicates the magnitude of the dispersion of the magnitude of the error associated with the MAE. Obviously, the lower this index, the model error in the whole set is closer to the average value and the model shows a more stable behavior. In this research, four first indicators were used to evaluate and compare the models and structures. SDAE was also presented as a statistical indicator of different models and structures and has been considered in the secondary assessment.

7 PROCESSING OF NEURAL NETWORK DATA

The data needed for the network training was obtained from laboratory and field experiments. In this research, PDA testing results with a capacity of between 50 and 400 tons were used. Given the drilling of bores at the test site, the input data is selected from geotechnical reports. The number of data used in the prediction stage was 100 data, according to the PDA test charts.

8 IMPLEMENTATION OF NEURAL NETWORKS, TRAINING AND STOP

To implement the neural networks, training and evaluation of them from the neural network toolbox is used in the MATLAB (2013a) software. This software has been of great interest to researchers in the light of numerous functions, programming capabilities, educational algorithms and multiple structures for neural networks and the power of processing and statistical analysis in solving engineering problems. As mentioned above, a two-layer or three-layer perceptron network with different inputs in this research has been used for the prediction, and according to the capabilities, the ML method is used. In this research, the coefficients of the method including μ and β are considered to be 0.011 and 0.01, respectively, for the default values in the MATLAB software, respectively. Cross-validation is used to increase the power of the network generalization to stop the learning. In this regard, the database is divided into three educational,

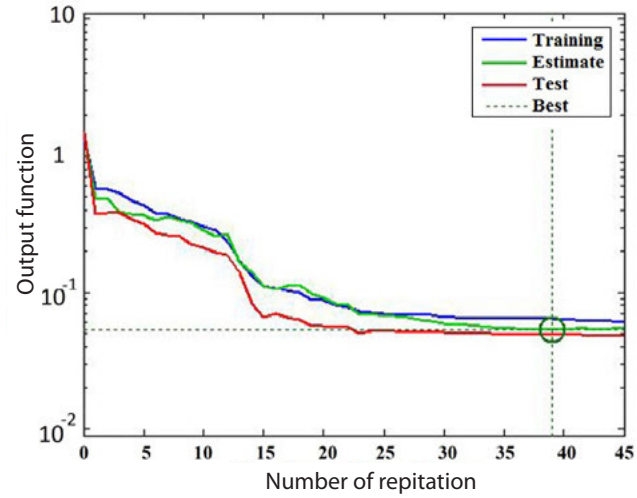

Figure 2. Layered perceptron network learning with hidden layer and 11 neurons.

evaluation and experimental sets, and all the evaluation indicators are used to determine the efficiency and accuracy of the network. In this regard, there are 70 data for the training, 15 data for the evaluation set and 15 data for the experimental set. Figure 2 shows the curve for a perceptron multi-layered network with a hidden layer. After training, the weights are stored and the network is ready. As active functions in the hidden layers, the hyperbolic tangent function and the sigmoid function for the output layer are used. Since the number of hidden-layer neurons plays a major role in the network behavior, the study of the performance of these networks was done with a number of different neurons.

Neuro-Fractional Network - The learning algorithm in MATLAB software (ANFIS) involves a fuzzy system using the post-error learning process. In the same system as the neural network, the inputs enter the input membership functions and, after passing through the membership functions of the output, the output of the

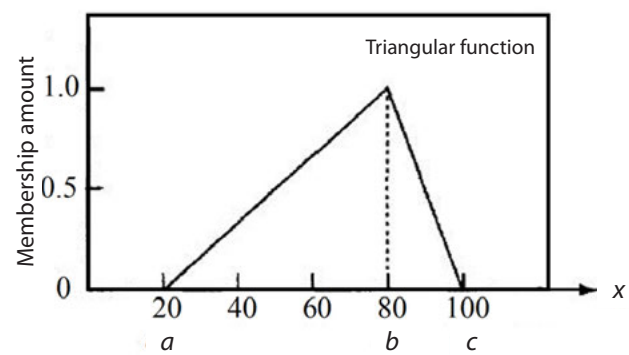

Figure 3. Triangular membership function.

network is generated. In this research, the best use is made in using the triangular membership function with relation 10 in the input layer. Figure 3 shows this membership function [25].

$$\mu(x, a, b, c) = \max\left(\min\left(\frac{x-a}{b-a}, \frac{c-x}{c-b}\right), 0\right),$$
$$a \neq b \text{ and } c \neq d \qquad (7)$$

The database used in this way is divided into two categories of training data and experimental data. There are 80 data in the training phase and 20 data for the testing. The evaluation indicators in this model are, like multi-layered perceptron model and neo-fuzzy network model, used for prediction. Figure 4 shows the training curve for the neuro-fuzzy network. After training, the weights are stored and the network is ready. In the first model, the network error indicators versus the training sets for the neo-Frazy network are shown in Table 6. All the networks have an acceptable performance. In this way, two networks with 2 and 3 input and output membership functions are selected.

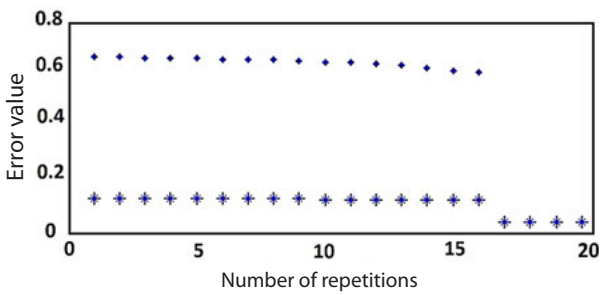

Figure 4. Neuro-fuzzy network learning curve with triangular membership function.

The network has a dual-core radial basis and is a special mode of post-transmission network. Each unit in the hidden layer uses a radial base function, such as a Gaussian node, as the activation function, while the output units use the same function as the activation function. The center of this radial base function (or core function) is determined by the weight vector of each unit, and the position and width of these cores should be learned from the training patterns.

The network implementation of the radial basis function is also used in the MATLAB toolbox. The hybrid learning algorithm in this model involves uncontrolled clustering using the least-squared mean (LMS), monitored to determine the bond weights between the layers and the output layers.

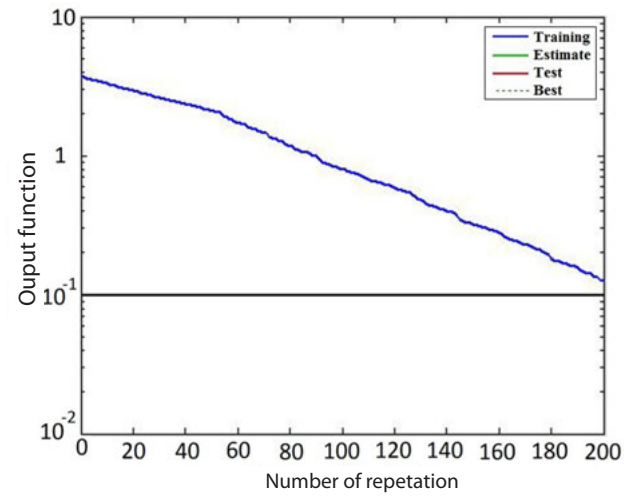

Figure 5. Grid training curve of the radial basis function.

Table 6. Comparison of error indicators in the neural network models.

Collection	Type of network	Total square error	Standard deviation module error	Maximum module error	Average module error	Root mean square error	Correlation coefficient	Number of neurons
Estimates	Multi-layer perceptron	0.75	0.75	0.37	0.033	0.061	0.91	20 20
Education	Multi-layer perceptron	0.48	0.021	0.27	0.007	0.022	0.84	20 20
	Neuro-fuzzy	2.5	0.055	0.55	0.042	0.050	0.88	3
	Radial basis function	1.1	0.027	0.32	0.018	0.033	0.88	250
Test	Multi-layer perceptron	1.35	0.045	0.30	0.057	0.080	0.81	20 20
	Neuro-fuzzy	3.7	0.065	0.50	0.065	0.080	0.82	3
	Radial basis function	1.8	0.053	0.46	0.042	0.072	0.84	250

In this research, the network of radial basis functions for the prediction phase was used. The evaluation indicators are for radial basis function models such as neuro-fuzzy networks. There are 80 data in the training phase and 20 data for the testing. In Figure 5, the educational curves for the grid are shown by the radial basis function.

9 COMPARISON OF THE EFFICIENCY OF NEURAL NETWORK MODELS

The efficiency of the optimal structures in all three models of the neural network is shown in Table 7 by comparing the error indices for the educational, experimental and evaluation sets. As the results show, the MLP network with the two hidden layers of 20 neurons has a better performance than the other three models. Therefore, the network is selected as the most successful model in predicting the PDA test results.

Table 7. Statistical analysis of absolute sensitivity to the desired input.

Input	Maximum	Minimum	Average	Standard deviation
Diameter	4.045	0.361	0.950	0.535
Length	3.201	-1.218	1.482	0.984
Internal friction	2.068	-11.78	-1.593	1.188
Modulus of elasticity	6.422	-17.34	-1.427	1.387

10 SENSITIVITY ANALYSIS

In order to evaluate the sensitivity, the final structure of the models consists of a double-layer neural network with 20 neurons and one output layer with a neuron. In this regard, the indeterminate analysis and sensitivity analysis on the model have been made to determine the efficiency and importance of the variables. The sensitivity of the output of the neural network is comparable to the inputs, similar to the regression method, with the derivative relative to the input to the desired input. In this research, due to the general structure of the behavioral models based on neural networks, part of the inputs are independent of the output, and the other part is the net output in the development or previous development. Therefore, in this research, the relative derivative of the output of the model is compared with the independent inputs. In this regard, the sensitivity analysis was performed on four inputs, including length, diameter, internal friction and soil elastic modulus. In this analysis, 200 data points in the four-dimensional space of the input parameters corresponding to the normal distribution function are selected using the Simlab 3.0 software.

For each of these points with the input values, the relative derivative values of the bearing capacity for the optimal structure in each step are calculated, and its statistical analysis is presented in Table 5. As expected, the relative derivative of each output is different in relation to each input (at the points of the input space). The negativity of

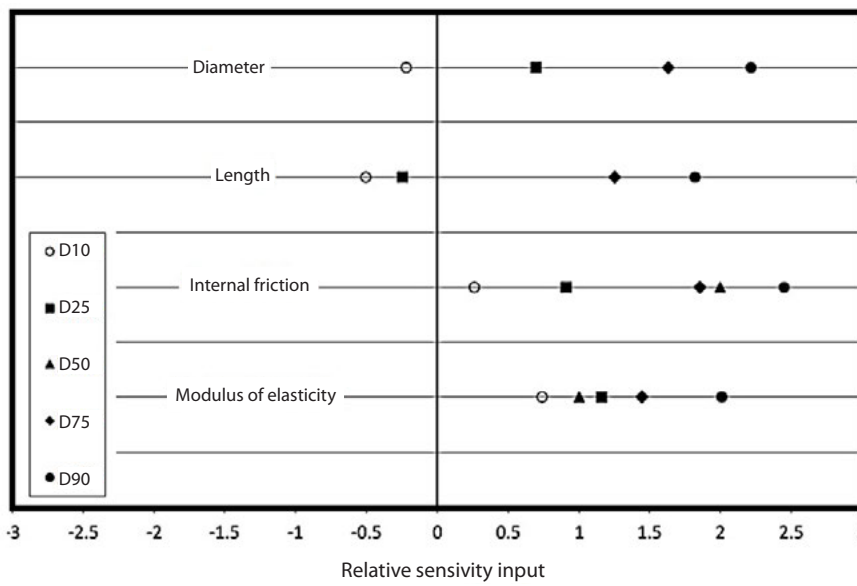

Figure 6. Neural network sensitivity analysis.

the sensitivity values in this table has a decreasing effect on the load-capacity parameter. To analyze and explain this change if the distribution of derived quantities is available in real time, this distribution can be compared with the real distribution and thus evaluate the model. But, due to the complexity of issues in geotechnical engineering, this distribution is not available.

Statistical values of the relative sensitivity of the load capacities versus the four inputs for the multi-layered perceptron network with 20 neurons in the hidden layer are shown in Figure 6. In the input variable length (L) this figure shows that there are more values of the relative sensitivity in this variable, but positive values account for an increase in the amount of bearing capacity due to the increase in the length of the candle. As Figure 6 shows, the other three input variables have the same relative sensitivity values, and this result shows the almost similar effect of these three variables on the bearing capacity of the candle.

11 CONCLUSION

In this research, three types of neural networks were used to predict and interpret the results of the PDA method in estimating the bearing capacity of the pile. These three types of neural networks include the perceptron multi-layer network, the neuro-fuzzy network, and the radial-base network. In this research, the parameters are available, including the length of the pile, the diameter of the pile, the modulus of the elasticity and the internal friction angle of the soil, and the pressure bearing of the pile is considered as an outlet. In a multi-layer perceptron network using a part of the database, the networking constituents of the models were trained with a quick training method, and, in contrast to another part of the database, was used to evaluate the predictability of the model. The evaluation method was also used to increase the power of the generalization of the neural networks. Two types of triangular and four-layered perceptron were used in this study. In their structure, the number of optimal hidden neurons was chosen. In this research, a variety of evaluation indices, including the correlation coefficient, mean square error, total square error, absolute error average, absolute error, and standard deviation of the magnitude error were used to evaluate the performance of the networks. Finally, the network with the best performance against the evaluation indicators was selected as the most successful network model. In total, by comparing the performance of different models of the perceptron network with the four input parameters and 15 neurons in the hidden layer as the most successful network in the prediction phase was introduced.

REFERENCES

[1] Mandolini, A., Laora, A. and Mascarucc, Y .2011. Rational Design of the Piled Raft. Proc. Int. conf. on Modern Building Materials, Structures and Techniques. Vilnius Gediminas Technical University, pp. 45-52 https://doi.org/10.1016/j.proeng.2013.04.008

[2] Alnuaim, A.M., Naggar, M.H. El, and Naggar, H. El. 2011. Performance of the Micropiled Raft in Sand Subjected to Vertical Concentrated Load: Centrifuge Modeling. Canadian Geotechnical Journal 52(1), 33-45. https://doi.org/10.1139/cgj-2014-0448

[3] Shahin, M. A. 2014. Load-settlement modeling of axially loaded steel driven piles using CPT-based recurrent neural networks. Soils and Foundations 54(3), 515-522. https://doi.org/10.1016/j.sandf.2014.04.015

[4] Lee, K.M. and Xiao, Z. R. 2013. A Simplified Nonlinear Approach for Pile Group Settlement Analysis in Multilayered Soils. Canadian Geotechnical Journal 38(5), 1063-1080. https://doi.org/10.1139/t01-034

[5] Kim, H.T., Yoo, H.K., and Kang, I.K. 2002. Genetic Algorithm-Based Optimum Design of Piled Raft Foundations with Model Tests. Geotechnical Engineering 33, 1-11.

[6] Belevicius, B., Ivanikovas S., Shelkov, D., Valentinavičius, S., Zilinskas, J. 2011. Optimal placement of piles in real grillages: experimental comparison of optimization algorithms. Information Technology and Control 40(2), 22-36. https://doi.org/10.5755/j01.itc.40.2.427

[7] Momeni, E., Nazir, R., Jahed Armaghani, D., and Maizir, H. 2014. Prediction of pile bearing capacity using a hybrid genetic algorithm-based ANN. Measurement 57, 122-131. https://doi.org/10.1016/j.measurement.2014.08.007

[8] Golshani, A., Baranti, M. and Yasrebi, S. 2014. Determination of Bearing Capacity for Driven Piles in Sandy Soils by Using an Artificial Neural Network Method. Modares Civil Engineering Journal 14(20), 27-36. https://mcej.modares.ac.ir/article-16-9187-en.html

[9] Padfield, C.J., Sharrock, M.J. 1983. Settlement of Structures on Clay Soils. Construction Industry Research and Information Association, U.K.

[10] Hwang, J., Chung, M., Juang, D., Lyu, Y., and Juang, C. 2011. Practical optimization of group piles using a discrete Lagrange multiplier method. Optimization and Engineering 12 (1-2), 83-109. https://doi.org/10.1007/s11081-010-9117-z

[11] Reul, O., Randolph, M. F. 2003. Piled rafts in

over consolidated clay, Comparison of in situ measurements and numerical analyzes. Geotechnique 53 (3), 301- 315. https://doi.org/10.1680/geot.2003.53.3.301
[12] Fellenius, B. H. 1980. The Analysis of Results from Routine Pile Load Test, Ground Engineering. Geotechnical News Magazine 13(6), 19-31.
[13] Smith EA. 1986. Pile Driving Analysis by the Wave Equation. Journal of Soil Mechanics and Foundations 86(4), 35-61.
[14] Goble G., Rausche F., Moses F. 1970. Dynamic Studies on the Bearing Capacity of Piles - Phase III. Final Report to the Ohio Department of Highways, Case Western Reserve University, Cleveland, Ohio.
[15] Kordjezi, A. Pooyanejad, F. 2014. Prediction of ultimate axial load-carrying capacity of piles using a support vector machine based on CPT data, Computers and Geotechnics 55(1), 91-102. http://dx.doi.org/10.1016/j.compgeo.2013.08.001
[16] Maizir, H, Kassim, K.A. (2013). Neural network application in prediction of axial bearing capacity of driven piles, Proceedings of the International Multi Conference of Engineers and Computer Scientists, IMECS, Hong Kong.
[17] McVay, M.C., Klammler H. Tran K. 2014. Pile Shaft Designs Using Artificial Neural Networks (Genetic Programming) with Spatial Variability Considerations, University of Florida (UF Contract No.: 00100800).
[18] Beraja M. D., Nagaratnam, S. 2014. Principles of Foundation Engineering, Cengage Learning.
[19] Rojhani M., Fakher A. 2005. Evaluation of the Haley Formula to Determine Bearing in Place of Piles. Second National Congress of Civil Engineering, Tehran, University of Science and Technology (in Persian)
[20] Kehanian, A., Mohammadi, A. and Dehghani, M. 2006. Determining the accuracy of the PDA test based on the results of dynamic and static loading tests in Bandar Abbas dock projects and the 150,000-ton quay of Imam Port. Seventh International Conference on Shores, Ports and Offshore Structures, Tehran, Ports and Shipping Organization (in Persian).
[21] Seyed, H. E. 2006. Study of the Number of Pile Dynamic Testing Results using PDA and describing the lessons learned", 7th International Conference on Coasts, Ports and Marine Structures, Code 278.
[22] Fakhaian, K. and Hoseinzade, E. 2010. Case Study Comparison of Static Test and Dynamic Test in Determination of Pile Resistance. 5th National Congress of Civil Engineering, Mashhad, Ferdowsi University of Mashhad.
[23] Fachaian, K., Hoseinzade, E. 2011. Application of the Pilot Dynamic Test (PDA) to evaluate the possibility of knocking steel tube piles at the Chabahar Port Pier. 6th National Congress on Civil Engineering, Semnan, Semnan University (in Persian)
[24] Nejadqomi, N., Morani, M. 2013. Comparison of the results of dynamic coupling and PDA test with case study. International Conference on Civil Engineering, Architecture and Sustainable Urban Development, Tabriz (in Persian).
[25] Kennedy, J. B., Neville, A.D. 1966. Basic statistical methods for engineers and scientists, Longman Higher Education; 3rd edition.
[26] AlHolou, N., Lahdhiri, T., Sung, J. D., Weaver, J., Al-Abbas, F. 2002. Sliding Mode Neural Network Inference Fuzzy Logic Control for Active Suspension Systems. IEEE Trans. Fuzzy Syst. 10(2), 234-246. https://doi.org/10.1109/91.995124
[27] Smith G. N. 1986 "Probability and Statistics in Civil Engineering: An Introduction" Collins Publisher, London (ISBN: 000383154X, 9780003831542).

MECHANICAL PROPERTIES AND CONSTITUTIVE MODEL FOR ARTIFICIALLY STRUCTURED SOILS WITH AN INITIAL STRESS-INDUCED ANISOTROPY

MEHANSKE LASTNOSTI IN KONSTITUTIVNI MODEL ZA UMETNO STRUKTURIRANE ZEMLJINE PRI ZAČETNI ANIZOTROPNI NAPETOSTI

Chuan He
Sichuan university,
College of water resource and hydropower
Chengdu 610065, China

Enlong Liu *(corresponding author)*
Sichuan university,
College of water resource and hydropower
Chengdu 610065, China *and*
Northwest institute of eco-environment and resources
Lanzhou 730000,China
E-mail: liuenlong@scu.edu.cn

Qing Nie
Sichuan university,
College of water resource and hydropower
Chengdu 610065, China

DOI https://doi.org/10.18690/actageotechslov.17.2.46-55.2020

Keywords

constitutive model, artificially structured soils, breakage ratio, local strain coefficient, initial stress-induced anisotropy

Ključne besede

konstitutivni model, umetno strukturirane zemljine, razmerje loma, lokalni koeficient specifične deformacije, začetna anizotropna napetost

Abstract

A series of triaxial compression tests was performed on artificially structured soil samples with an initial stress--induced anisotropy at confining pressures of 25, 37.5, 50, 100, 200, and 400 kPa. Based on the results of these tests, a constitutive model for structured soils with initial stress-induced anisotropy was formulated. In the proposed model, the initially anisotropic structured soils are regarded as heterogeneous materials composed of bonded blocks and weaker bands. The bonded blocks (denoted as bonded elements) are described as transversely isotropic elastic–brittle materials, while the weaker bands (denoted as frictional elements) are described by the Lade–Duncan model of elastic–plastic materials. Based on the homogenization theorem for heterogeneous materials, and the introduction of structural parameters such as the breakage ratio and the local strain coefficient, the non-uniform distribution of stress and strain within a representative volume element was obtained. Finally, the parameters of the model were determined based on experimental results. The model was verified with test results, demonstrating that it can effectively capture many important features of artificially structured soils with an initial stress-induced anisotropy.

Izvleček

Na umetno strukturiranih vzorcih zemljine pri začetni anizotropni napetosti, pri bočnih tlakih 25, 37.5, 50, 100, 200 in 400 kPa je bila izvedena vrsta triosnih tlačnih preizkusov. Na podlagi rezultatov teh preizkusov je bil oblikovan konstitutivni model za strukturirane zemljine pri začetni anizotropni napetosti. V predlaganem modelu se prvotno anizotropne strukturirane zemljine obravnavajo kot heterogeni materiali, sestavljeni iz vezanih blokov in šibkejših pasov. Vezani bloki (označeni kot vezni elementi) so opisani kot prečno izotropni elastično-krhki materiali, šibkejši trakovi (označeni kot trenjski elementi) pa so opisani z modelom elastično-plastičnih materialov Lade-Duncan. Na podlagi teorema homogenizacije heterogenih materialov in uvedbe strukturnih parametrov, kot sta razmerje loma in lokalni koeficient specifične deformacije, je bila dobljena neenakomerna porazdelitev napetosti in specifične deformacije znotraj reprezentativnega volumskega elementa. Na koncu so bili parametri modela določeni na podlagi eksperimentalnih rezultatov. Model je bil preverjen z rezultati preizkusov, kar kaže, da lahko učinkovito zajame številne pomembne značilnosti umetno strukturiranih zemljin pri začetni anizotropni napetosti.

1 INTRODUCTION

Soil structures are a combination of the fabric, components and inter-particle bonding [1], which together with the initial stress anisotropy, strongly affects the mechanical properties of natural or structured soils. As a result of the non-uniform distribution of the stress in the vertical and horizontal directions, an initial stress-induced anisotropy is formed via precipitation. These two factors cause the mechanical behaviour of natural soils and re-moulded soils to differ significantly, even though the soils are composed of the same materials [2-3]. Therefore, the impacts of variables related to the stress history, bonding, fabric and current stress state should be considered in the formulation of a constitutive model. During the process of loading, the bonds between the soil particles in structured soils can be destroyed, and this phenomenon of bond loss is referred to as destructuration. To date, many constitutive models have been proposed to describe the stress–strain relationships in re-moulded soils, such as the modified Cam clay model [4-6] and the Lade–Duncan model [7-8]. These models can be utilized to solve soil engineering problems relatively satisfactorily. The modified Cam–clay model is widely used, but it has some limitations when used to simulate the strain softening and volumetric dilatancy of natural or structured soils at low confining pressures under the conditions of triaxial compression [9].

The mechanical features of structured soils have been investigated under drained and undrained conditions, including with triaxial tests and true triaxial tests. The samples tested included artificially structured soils [10-12], intact soil samples extracted from construction fields [13-22], and cemented and uncemented sands [23, 24]. Through these tests, the yielding, strength, deformation properties, aging, anisotropy and stress path of the structured soils were analysed. Many constitutive models for structured soils have been formulated based on macroscopic observations of the stress–strain properties of structured soils in laboratory tests, including the revised Cam–clay model [25-33], damage mechanical models [34–36], the disturbed state concept (DSC) model [37], kinematic or bounding models [38-41], micromechanical models [42], a bounding surface constitutive model under monotonic loading conditions [23], and a critical state bounding surface plasticity model considering the fabric anisotropy and intermediate principal stress effects [24]. However, only a few of these models are able to consider the deformation or breakage mechanism of structured soils. In addition, there is currently no widely accepted constitutive model for structured soils.

A structured soil sample with an initial stress-induced anisotropy initially exhibits strain softening and volumetric contraction behaviours, followed by dilatancy under a relatively low stress state [42]; however, strain hardening and volumetric contraction occur continuously under a relatively high stress state. Upon loading, the stress and strain distributed within a soil element will not be uniform, accompanied by the breaking of bonds between the soil particles. Thus, when formulating a constitutive model for structured soils, the non-uniform distribution of stress and strain in the soil element should be considered, and the macroscopic strain softening should be reflected through the use of parameters that consider the micro-deformation mechanism.

In this study, triaxial tests of artificially structured soils with an initial stress-induced anisotropy were performed at confining pressures ranging from 25 to 400 kPa under conditions of drained consolidation. Based on the test results, a binary-medium model for initially anisotropic structured soils was formulated by regarding the structured soils as a binary medium consisting of bonded blocks and weakened bands. Finally, the model parameters were determined and the model was verified through a comparison with the test results for anisotropic, artificially structured samples.

2 TEST CONDITIONS AND RESULTS

2.1 Sample Preparation

According to our previously described sample-preparation method [43], the materials for the artificially structured soils are silty clay, kaolin clay, cement and high-purity salt particles. Silty clay is the primary substrate, while cement provides the bonding between the grains. Moreover, kaolin clay can increase the content of fine particles in the samples, and large pores can be formed within the sample after the dissolution of the salt particles. The silty clay was obtained from a construction site in Chengdu with G_s=2.72, w_l=29.11 % and w_p=17.06 %, where G_s is the specific gravity, w_l is the liquid limit, and w_p is the plastic limit, respectively. After drying and sieving through a 0.5-mm screen, the silty clay was mixed evenly with the other dried components at a weight ratio of 65 % silty clay, 20 % kaolin clay, 5 % 32.5R cement, and 10 % salt grains. The uniform dry mixture was then compacted to a dry density of 1.49 g/cm^3, followed by storage under vacuum for approximately 3 h before being refilled gradually with distilled water. After full immersion, the samples were cured in running water for 7 d, and the salt content of the water was measured during the curing process to

ensure complete dissolution of the salt particles. Finally, samples were obtained with $\gamma_d = 1.34$ g/cm^3 and a void ratio, e, of 1.253, where γ_d is the dry density.

When natural soils form through sedimentation over a long geological duration, the resulting mechanical properties in the vertical and horizontal directions are different. To simulate this anisotropy induced by the initial stress in natural soils, a constant external load of 70 kPa is applied to the upper surface of the sample during the curing process. As a result of the vertical application of this external load and the confining restraint of the mould in the horizontal direction, different mechanical features will be produced in the samples in the vertical and horizontal directions. After the hydration of the cement and the dissolution of the salt particles, the bonding and fabric of the distribution of large pores among the soil particles are formed within the artificial samples with a cross-anisotropy similar to that of natural soils.

2.2 Test Results and Analysis

Drained triaxial consolidation experiments were carried out with the artificially structured samples having an initial stress-induced anisotropy under monotonic loading at confining pressures of 25, 37.5, 50, 100, 200, and 400 kPa and a loading speed of 0.06 mm/min. The apparatus employed was a GCTS triaxial system.

The test results are shown in Fig. 1(a)–(b), where "Ani–CD–xx kPa" is used to denote the artificially structured sample with an initial stress-induced anisotropy tested under drained consolidation conditions at a confining pressure of xx kPa. The results show that: (i) both the deviatoric stress and the volumetric strain increase with an increasing confining pressure. Under lower confining pressures, i.e., 25, 37.5, and 50 kPa, the samples exhibit the features of strain softening and an initial contraction, followed by dilatancy. The lower the confining pressure, the more the sample will dilate. (ii) Under higher confining pressures, i.e., 100, 200, and 400 kPa, the samples exhibit the features of strain hardening and contract continuously; the higher the confining pressure, the more the samples will contract. These features are similar to those of initially isotropic structured samples [43]. Because the structured samples with an initial stress-induced anisotropy were preloaded with a vertical load during the sample preparation (thus forming stronger bonds between the soil particles), these samples have a greater strength and smaller volumetric contraction compared with the initially isotropic structured samples.

The failure modes are depicted in Fig. 2(a)–(f). These demonstrate that obvious shear bands appear in the samples at relatively low confining pressures, while a bulging deformation occurs in the middle of the samples at relatively high confining pressures, which becomes less apparent as the pressure increases. This might be because a lower confining pressure contributes only little to damaging the bonds during the consolidation process, leading to progressive failure upon loading. However, at higher confining pressures, the bonds can be largely destroyed during the consolidation process, eventually resulting in the sliding between the soil particles bearing most of the external load. Thus, strain softening and shear bands appear at lower confining pressures, while strain hardening and bulging appear at higher confining pressures.

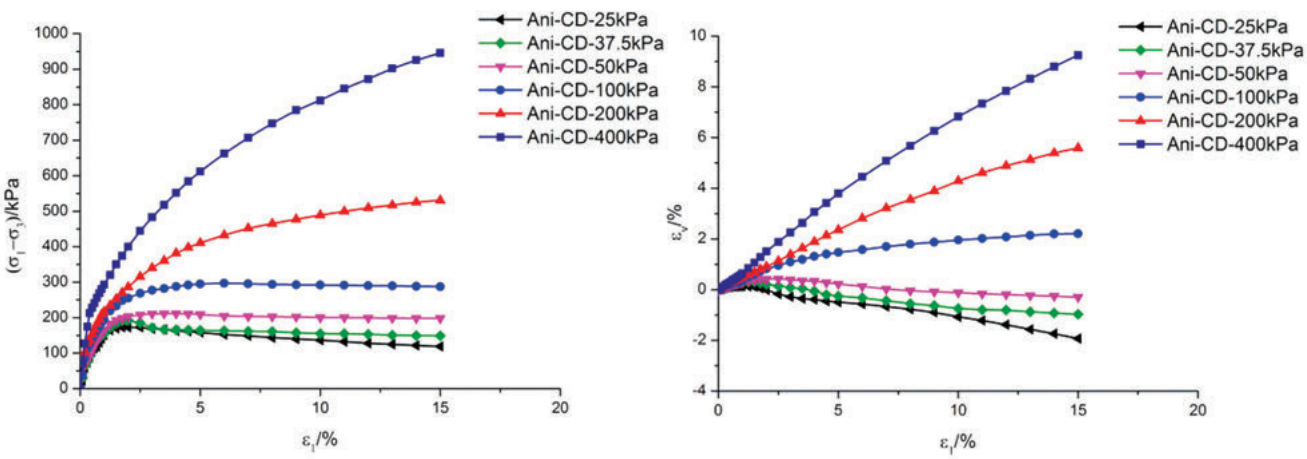

(a) Deviatoric stress vs. axial strain curves

(b) Volumetric strain vs. axial strain curves

Figure 1. Stress–strain curves for the structured samples with an initial stress-induced anisotropy.

(a) σ_c = 25 kPa (b) σ_c = 37.5 kPa (c) σ_c = 50 kPa (d) σ_c = 100 kPa (e) σ_c = 200 kPa (f) σ_c = 400 kPa

Figure 2. Failure modes of samples with initial stress-induced anisotropy.

3 CONSTITUTIVE MODEL FOR STRUCTURED SOILS WITH AN INITIAL STRESS-INDUCED ANISOTROPY

3.1 Formulating the constitutive model

Soil structures have a significant impact on the mechanical properties of intact soils [1]. The cohesive force reaches a maximum value at relatively small strains, while the frictional resistance plays an important role with relatively large strains [46]. This illustrates that cohesion and friction do not work simultaneously. Owing to the cohesion that is mainly produced by bonded blocks, the effect of friction arises gradually only after the bonded blocks are damaged. Structured soils are heterogeneous materials, which is consistent with the fact that a stronger bonding intensity produces bonded blocks, while weaker bonding produces weaker bands. Moreover, in the process of loading, the bonded blocks gradually break and transform into weaker bands, which are elastic–plastic. According to the theorem of binary-medium materials [36], the bonded blocks can be characterized as bonded elements, while the weaker bands can be described as frictional elements. The progressive failure process of structured soils can thus be idealized as the process of transformation from bonded elements to frictional elements. Whether softening or hardening occurs will depend on the reduction in the bearing capacity of bonded elements and increase in the bearing capacity of frictional elements.

To derive the relationship between stress and strain in artificially structured soils with initial stress-induced anisotropy, the soil is regarded as a binary-medium material, i.e., composed of bonded elements and frictional elements. The homogenization theorem is then applied to this heterogeneous material by considering a representative volume element (RVE) [36,43,44], yielding the following:

$$\{\sigma\} = (1-\lambda)\{\sigma\}_{\mathrm{b}} + \lambda\{\sigma\}_{\mathrm{f}} \ , \qquad (1)$$

$$\{\varepsilon\} = (1-\lambda)\{\varepsilon\}_{\mathrm{b}} + \lambda\{\varepsilon\}_{\mathrm{f}} \ , \qquad (2)$$

where $\{\sigma\}$, $\{\sigma\}_b$ and $\{\sigma\}_f$ are the average stress of the RVE, the stress of the bonded elements and the stress of the frictional elements, respectively; $\{\varepsilon\}$, $\{\varepsilon\}_b$ and $\{\varepsilon\}_f$ are the average strain of the RVE, the strain of the bonded elements and the strain of the frictional elements, respectively; and λ is the breakage ratio describing the ratio of the volume of frictional elements, v_f, to the whole volume, v, of the RVE. This ratio can be expressed as follows:

$$\lambda = \frac{v_{\mathrm{f}}}{v} \ . \qquad (3)$$

The breakage ratio is an internal variable similar to the damage factor used in damage mechanics or the hardening parameter used in plasticity [47], and it varies with the stress or strain upon loading. Here the breakage ratio is assumed to be a function of the strain:

$$\lambda = f(\{\varepsilon\}) \ . \qquad (4)$$

To derive the stress–strain relationships for bonded elements and frictional elements, $[D]_b$ and $[D]_f$ were defined as the tangential stiffness matrixes of the two media, respectively, yielding the following:

$$\{\Delta\sigma\}_{\mathrm{b}} = [D]_{\mathrm{b}}\{\Delta\varepsilon\}_{\mathrm{b}} \quad \text{and} \qquad (5)$$

$$\{\Delta\sigma\}_{\mathrm{f}} = [D]_{\mathrm{f}}\{\Delta\varepsilon\}_{\mathrm{f}} \ . \qquad (6)$$

Equation (1) can be written in incremental form as follows:

$$\begin{aligned}\{\Delta\sigma\} = {} & (1-\lambda^0)\{[D]_{\mathrm{b}} - [D]_{\mathrm{f}}\}\{\Delta\varepsilon\}_{\mathrm{b}} + [D]_{\mathrm{f}}\{\Delta\varepsilon\} \\ & - \Delta\lambda[D]_{\mathrm{f}}\{\{\varepsilon\}_{\mathrm{f}}^0 - \{\varepsilon\}_{\mathrm{b}}^0 + \Delta\lambda\{\{\varepsilon\}_{\mathrm{f}}^0 - \{\varepsilon\}_{\mathrm{b}}^0\} \ ,\end{aligned} \qquad (7)$$

in which the superscript 0 denotes the values of the breakage ratio, the stress and the strain in the initial state.

The local strain-coefficient matrix, [C], relating the strain of the bonded elements and the average strain of the RVE is introduced as follows:

$$\{\varepsilon\}_{\mathrm{b}} = [C]\{\varepsilon\} \ . \qquad (8)$$

The incremental form is given by the following:

$$\{\Delta\varepsilon\}_{\mathrm{b}} = [C]^0\{\Delta\varepsilon\} + [\Delta C]\{\varepsilon\}^0 \ . \qquad (9)$$

Combining Equations (7) and (8) yields:

$$\begin{aligned}\{\Delta\sigma\} = {} & \{(1-\lambda^0)\{[D]_{\mathrm{b}} - [D]_{\mathrm{f}}\}[C]^0 + [D]_{\mathrm{f}}\}\{\Delta\varepsilon\} + (1-\lambda^0) \\ & \{[D]_{\mathrm{b}} - [D]_{\mathrm{f}}\}[\Delta C]\{\varepsilon\}^0 - \frac{\Delta\lambda}{\lambda^0}[D]_{\mathrm{f}}\{\{\varepsilon\}^0 - \{\varepsilon\}_{\mathrm{b}}^0\} + \frac{\Delta\lambda}{\lambda^0}\{\{\sigma\}^0 - \{\sigma\}_{\mathrm{b}}^0\} \ . \end{aligned} \qquad (10)$$

Given that λ^0=0, $\{\varepsilon\}^0$=0, $\{\varepsilon\}_{\mathrm{b}}^0 = 0$ and $\{\varepsilon\}_{\mathrm{f}}^0 = 0$ at the initial loading, the incremental stress expression at the initial moment can be obtained from Equation (9) as follows:

$$\begin{aligned}\{\Delta\sigma\} = {} & \{(1-\lambda^0)\{[D]_{\mathrm{b}} - [D]_{\mathrm{f}}\}[C]^0 + [D]_{\mathrm{f}}\}\{\Delta\varepsilon\} \\ & + (1-\lambda^0)\{[D]_{\mathrm{b}} - [D]_{\mathrm{f}}\}[\Delta C]\{\varepsilon\}^0 \ . \end{aligned} \qquad (11)$$

There are four sets of parameters to be determined in Equation (11), including the constitutive relationships for the bonded elements and the frictional elements, the breakage parameter, and the local strain matrix, which will be discussed in the following sections.

3.2 Constitutive relationship for the bonded elements

In general, soils are anisotropic materials. Here, it is assumed that the bonded elements are transversely isotropic, elastic brittle materials because the mechanical features of the structured soils formed during the sedimentation process are in the vertical and horizontal directions. Setting the axis of symmetry along the z-direction, and defining the x-axis and y-axis in the horizontal plane in which the mechanical properties are isotropic, the following stress–strain relationship can be obtained from Equation (5):

$$\begin{pmatrix} \Delta\sigma_x \\ \Delta\sigma_y \\ \Delta\sigma_z \\ \Delta\sigma_{yz} \\ \Delta\sigma_{zx} \\ \Delta\sigma_{xy} \end{pmatrix}_{\mathrm{b}} = \begin{pmatrix} D_{11} & D_{12} & D_{13} & 0 & 0 & 0 \\ D_{12} & D_{11} & D_{13} & 0 & 0 & 0 \\ D_{13} & D_{13} & D_{33} & 0 & 0 & 0 \\ 0 & 0 & 0 & D_{44} & 0 & 0 \\ 0 & 0 & 0 & 0 & D_{44} & 0 \\ 0 & 0 & 0 & 0 & 0 & \dfrac{D_{11}-D_{12}}{2} \end{pmatrix}_{\mathrm{b}} \begin{pmatrix} \Delta\varepsilon_x \\ \Delta\varepsilon_y \\ \Delta\varepsilon_z \\ \Delta\varepsilon_{yz} \\ \Delta\varepsilon_{zx} \\ \Delta\varepsilon_{xy} \end{pmatrix}_{\mathrm{b}} , \qquad (12)$$

which contains five material constants, D_{11}, D_{12}, D_{13}, D_{33}, and D_{44}. These can be determined from the stress–strain curves of the tested samples at the initial loading stage; at this stage, the structured samples are not yet destroyed and can be regarded as bonded elements [45].

Under conventional triaxial stress conditions, the relationship between the stress and the strain of the bonded elements, i.e., Equation (12), can be simplified as follows:

$$\begin{pmatrix} \Delta\sigma_1 \\ \Delta\sigma_3 \end{pmatrix}_{\mathrm{b}} = \frac{E_{\mathrm{vb}}}{(1-v_{\mathrm{hhb}})E_{\mathrm{vb}} - 2v_{\mathrm{vhb}}^2 E_{\mathrm{hb}}} \begin{pmatrix} (1-v_{\mathrm{hhb}})E_{\mathrm{vb}} & 2v_{\mathrm{vhb}}E_{\mathrm{hb}} \\ v_{\mathrm{vhb}}E_{\mathrm{hb}} & E_{\mathrm{hb}} \end{pmatrix} \begin{pmatrix} \Delta\varepsilon_1 \\ \Delta\varepsilon_3 \end{pmatrix}_{\mathrm{b}} . \qquad (13)$$

Equation (13) contains four material parameters, i.e., E_{vb}, E_{hb}, ν_{vhb}, and ν_{hhb}, where E_{vb} and E_{hb} represent the elastic moduli of the bonded elements in the vertical and horizontal directions, respectively, and ν_{vhb} and ν_{hhb} are the Poisson's ratios of the bonded elements in the vertical and horizontal planes, respectively.

During initial loading under the conditions of low strain, the value of λ is small because the proportion of bonded elements is high. Thus, the mechanical properties of bonded elements can be effectively approximated by the stress–strain curve of the artificially structured samples. Here, a strain of 0.25 % of the artificially structured samples tested is used to determine E_{vb}, E_{hb}, ν_{vhb}, and ν_{hhb}. Using Equation (13), only the values of E_{vb} and ν_{vhb} can be solved. Note that when E_{vb}= E_{hb} and ν_{vhb}= ν_{hhb}, the samples with initial stress-induced anisotropy become initially isotropic samples, and thus it is assumed that the values of E_{hb} and ν_{hhb} for the samples with an initial stress-induced anisotropy are the same as those for the initially isotropic structured samples. E_{vb}, E_{hb}, ν_{vhb}, and ν_{hhb} are functions of the confining pressure, σ_3, and can be expressed as $E_{\mathrm{vb}}(\text{or } E_{\mathrm{hb}}) = b_1 \ln\left(\dfrac{\sigma_3}{p_a}\right) + b_2$ and $\nu_{\mathrm{hhb}}(\text{or } \nu_{\mathrm{vhb}}) = b_3\left(\dfrac{\sigma_3}{p_a}\right)^{b_4}$, in which b_1, b_2, b_3, and b_4 are material constants, and p_a=101.4 kPa is the atmospheric pressure.

3.3 Constitutive relationship for frictional elements

For structural soils with an initial stress-induced anisotropy, the bonds between grains are gradually broken as the load increases, and an increasing number of bonded elements become frictional elements. Thus, it is assumed that the mechanical properties of the frictional elements can be described by re-moulded soils, and a nonlinear elastic model is used. The test results for re-moulded soils [43] have shown that the stress–strain relationship of frictional elements can be described by the Lade–Duncan model [7,8]. In the Lade–Duncan model, the incremental expression for the strain can be written as follows:

$$\{\Delta\varepsilon\}_{\mathrm{f}} = \{\Delta\varepsilon^e\}_{\mathrm{f}} + \{\Delta\varepsilon^p\}_{\mathrm{f}} , \qquad (14)$$

where $\{\Delta\varepsilon^e\}_{\mathrm{f}}$ represents the incremental elastic strain and $\{\Delta\varepsilon^p\}_{\mathrm{f}}$ is the incremental plastic strain.

According to the Lade–Duncan model, the incremental relationship between the elastic strain and the stress

can be expressed using the generalized Hooke's law as follows:

$$\begin{pmatrix}\Delta\varepsilon_x^e\\ \Delta\varepsilon_y^e\\ \Delta\varepsilon_z^e\\ \Delta\varepsilon_{yz}^e\\ \Delta\varepsilon_{zx}^e\\ \Delta\varepsilon_{xy}^e\end{pmatrix}_{\mathrm{f}}=\frac{1}{E_{\mathrm{f}}}\begin{pmatrix}\Delta\sigma_x-v_{\mathrm{f}}(\Delta\sigma_y+\Delta\sigma_z)\\ \Delta\sigma_y-v_{\mathrm{f}}(\Delta\sigma_z+\Delta\sigma_x)\\ \Delta\sigma_z-v_{\mathrm{f}}(\Delta\sigma_x+\Delta\sigma_y)\\ 2(1+v_{\mathrm{f}})\Delta\tau_{yz}\\ 2(1+v_{\mathrm{f}})\Delta\tau_{zx}\\ 2(1+v_{\mathrm{f}})\Delta\tau_{xy}\end{pmatrix}_{\mathrm{f}}, \quad (15)$$

where E_f and v_f are the tangential deformation modulus and the tangential Poisson's ratio, respectively, of the frictional elements in the re-moulded samples. For the Lade–Duncan model, the failure criterion is $f_1 = I_1^3 / I_3 = K_{\mathrm{f}}$, the yielding function is $f = I_1^3 / I_3 = K_0$ and the plastic potential function is $g = I_1^3 - K_2 I_3$, where I_1 and I_3 are the first and third invariants of the stress tensor, and K_f=K_0 at failure. Then, the incremental relationship between the plastic strain and stress of the frictional elements is:

$$\begin{pmatrix}\Delta\varepsilon_x^p\\ \Delta\varepsilon_y^p\\ \Delta\varepsilon_z^p\\ \Delta\varepsilon_{yz}^p\\ \Delta\varepsilon_{zx}^p\\ \Delta\varepsilon_{xy}^p\end{pmatrix}_{\mathrm{f}}=\Delta\vartheta\cdot K_2\begin{pmatrix}\frac{3I_1^2}{K_2}-\sigma_y\sigma_z+\tau_{yz}^2\\ \frac{3I_1^2}{K_2}-\sigma_z\sigma_x+\tau_{zx}^2\\ \frac{3I_1^2}{K_2}-\sigma_x\sigma_y+\tau_{xy}^2\\ 2\sigma_x\tau_{yz}-2\tau_{xy}\tau_{zx}\\ 2\sigma_y\tau_{zx}-2\tau_{xy}\tau_{yz}\\ 2\sigma_z\tau_{xy}-2\tau_{yz}\tau_{zx}\end{pmatrix}_{\mathrm{f}}, \quad (16)$$

where $\Delta\vartheta$ and K_2 are model constants. A more detailed description of the Lade–Duncan model can be found in the references by Lade et al. [7,8].

Next, the parameters of the frictional elements are determined. First, the following can be obtained from Equation (14):

$$\begin{pmatrix}\Delta\sigma_1\\ \Delta\sigma_3\end{pmatrix}_{\mathrm{f}}=\left[D^{ep}\right]_{\mathrm{f}}\begin{pmatrix}\Delta\varepsilon_1\\ \Delta\varepsilon_3\end{pmatrix}_{\mathrm{f}}, \quad (17)$$

where $\left[D^{ep}\right]_{\mathrm{f}}=\left[D^{e}\right]_{\mathrm{f}}-\left[D^{p}\right]_{\mathrm{f}}$ is the elastic–plastic stiffness matrix of the frictional elements, and $\left[D^{e}\right]_{\mathrm{f}}$ and $\left[D^{p}\right]_{\mathrm{f}}$ are the corresponding elastic and plastic stiffness matrixes, respectively. Note that the discussion presented here is based on conventional triaxial stress conditions, and thus $\left[D^{e}\right]_{\mathrm{f}}$ can be derived by rewriting Equation (15) as follows:

$$\left[D^{e}\right]_{\mathrm{f}}=m_1\begin{bmatrix}1 & \frac{2v_{\mathrm{f}}}{1-v_{\mathrm{f}}}\\ \frac{v_{\mathrm{f}}}{1-v_{\mathrm{f}}} & \frac{1}{1-v_{\mathrm{f}}}\end{bmatrix}, \quad (18)$$

in which m_1 is $\frac{E_{\mathrm{f}}(1-v_{\mathrm{f}})}{(1+v_{\mathrm{f}})(1-2v_{\mathrm{f}})}$. Here, E_f and v_f are determined via a nonlinear Duncan–Chang elastic model expressed approximately by the hyperbola as follows:

$$E_{\mathrm{f}}=Kp_a\left(\frac{\sigma_3}{p_a}\right)^n\left[1-\frac{R_{\mathrm{f}}(\sigma_1-\sigma_3)(1-\sin\varphi)}{2c\cos\varphi+2\sigma_3\sin\varphi}\right]^2, \quad (19)$$

$$v_{\mathrm{f}}=\frac{G-F\lg(\sigma_3/p_a)}{\left(1-\frac{D(\sigma_1-\sigma_3)}{Kp_a\left(\frac{\sigma_3}{p_a}\right)^n\left[1-\frac{R_{\mathrm{f}}(\sigma_1-\sigma_3)(1-\sin\varphi)}{2c\cos\varphi+2\sigma_3\sin\varphi}\right]}\right)^2}, \quad (20)$$

where K, n, R_f, G, F, and D are material constants; c and φ are the cohesion and internal frictional angle of the re-moulded soils, respectively; p_a=101.4 kPa is the standard atmosphere pressure; and the stress is that of the frictional elements.

Next, Equation (16) along with the plastic theorem can be used to obtain the following:

$$\left[D^{p}\right]_{\mathrm{f}}=\begin{bmatrix}\frac{n_3}{n_9} & \frac{n_4}{n_9}\\ \frac{n_5}{n_9} & \frac{n_6}{n_9}\end{bmatrix}. \quad (21)$$

Finally:

$$\left[D^{ep}\right]_{\mathrm{f}}=\begin{bmatrix}m_1-\frac{n_3}{n_9} & \frac{2m_1v_f}{1-v_f}-\frac{n_4}{n_9}\\ \frac{m_1v_f}{1-v_f}-\frac{n_5}{n_9} & \frac{m_1}{1-v_f}-\frac{n_6}{n_9}\end{bmatrix}, \quad (22)$$

in which n_1, n_2, n_3, n_4, n_5, n_6, n_7, n_8, and n_9 can be found in Liu et al.[43].

K_2 and the stress, f, can be expressed as follows:

$$K_2=\mathrm{A}f+27(1\text{-}\mathrm{A}), \quad (23)$$

where A is a material constant, and f has the following relationship with plastic work:

$$f-f_{\mathrm{t}}=\frac{W_{\mathrm{p}}}{\alpha'+\beta'W_{\mathrm{p}}}, \quad (24)$$

in which f_t=27 for the re-moulded soils tested, and α' and β' are model parameters. Bearing in mind again that the discussion presented here is subject to conventional triaxial stress conditions, $f=\frac{\left[(\sigma_1-\sigma_3)+3\sigma_3\right]^3}{\left[(\sigma_1-\sigma_3)+\sigma_3\right]\sigma_3^2}$ and $W_{\mathrm{p}}=\int\sigma_{ij}d\varepsilon_{ij}^p$. Using the test results for re-moulded soils yields β'=0.01 and $\alpha'=r_1\left(\frac{\sigma_3}{p_a}\right)+r_2$, which varies with the confining pressure; r_1 and r_2 are material constants.

3.4 Structural parameters of the breakage ratio and local strain-coefficient matrix

In Equation (3), the breakage ratio, λ, is introduced as a structural parameter to reflect the degree to which the bonded elements are transformed into frictional elements upon loading. Therefore, λ is near zero during the initial loading and will ultimately have a value close to 1, with frictional elements mainly carrying the external load. Given this evolution of λ, it can be expressed as follows:

$$\lambda = 1 - \exp\left(-\beta(\alpha\varepsilon_z + \varepsilon_x + \varepsilon_y)^{\psi} - (\xi\varepsilon_s)^{\theta}\right), \quad (25)$$

where $\varepsilon_s = \sqrt{2e_{ij}e_{ij}/3}$ is the generalized shear strain, $e_{ij} = \varepsilon_{ij} - \varepsilon_{kk}\delta_{ij}/3$, δ_{ij} is the Kronecker delta, and α, β, ξ, ψ, and θ are material parameters. For conventional triaxial tests, $\varepsilon_s = 2(\varepsilon_1 - \varepsilon_3)/3$ and thus:

$$\lambda = 1 - \exp\left(-\beta(\alpha\varepsilon_1 + 2\varepsilon_3)^{\psi} - \left(\frac{2}{3}\xi(\varepsilon_1 - \varepsilon_3)\right)^{\theta}\right). \quad (26)$$

For the artificially structured soils with an initial stress-induced anisotropy, the parameters β and ψ are constants; α, ξ and θ vary with the confining pressure as $\alpha = e_1\left(\frac{\sigma_3}{p_a}\right)^{e_2}$ and $\xi(\text{or }\theta) = e_1\left(\frac{\sigma_3}{p_a}\right) + e_2$, in which e_1 and e_2 are constants.

Recalling Equation (8), the following can be defined:

$$[C] = \begin{bmatrix} m_3 & 0 \\ 0 & m_3 \end{bmatrix} \text{ and } \quad (27)$$

$$m_3 = \exp\left(-\left[t_c \times \frac{2}{3}(\varepsilon_1 - \varepsilon_3)\right]^{r_c}\right), \quad (28)$$

where t_c and r_c are material parameters determined by fitting the experimental results. It is assumed that $t_c = s_1\left(\frac{\sigma_3}{p_a}\right) + s_2$, r_c=1.5, s_1 and s_2 are constants, and p_a is the standard atmospheric pressure.

Here, it should be emphasized that both the breakage ratio and the local strain coefficient are internal variables, which means that they should be determined through the mesomechanics on a mesoscopic scale. However, owing to the difficulty of determining meso-parameters for structured soils with an initial stress-induced anisotropy, a similar method for the determination of the hardening parameters in plasticity and damage factor in damage mechanics is employed to build the evolutionary relationships of these internal variables. Then, expressions are formulated based on the analysis of the breakage mechanism, and then the structural parameters can be determined from experimental data.

3.5 Model verification and analysis

The parameters that correspond to the bonded elements, frictional elements, and structures are summarized in Tables 1, 2, and 3, respectively.

A program is developed to perform the computation using the above parameters, from which the deviatoric stress vs. axial strain and volumetric strain vs. axial strain curves can be obtained, as shown in Fig. 3(a) and 3(b), respectively.

From Fig. 3(a) we can see that despite some errors, the calculated deformation characteristics are qualitatively well matched with the experimental results. At low confining pressures of 25, 37.5, and 50 kPa, both curves exhibit strain-softening behaviour, while at high confining pressures of 200 and 400 kPa, both curves exhibit strain-hardening behaviour. At a confining pressure of 100 kPa, the curves enter the plastic flow state at the same time. Fig. 3(b) shows that the main trends in the calculated and tested results are basically similar, exhibiting dilation at low confining pressures and contraction at high confining pressures.

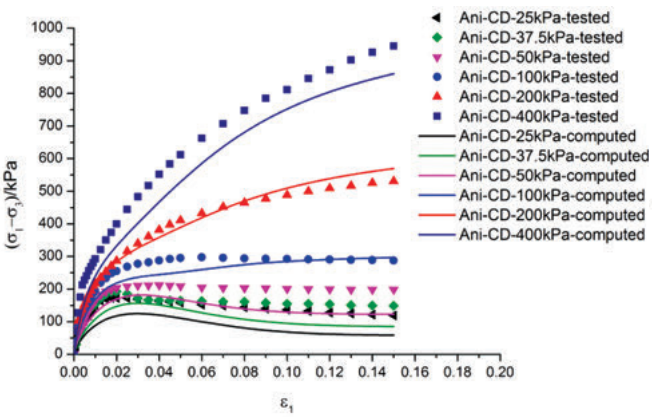

(a) Curves of the relationship between the deviatoric stress and the axial strain of structured soils with an initial stress-induced anisotropy

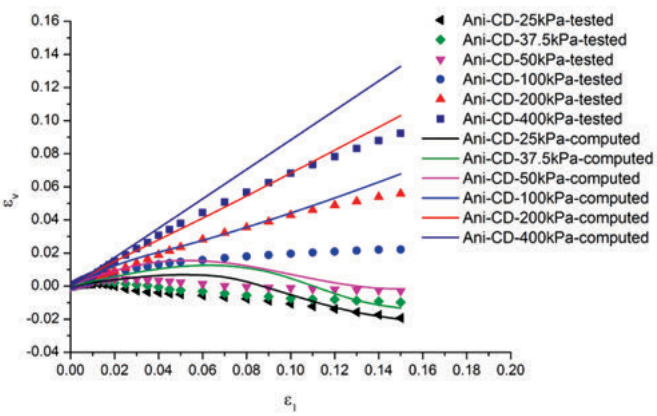

(b) Curves of the relationship between the volumetric strain and the axial strain of structured soils with an initial stress-induced anisotropy

Figure 3. Comparison of experimental and calculated results for structured samples with an initial stress-induced anisotropy.

Table 1. Parameters for the bonded elements.

E_{vb}		E_{hb}		ν_{vhb}		ν_{hhb}	
b_1	b_2	b_1	b_2	b_3	b_4	b_3	b_4
9.8383	30.37	9.1511	28.61	0.1389	-0.668	0.2134	-0.41

Table 2(a). Determination of parameter A for the frictional elements.

r \ σ_3	σ_3 < 100kPa	$\sigma_3 \geq$ 100kPa
r_1	-14.0	-155.0
r_2	-10.0	-66.67

Table 2(b). Parameters for the frictional elements.

K	n	R_f	G	F	D	c	φ
88.797	0.3425	0.95	0.242	0.313	0.0113	0	32.062

Table 3(a). Determination of structural parameters α, θ, and ξ.

Parameters	α	θ		ξ	
		σ_3<100kPa	σ_3≥100kPa	σ_3<100kPa	σ_3≥100kPa
e_1	105.58	0	0.0435	40.56	2.535
e_2	0.1081	0.15	0.325	40.0	100.0

Table 3(b). Structural parameters.

ψ	β		s_1	s_2
	σ_3 < 100kPa	$\sigma_3 \geq$ 100kPa		
1.0	0.4	0.5	11.859	30.854

4 CONCLUSIONS

Triaxial tests under the conditions of drained consolidation and monotonic loading were carried out at confining pressures of 25, 37.5, 50, 100, 200, and 400 kPa on artificially structured soil samples with an initial stress-induced anisotropy. An incremental constitutive model is proposed based on the binary-medium theorem and the Lade–Duncan model. The following conclusions can be drawn:

(1) At relatively low confining pressures, i.e., 25, 37.5, and 50 kPa, the artificially structured samples with an initial stress-induced anisotropy exhibit strain--softening behaviour and initially contract, followed by subsequent dilation. There are also apparent shear bands in the samples at failure. Under relatively large confining pressures of 200 and 400 kPa, the samples exhibit strain-hardening and contract continuously with bulging in the middle at failure. At a confining pressure of 100 kPa, the samples exhibit a plastic flow state along with contracting and bulging at failure.

(2) Based on the binary-medium theorem and by introducing structural parameters together with the Lade–Duncan elastic plastic model, an incremental constitutive model is proposed for artificially structured soils with an initial stress-induced anisotropy. Different material parameters are defined for confining pressures above and below 100 kPa because the structural yield strength of the samples is approximately 100 kPa. Through verification and a comparison between the test data and the calculation results, it is clear that the model can replicate the main mechanical features, particularly the strain softening and dilatancy at relatively low stress states.

Acknowledgments

The authors thank the reviewers and editor for their comments and appreciate the financial support from the National Natural Science Foundation of China (NSFC) (Grant No. 51009103).

REFERENCES

[1] Mitchell, J. K. (1976). Fundamentals of soil behavior. Wiley, New York.

[2] Burland, J. B. (1990). On the compressibility and shear strength of natural clays. Géotechnique 40(3), 329-378. DOI: 10.1680/geot.1990.40.3.329

[3] Leroueil, S., Vaughan, P.R. (1990). The important and congruent effects of structure in natural soils and weak rocks. Géotechnique40(3), 467-488. DOI: 10.1680/geot.1990.40.3.467

[4] Schofield, A. N., Worth, C. P. (1968). Critical State Soil Mechanics. MacGraw-Hill, London.

[5] Yao, Y. P., Hou, W., Zhou, A. N. (2009). UH model: three-dimensional unified hardening model for overconsolidated clays. Géotechnique 59(5), 451-469. DOI: 10.1680/geot.2007.00029

[6] Yao, Y. P., Kong, L. M., Zhou, A. N., Yin, J. H. (2015). Time-dependent unified hardening model: three-dimensional elasto-visco-plastic constitutive model for clays. ASCE, Journal of Engineering Mechanics141(6), 04014162. DOI: 10.1061/(ASCE)EM.1943-7889.0000885

[7] Lade, P. V., Duncan, J. M. (1975). Elasto-plastic stress-strain theory for cohesionless soil. Journal of the Geotechnical Engineering Division 101(10), 1037-1053.

[8] Lade, P. V. (1977). Elasto-plastic stress-strain theory for cohesionless soil with curved yield surfaces. International Journal of Solids and

Structures 13(11), 1019-1035. DOI: 10.1016/0020-7683(77)90073-7
[9] Smith, P. R., Jardine, R. J., Hight, D. W. (1992). On the yielding of Bothkennar clay. Géotechnique 42(2), 257-274. DOI: 10.1680/geot.1992.42.2.257
[10] Maccarini, M. (1987). Laboratory studies of a weakly bonded artificial soil. Ph.D. thesis, University of London, London. URL: http://hdl.handle.net/10044/1/8129
[11] Bressani, L. A. (1990). Experimental properties of bonded soils. Ph.D. thesis, University of London, London. URL: http://hdl.handle.net/10183/170716
[12] Malanraki, V., Toll, D. G. (2001). Triaxial tests on weakly bonded soil with changes in stress path. J. of Geotech. and Geoenv. Eng. 127(3), 282-291. DOI: 10.1061/(ASCE)1090-0241(2001)127:3(282)
[13] Lo, K. Y., Morin, J. P. (1972). Strength anisotropy and time effects of two sensitive clays. Can. Geotech. J. 9(3), 261-277. DOI: 10.1139/t72-030
[14] Sangrey, D. (1972). On the causes of natural cementation in sensitive soils.Can. Geotech. J.9(1), 117-119. DOI: 10.1139/t72-010
[15] Baracos, A., Graham, J., Domaschuk, L. (1980). Yielding and rupture in a Lacustrine clay.Can. Geotech. J. 17(4), 553-559. DOI: 10.1139/t80-063
[16] Schmertmann, J. H. (1991). The mechanical aging of soils. J. of Geotech. Eng. 117(9), 1288-1330. DOI: 10.1061/(ASCE)0733-9410(1991)117:9(1288)
[17] Diaz-Rodriguez, J. A., Leroueil, S., Aleman, J. D. (1992). Yielding of Mexico city and other natural clays. J. Geotech. Eng.118(7), 981-995. DOI: 10.1061/(ASCE)0733-9410(1992)118:7(981)
[18] Callisto, L., Calabresi, G. (1998). Mechanical behaviour of a natural soft clay. Géotechnique 48(4), 495-513. DOI: 10.1680/geot.1998.48.4.495
[19] Cotecchia, F., Chandler, R. J. (2000). A general framework for the mechanical behaviour of clays. Géotechnique 50(4), 431-447. DOI: 10.1680/geot.2000.50.4.431
[20] Dudoignon, P., Pantet, A., Carra, L., Velde, B. (2001). Macro-micro measurement of particle arrangement in sheared kaolinitic matrices. Géotechnique 51(6), 493-499. DOI: 10.1680/geot.2001.51.6.493
[21] Callisto, L., Gajo, A., Wood, D.M. (2002). Simulation of triaxial and true triaxial tests on natural and reconstituted Pisa clay. Géotechnique 52(9), 649-666. DOI: 10.1680/geot.52.9.649.38840
[22] Rocchi, G., Vaciago, G., Fontana, M., Prat, M. D. (2013). Understanding sampling disturbance and behavior of structured clays through constitutive modelling. Soils Found53(2), 315-334. DOI: 10.1016/j.sandf.2013.02.011
[23] Rahimi, M., Chan, D., Nouri, A. (2015). Bounding Surface Constitutive Model for Cemented Sand Under Monotonic Loading. International Journal of Geomechanics 16(2), 04015049-1:11. DOI: 10.1061/(ASCE)GM.1943-5622.0000534
[24] Rahimi, M., Chan, D., Nouri, A., Rasouli, R. (2016). Effects of inherent fabric anisotropy and intermediate principal stress on constitutive behavior of uncemented and cemented sands. Computers and Geotechnics 80, 237-247. DOI: 10.1016/j.compgeo.2016.08.024
[25] Kavvads, M., Amorosi, A. (2000). A constitutive model for structured soils. Géotechnique 50(3), 263-273. DOI: 10.1680/geot.2000.50.3.263
[26] Asaoka, A., Nakano, M., Noda, T. (2001). The decay of structure and the loss of overconsolidation. Proc. 15th Int. Conf. on Soil Mechanics and Geotechnical Engineering, Lisse, pp. 19-22. DOI: 10.1061/40797(172)7
[27] Liu, M.D., Carter, J. P. (2002). A structured cam-clay model. Can. Geotech. J. 39(6), pp. 1313-1332. DOI: 10.1139/t02-069
[28] Wheeler, S. J., Näätänen, A., Karstunen, M., Lojander, M. (2003). An anisotropic elastoplastic model for soft clays. Can. Geotech. J. 40(2), pp. 403-418. DOI: 10.1139/t02-119
[29] Belokas, G. Kavvadas, M. (2010). An anisotropic model for structured soils. Comput. Geotech. 37(6), pp. 737-747. DOI: 10.1016/j.compgeo.2010.05.001
[30] Suebsuk, J., Horpibulsuk, S., Liu, M. D. (2011). A critical sate model for overconsolidated structured clays. Comput.Geotech. 38(5), pp. 648-658. DOI: 10.1016/j.compgeo.2011.03.010
[31] Zhu, E. Y., Yao, Y. P. (2013). A Structured UH Model. In Constitutive modelling of geomaterials (Yang, Q. et al. (Eds)), Springer-Verlag: Berlin, pp. 675-689. DOI: 10.1007/978-3-642-32814-5_90
[32] Liu, M. D., Carter, J. P., Airey, D. W. (2011). Sydney Soil model: (I) theoretical formulation. International J. of Geomechanics, ASCE, 11(3), pp. 211-224. DOI: 10.1061/(ASCE)GM.1943-5622.0000078
[33] Liu, W., Shi, M., Miao, L., Xu, L., Zhang, D. (2013). Constitutive modelling of the destructuration and anisotropy of natural soft clay. Comput. Geotech. 51, pp. 24-41. DOI: 10.1016/j.compgeo.2013.01.011
[34] Shen, Z. J. (1997). Development of structural model for soils. Proc.,9th Conf. on Computational Methods and Advance in Geomechics, China, pp. 235-240.
[35] Zhao, X. H., Sun, H., Lo, K. W. (2002). An elasto-plastic damage model of soil. Géotechnique, 52(7), pp. 533-536. DOI: 10.1680/geot.2002.52.7.533
[36] Shen, Z. J. (2006). Progress in binary medium

modeling of geological materials. In Modern Trends in Geomechancis (Wu, W. and Yu, H.S. (Eds)), Springer: Berlin, pp. 77-99. DOI: 10.1007/978-3-540-35724-7_5
[37] Liu, M. D., Carter, J. P., Desai, C. S. (2003). Modelling compression behavior of structured geomaterials. Int. J. Geomech., 3(2), pp. 191-204. DOI: 10.1061/(ASCE)1532-3641(2003)3:2(191)
[38] Rouainia, M., Wood, D. M. (2000). A kinematic hardening constitutive model for natural clays with loss of structure. Géotechnique, 50(2), pp. 153-164. DOI: 10.1680/geot.2000.50.2.153
[39] Gajo, A., Wood, D. M. (2001). A new approach to anisotropic, bounding surface plasticity: general formulation and simulations of natural and reconstituted clay behavior. Int.J. Numer. Anal. Meth. Geomech. 25(3), pp. 207-241. DOI: 10.1002/nag.126
[40] Baudet, B., Stallebrass, S. (2004). A constitutive model for structured clays. Géotechnique, 54(4), pp. 269-278. DOI: 10.1680/geot.2004.54.4.269
[41] Huang, M., Liu, Y., Sheng, D. (2011). Simulation of yielding and stress-strain behavior of shanghai soft clay. Comput. and Geotech. 38(3), pp. 341-353. DOI: 10.1016/j.compgeo.2010.12.005
[42] Gao, Z., Zhao, J. (2012). Constitutive modelling of artificially cemented sand by considering fabric anisotropy. Comput.Geotech.41, pp. 57-69. DOI: 10.1016/j.compgeo.2011.10.007
[43] Liu, E., Yu, H. S., Zhou, C., Nie, Q., Luo, K. T. (2017). A binary-medium constitutive model for artificially structured soils based on the disturbed state concept and homogenization theory. International J. of Geomechanics, ASCE, 04016154-1:15. DOI: 10.1061/(ASCE)GM.1943-5622.0000859
[44] Wang, J. G., Leung, C. F., Ichicawa, Y. (2002). A simplified homogenization method for composite soils. Comput.Geotech. 29(6), pp. 477-500. DOI: 10.1016/S0266-352X(02)00004-6
[45] Graham, J., Houlsby, G. T. (1983). Anisotropic elasticity of a natural clay. Géotechnique33(2), pp. 165-180. DOI: 10.1680/geot.1983.33.2.165
[46] Lambe, T. W. (1960). A mechanical picture of shear strength in clay. In Research Conference on Shear Strength of Cohesive Soils. University of Colorado, Colorado, pp. 555-580.
[47] Krajcinovic, D., Mastilovic, S. (1995). Some fundamental issues of damage mechanics. Mechanics of Materials 21(3), pp. 217-230. DOI: 10.1016/0167-6636(95)00010-0.

THE CONSOLIDATION MATRIX AND THE CONSOLIDATION CIRCLE

KONSOLIDACIJSKA MATRIKA IN KONSOLIDACIJSKI KROG

Houssam Khelalfa
Selinus university of science and literature, Faculty of engineering and technology, Department of civil engineering
94277 Bologna, Italy and
University of Jijel, Civil Engineering and environment laboratory (LGCE), Jijel, Algeria.
E-mail: khelalfahoussam@gmail.com

DOI https://doi.org/10.18690/actageotechslov.17.2.56-64.2020

Keywords
consolidation, soil properties, compression index, correlations, geotechnical engineering, new concept

Ključne besede
konsolidacija, lastnosti zemljin, indeks stisljivosti, korelacije, geotehnično inženirstvo, novi koncept

Abstract

In geotechnical engineering, the consolidation and settlement of structures are among the major problems an engineer must deal with. An appropriate estimation of a soil's settlement is of significant importance, since it directly influences the performance of buildings and infrastructures that are built on soil.The compressibility characteristics of soils form one of the most important parameters required in the design of foundations. The compressibility behaviour of soils islargely dependent on the compression index, the properties and the parameters of the soil. A number of empirical correlations have been developed in the literature that aresupposedto connect the compression index to other soil parameters. The main objectives of this research were to study the relationships between the compression index (C_c) and the swelling index (C_s), and to investigate the effects of the natural void ratio (e_0) and the over-consolidation ratio (OCR) on C_c and C_s, in order to combine them with the pre-compression stress (P_c), the consolidation duration (T_c) and the settlement (S_u).Consequently, aconsolidation matrix and a consolidation circle are proposed, which gives us a new method and model to facilitate the calculations of the parameters involved in the soil consolidation, so as to summarize the consolidation phenomenon.

Izvleček

V geotehničnem inženirstvu spadata določitev konsolidacije zemljin in posedkov konstrukcij med glavne naloge, s katerimi se mora soočiti inženir. Ustrezna ocena posedanja zemljin je zelo pomembna, saj neposredno vpliva na delovanje zgradb in infrastrukture, ki so zgrajene na zemljinah. Lastnosti stisljivosti zemljin tvorijo enega najpomembnejših parametrov, ki se zahtevajo pri zasnovi temeljev. Obnašanje stisljivosti tal je močno odvisno od indeksa stisljivosti, lastnosti in parametrov zemljin. V literaturi so bile razvite številne empirične korelacije, ki naj bi povezovale indeks stisljivosti z drugimi parametri tal. Glavna cilja te raziskave sta bila preučiti razmerja med indeksom stisljivosti (C_c) in indeksom nabrekanja (C_s) ter raziskati učinke količnika por v naravi (eo) in prekonsolidacijskega razmerja (OCR) na C_c in C_s, da jih povežemo s prekompresijsko napetostjo (P_c), trajanjem konsolidacije (T_c) in posedanjem (S_u). Posledično sta predlagani matrika konsolidacije in konsolidacijski krog, ki podajata novo metodo in model za olajšanje izračunov parametrov, vključenih v konsolidacijo zemljin, tako da zajamejo pojav konsolidacije.

1 INTRODUCTION

Soils represent one of the most widely encountered materials in geotechnical engineering work [1]. Because of their heterogeneity, anisotropic nature, and nonlinear stress-strain curves, the characterizationand prediction of the engineering behaviour of soils is a challenging task that requires significant experimental work and a good sense of judgment [2]. Many civil engineering and hydraulic structures are either made of soil material or they are basedon soils. The design and stability of these structures depend heavily on the shear strength characteristics of the soils involved that, in turn, are greatly influenced by their geotechnical engineering properties. The aim of the evaluation of the geo-mechanical parameters is to determine the sub-surface condition and the soil strength that help to develop the structure or foundation in an area [3]. Soil settlements are very important, both in terms of the safety and the serviceability of the structures. Even though the settlements mightnot be excessive so as to causestructural damage, they may be largeenough to affect the serviceability of a structure in some cases.An accurate prediction of the settlements is especially importantwhen cohesive soils are present at a project site, because theconsolidation process cancontinue to occur over a very longperiod of time.Therefore, it is necessary to know the field consolidation curve in order to calculate the soil settlement caused by the structures. A knowledge of the rate at which the compression of the soil layer takes place is essential from design considerations. This canbe achieved by determining the value of the coefficient of the consolidation. The compression index is one of the most important parameters in soil mechanics forcalculating the settlement of different geotechnical structures, which can be achieved by spending a great deal oftime and expense usinga one-dimensional consolidation test. Attention was first drawn to the problem of the long-term consolidation of clays by Terzaghi (1925) [4], and proposed a theoretical approach to the consolidation process, and he had already designed the first consolidation apparatus,named an "oedometer" [5]. But, an estimation of the compression index from a laboratory oedometer test requires considerable time, cost and effort. An undisturbed soilsample needs to be obtained during the sub-surface investigations,carefully handled, and prepared for testing. The test results must also be analysed and interpreted accurately, otherwise all theeffort spent during sampling and testing would be useless sincethe parameters obtained from the tests at the end would beinaccurate. In addition, the test results should be interpreted insuch a way that the soil properties obtained should be uniformacross the practice. Unfortunately, the current standard procedures for consolidation testing do not give clearguidance for the unloading stress levels, the void ratio and the number of unloading decrements [6]. Numerous correlations have been developed in the literature relating the compression index of soft soils to the simple index properties that serve as a useful reality check on the oedometer test results [7-14].These equations were mainly developed based on traditional statistical analyses. Nevertheless, they include a number of drawbacks such as the low correlation of the input and output parameters [15]. However, many of these empirical correlations are specific to soils of a certain geographic region and/or geological origin and therefore may not be applicable in other contexts.This parameter, which has a major influence, is determined experimentally from the oedometric tests according to the procedures described in the technical standards, which requires a qualified workforce and a relatively long time. Also, the fact that many curve-fitting procedures are available in the literature suggests that none of them are completely satisfactory in evaluating the compression index.The multitude of equations reported in the literature indicates that none of them can be assumed to have general validity, but that each of them can be acceptable within defined ranges only.

In this paper, a relationship between all the main parameters and indices involved in thesoil-consolidation phenomenon are studied and summarized.The main objectives of this research were to study the relationships between the compression index (C_c) and the swelling index (C_s), and to investigate the effects of the natural void ratio (e_0) and over-consolidation ratio (OCR) on C_c and C_s, in order to combine with the pre-compression stress (P_c), consolidation duration (T_c) and settlement (S_u). Consequently, a consolidation matrix and a consolidation circle are proposed, which gives us a new method and model to facilitate the calculations of the parameters involved in the soil consolidation; so as to summarize the consolidation phenomenon.

2 SOIL PROPERTIES AND SOIL INDEX RELATIONSHIP

When thedistributed load from a structure is applied to a soft soil stratum, there will be some settlement of the structure. The term settlement refers to the vertical downward displacement at the base of a foundation or other structure due to ground improvements. This settlement may be due moisture movement, seismic disturbance, and adjacent excavation and so on.In soil mechanics, the settlement prediction of soft clay is a critical problem and very crucial. Soil settlement is controlled by its compressibility. Currently, the proce-

dure to obtain thecompressibility characteristic through in-situ or in the laboratory is quite complicated and time consuming. In order to havea simple and quick method, but give a significant and trusted result, some researcherspublished a relationship between the compression index and the basic physical properties of soil. Since the 1960s, many models have been developed by researchers to predict the compression index, in order to reduce costs and save time. A simple regression analysis aims to verify the validity of the available correlations between the compression index and other soil properties such as moisture content, initial void ratio and moisture content from simple lab testing and low in cost compared to an oedometer test [16-41].

Deformation due to elastic compression and that due to expulsion of the air from voids, take place immediately on the application of load, but deformation due to the removal of water takes place gradually. Itisleft with only two types of compression deformations, which cause a reduction in the volume of the soils. Out of these two, the first one is caused by compaction, i.e., a change in the volume due the removal of air and a reduction of the pore space and is an immediate process, whereas the second one occurs due to the removal of water from the pores on sustained loading, and is caused by consolidation, which is a slow and a gradually process. The soil-compression characteristic is a fundamental mechanical property of the soil that relates the effect of compressive stress on a soil volumetric parameter [42-52].The recompression index (C_s) and the recompression ratio (C_s) are considered as one of the most important parameters used in the settlement calculations.The recompression index, C_s, (or swell index) is needed to beable to calculate the consolidation settlements of over-consolidatedclays. The recompression index is usually obtained from one-dimensional consolidation tests.The compression (C_c) and recompression (C_s) indices obtained from the oedometer test are necessary for asettlement calculation ofclayey soil layers. However, the oedometer test takes a long time to measure the compression of clays. This will lead to a very demanding experimental working program in the laboratory. In the literature, a number of researchers have been looking for a possible relationship between C_c and C_s indices and the general characteristics of clays. A number of parameters appear to have an effect on the compression of clays. One of these parameters is the over-consolidation ratio (OCR). The results indicate that the C_c and C_s indices were influenced by the OCR and e_0, and, in most cases, a linear relationship between the C_c and C_s indices was observed. The results of this research can provide valuable contributions for academics and practitioners [53- 74].

Soil with a moisture content more than optimum is always close to the saturated condition. The compressibility of soil like this depends on the natural characteristic. This characteristic can be pictured with a liquid limit and a plasticity index. Besides that, it also depends on the moisture content and the degree of saturation. From the study of Md. Wasif Zaman et al. 2016/2017, in Bangladesh [75, 76], various correlations that will help us determine the consolidation and index properties are suggested. It verifies that there is strong correlation between the compression index (C_c) vs. the liquid limit (L_L), the compression index (C_c) vs. the water content (w %), and the compression index (C_c) vs. the plasticity index (P_I). But there is amoderate relationship between the compression index (C_c) vs. the in-situ void ratio (e_0), and the swelling index (C_s) vs. the plasticity index (P_I). The results from several index tests obtained for a given site can be used to assess the variation in the properties of the soil mass, are aiming to provide a conservative correlation between the effective peak angle of the shearing resistance and the plasticity index (PI) [65]. While the drained angle of the shearing resistance is more naturally linked to the soil's mineral composition, as expressed partly by the (P_I) value, the apparent effective cohesion is more naturally linked to the soil's structure and dilative tendencies [77-81]. The values for C_c, C_s and P_c' have been found from the void ratio-pressure curve (e vs. log P). The standard test to determine the liquid limit, plastic limit, specific gravity and moisture content has also been conductedin the laboratory.It is seen that the e – log p curves for the remoulded samples tested are approximately straight lines, particularly at higher effective pressures and hence the compression index can be taken, for all practical purposes, as a constant. In all the analyses except that madewith porosity, the linear regression yielded the highest value of the correlation coefficient [73]. The empirical correlation can be considered quite logical, since the liquid limit and the shrinkage limit are important parameters controlling the compressibility behaviour. The liquid limit is the extreme limiting water content, above which the forces of the interaction between the particles become sufficiently weak so as to allow the easy movement of the particles relative to each other [74]. The void ratio at the shrinkage limit can be taken as the limiting void ratio, below which the volume change would be insignificant. The shrinkage index, which is the numerical difference between the liquid limit and the shrinkage limit, thus covers the entire range of water contents only within which any soil would undergo the volume change. It is interesting to note that one of the correlations reported in literature [75] also uses the shrinkage index as the independent variable for the prediction of the compression index of remoulded fine grained soils.

The results of previous studies clearly show that the shrinkage index, which takes into account the extreme limits of the water content within which volume change takes place, has a definite edge over other index properties in characterizing the compressibility behaviour of clays.

The engineering parameters that are of importance and how they affect a surcharge preloading scheme needs to be understood in order toachieve a good and effective design [65]. Useful correlations exist between the index properties obtained from simple routine testing and the strength and deformation properties of cohesive soils, among others. For practical purposes, the results of routine index tests and correlations can be used as a first approximation of the soil parameters for use in the preliminary design of geotechnical structures, and later as a mean to validate the results of laboratory tests [76]. Based on the data, the relationships between the drained peak angle and the plasticity index were proposed, which were dependent on the claysize fraction and the normal effective stress [76]. The findings suggest that the observed scatter in the reported data found in the literaturecan to a large extent be explained by variations in the stress level due to a non-linear strength envelope and additionally the claysize fraction, as both the soil mineralogy and the claysize fraction are not accounted for solely by the variation in the index properties. The datashows the relationship between the drained peak angle of the shearing resistance Φ'_{oc} and the plasticity index I_P (single log plot) as derived from the triaxial compression tests performed on the various over-consolidated undisturbed clays [76]. Φ'_{oc} has generally been derived as a tangent value, to minimize the otherwise largeinfluence of the stress level resulting from the initially curved failure envelope. A large scatter in the data and thetrend of a reducing Φ'_{oc} with an increasing I_P is generally seen as similar to that whichwas observed for NC clays. Variations in stress level, on the other hand, should have less of an influence, since a tangent value of Φ'_{oc} is derived from a failure envelope thatis approximately linear within the typical stress range. Alternatively, the strength parameters can be interpreted from the undrained compression effective stress path, since the effective stress path for over-consolidated clays will tend to climb the strength envelope as the soil dilates and the pore-water pressures decreases [76]. While the drained angle of the shearing resistance Φ'_{oc} is more naturally linked to the soil's mineralogy composition, as expressed partly by the I_P value, the apparent effective cohesion is more naturally linked to the soil's structure and the dilative tendencies. As the I_P value is determined from the reconstituted state it does not take account of the soil structure. Hence, the above relationship between the c'_{oc} and the I_P might not be the most appropriate one to use. As suggested in the previous Danish code of practice for foundations (Danish Standard DS 415) it is tobe expected that the value of c'_{oc} is better related to the undrained shear strength cu rather than the I_P. Both c_u and c'_{oc} are influenced by the soil structure and dilation, but as the stress level is likely to have a greater impact on cu than c'_{oc}, the relationship will not be unique [81]. The datashows the relationship between c'_{oc} and c_u based on the data from the performed tests. As before, both derived values from the tests and the estimated values of c'_{oc} are shown. As expected, the observed scatter is very significant, but there is a tendency forincreasing values of c'_{oc} with increasing values of c_u. Simple correlations between the plasticity index and the drained peak strength parameters in terms of Φ'_{oc} and c'_{oc} have been proposed on the basis of a comprehensive database of triaxial compression tests on undisturbed, over-consolidated Danish clays of very low to extremely high plasticity. The proposed correlations give cautious lower bound values of the drained strength parameters, which can be used as a first approximation in the preliminary design of geotechnical structures. Furthermore, the correlations can be used to evaluate the results of the laboratory effective strength tests, and as a means to assess how well these results represent the entire soil mass at a given site when viewed in connection withthe variations of the index properties in the soil mass.

3 CONSOLIDATION MATRIX

The compressionindex (C_c) and the recompression (or swelling) index (C_s) are necessary for acalculation of thesoil's consolidation. Increasing values of thevoid ratio (e_0) will decrease the C_c and C_s values. In contrast, when the OCR increases, the C_c and C_s values would also increase. It is possible to say that the C_c and C_s values are influenced by the same parameters. Therefore, it can be concluded that the amount of settlement depends on the swelling index, and that the amount of settlement(S_u) is proportional to the swelling index (C_s) [1-82]. When comparing the required time of consolidation to stabilize the settlement, it is a question of the OCR and C_c. Therefore, it can be concluded that the time of the consolidation depends on the compressionindex (C_c) and the over-consolidation ratio (OCR), and that the time of consolidation (T) is proportional to the compression index (C_c) and the over-consolidation ratio (OCR), and at the same time that the latter two are proportional [1- 82].

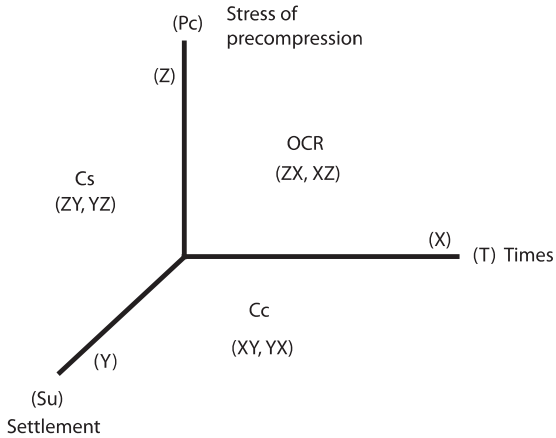

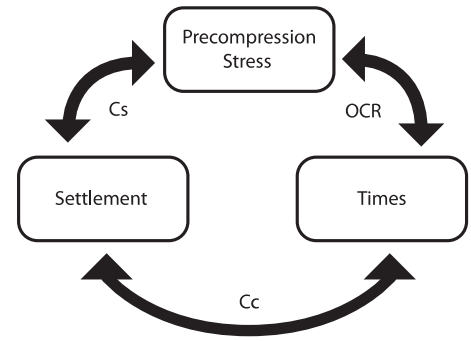

Figure 1. Soil consolidation cycle and its representation inthe Cartesian coordinate system according to our hypothesis.

As illustrated in Figure (1), according to our study; the consolidation phenomenon has been summarized in a consolidation cycle thatconsists of three basic components, i.e., the pre-compression stress (P_c), times (T) and settlement (S_u), that they are related to each other by three main index properties, i.e., the over-consolidation ratio (OCR), the compression index (C_c) and the swelling index (C_s). If taking all the previous data, and becauseit wasproventhat indexes and components are linearly dependent,wecan easily obtain a consolidation matrix, which clearly illustrates that the three basic components are the diagonal and the other three main index properties compose the rest of the matrix:

$$\begin{pmatrix} XX & XY & XZ \\ YX & YY & YZ \\ ZX & ZY & ZZ \end{pmatrix} = \begin{pmatrix} T & Cc & OCR \\ Cc & Su & Cs \\ OCR & Cs & Pc \end{pmatrix}$$

Consolidation Matrix

4 CONSOLIDATION CIRCLE

The nature of soil consolidation typically displays a complex concept as a result ofthe missing unified model about thisphenomenon. A key aspect for the selection of representative soil parameters is to consider a knowledge of its properties. This nature is based on our hypothesis to determine thesecharacteristics (compression index C_c, swelling index C_s, void ratio e_0, over-consolidation ratio OCR) of the soil; by using these compression parameters, it is possible to determine the settlement, the times of consolidation, and the amount of compression stress needed, etc. While the rigorous selection of soil parameters requires a deep understanding and proper knowledge of its behavior. Parameters such as the OCR, C_c and C_s play a key role inconsolidation and compression stress predictions.

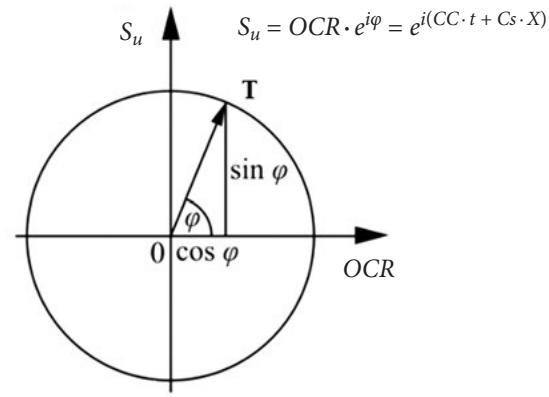

Figure 2. Consolidation circle according to our hypothesis.

Our theory introduced the following factors as the main causes of the Time of consolidation (T) according to the soilsettlement (Figure 2, Eq. 1, Eq. 2): the over curvature ratio (OCR), settlement (S_u), and phase (Phi/φ) (or time evolution), which depends on the compression index (C_c) as a function of the time (t) and swelling index (C_s) as a function of position (X). Thismeans that the change in the value (S_u) involves changing the value of (T).

$$S_u = OCR \cdot e^{i\varphi} = e^{i(Cc \cdot t + Cs \cdot x)} \qquad (1)$$

$$\varphi(X, t) = [0 \sim \Delta H] \,/\, \mathrm{Max} \cdot \Delta H = 2\pi \qquad (2)$$

where ΔH: is the maximum settlement.

In order to carry more than one value and for the indices to represent the consolidation Circle by using the complex number to explain the settlement characteristics of the soil. Thissimply concludes that the final state equals the initial state multipliedby the time of consolidation (T) (Eq. 3).

$$\varphi(X1, t1) = \varphi(X0, t0) \cdot T \qquad (3)$$

The most determining factor for the credibility consolidationCircle is its ability to contain all the characteristics and indices contributing to this phenomenon, as illustrated in Figure 2, Eq.1.

5 CONCLUSION

With animprovement in the knowledge of soil mechanics, the gap between the calculated values of the settlement and the settlement experienced throughout the life span of the structure has diminished. The settlement calculation of each soil stratum can be accomplished by various methods, ranging from Terzaghi's one-dimensional consolidation theory to stress path methods.Several empirical correlations based on the above approach have been developed by later researchers, each being applicable to a particular soil type. In view of the time, effort and cost involved in determining the compressibility characteristics through an odeometer test, it is very highly desirable that a predictive equation for the compression index is developed. Although several attempts have been made in the past to correlate the compression index with the index properties as well as the initial state parameters of the soils.

In our hypothesis, we looked for a possible relationship between the C_c and C_s indices and the general characteristics of the soil. One of these parameters is the over-consolidation ratio (OCR). In this research, the effect of the OCR and the void ratio (e_0) on the C_c and C_s indices was proven. Thus, the hypothesis indicates that the C_c and C_s indices were influenced by the OCR and e_0, and a linear relationship between them was proven. The consolidation matrix gives us a new method to facilitate the calculations of the parameters involved in the consolidation, which gives great credibility to our hypothesis. Indeed, the Consolidation Circle is consideredto bea good new tool to calculate and explain the consolidation; moreover, maybe it can summarize the phenomenon of consolidation.

Acknowledgment

This work was supported and funded by the K.E.C Laboratory, Department of Civil, Geotechnical & Coastal Engineering, under the project number (PN): KEC.LAB. DCGCE.M.DPED2019N001.

REFERENCES

[1] Taiba,A. C., Mahmoudi,Y., Belkhatir,M., and Schanz,T. 2018. Experimental Investigation into the Influence of Roundness and Sphericity on the Undrained Shear Response of Silty Sand Soils. Geotechnical Testing Journal 41(3), 619-633. DOI: 10.1520/GTJ20170118

[2] Lambe,T. W. 1967. Stress Path Method. JSMFD, ASCE, (SM6), 93, pp. 309–331.

[3] Md. EmdadulHaque, Hossain Md. Sayem, and Md. Hasan Imam. 2013. Evaluation of Some Geo Mechanical Parameters of the Soil Samples from Ganakbari Area, Dhaka, Bangladesh. ARPN Journal of Science and Technology 3(8), 850- 857.

[4] Terzaghi, K. 1925.Erdbaumechanik auf bodenphysikalischerGrundlage, Deuticke, Wien.

[5] Head, K. H. 1988. Manual of Soil Laboratory Testing, Volume 2 : Permeability, Shear Strength and Compressibility Tests. Plymouth, Devon, UK.ISBN: 9780727313058.

[6] Al-Khafaji A., Buehler A., Druszkowski E. 2019. Validation of Compression Index Approximations Using Soil Void Ratio. In: Hemeda S., Bouassida M. (eds) Contemporary Issues in Soil Mechanics. GeoMEast 2018. Sustainable Civil Infrastructures. Springer, Cham. Cairo, Egypt. DOI: 10.1007/978-3-030-01941-9_4

[7] Azzouz, A.S., Krizek,R.J., and Corotis,R.B. 1976. Regression analysis of soil compressibility. Soils and Foundations 16(2), 19-29.

[8] Cozzolino, V.1961. Statistical forecasting of compression index. Proc. Int. conf. The 5th international conference on soil mechanics and foundation engineering, Paris.

[9] Mayhe, P. 1980.Cam-clays predictions of undrained strength. Journal of Geotechnical and Geo-environmental Engineering, 106(ASCE 15816).

[10] Nishida, Y.1956. A brief note on compression index of soil. Journal of the Soil Mechanics and Foundations Division. 82(3), 1-14.

[11] Park, H.I. and S.R. Lee. 2011. Evaluation of the compression index of soils using an artificial neural network. Computers and Geotechnics. 38(4), 472-481.

[12] Skempton, A.W. and Jones,O.1944. Notes on the compressibility of clays. Quarterly Journal of the Geological Society. 100(1-4), 119-135.

[13] Terzaghi, K., Peck,R.B., and Mesri,G.1996. Soil mechanics in engineering practice. John Wiley & Sons, New York.

[14] Tsotsos, S.S. 1977. A New Relation Between Compressibility and Other Soil Parameters, Geotechnical Aspects of Clay.Proc. Int. conf.The International Symposium on Soft Clay. Asian Institute of Technology, Bangkok, pp 301- 310.

[15] Hossein,A. A. and Hossein, G.A.. (2011). A robust data mining approach for formulation of geotech-

nical engineering systems. Engineering Computations, 28(3), 242-274.
[16] Akayuli,C., Ofosu,B.2013. Empirical model for estimating compression index from physical properties of weathered birimianphyllites. Electron. J. Geotech. Eng. 18 (Z), 6135-6144.
[17] Singh,A., Noor,S. 2012. Soil compression index prediction model for fine grained soils. Int. J. Innov. Eng. Tech. 1(4), 34-37.
[18] Abbasi,N., Javadi,A.A., Bahramloo,R.2012. Prediction of Compression Behavior of Normally Consolidated Fine-Grained Soils. World Appl. Sci. J. 18(1), 6-14. doi:10.5829/idosi.wasj.2012.18.01.2675
[19] Kalantary,F., Kordnaeij,A.2012. Prediction of compression index using artificial neural network. Sci. Res. Essays 7(31), 2835-2848. doi:10.5897/SRE12.297
[20] Shahin,M.A., Jaksa,M.B., Maier,H.R.2008. State of the art of artificial neural networks in geotechnical engineering. Electron. J. Geotech. Eng. 8 (L), 1-26.
[21] Tang,Z., de Almeida,C., Fishwick,P.A. 1991. Time series forecasting using neural networks vs. Box-Jenkins methodology. Simulation 57(5), 303-310. doi:10.1177/003754979105700508
[22] Miller,G.F., Todd,P.M., Hegde,S.U. 1989. Designing neural networks using genetic algorithms. Proc. Int. conf. of the third international conference on Genetic algorithms, Fairfax, 379-384.
[23] Schiffmann,W., Joost,M., Werner,R. 1993. Application of Genetic Algorithms to the Construction of Topologies for Multilayer Perceptrons. In: Albrecht R.F., Reeves C.R., Steele N.C. (eds) Artificial Neural Nets and Genetic Algorithms. Springer. doi:10.1007/978-3-7091-7533-0_98
[24] Kitano,H. 1990. Empirical studies on the speed of Convergence of neural network training using genetic algorithms. Proc. Int. conf.of the eighth National conference on Artificial intelligence, Massachusetts, 789-795.
[25] Alsultanny,Y.A., Aqel,M.M.2000. Pattern recognition using multilayer neuralgenetic algorithm. Neurocomputing 51 (2003), 237-247. doi:10.1016/S0925-2312(02)00619-7
[26] Smith,G.N. 1986 Probability and statistics in civil engineering: an introduction. Nichols Pub. Co. London.
[27] Willmott,C.J., Matsuura,K. (2005). Advantages of the mean absolute error (MAE) over the root mean square error (RMSE) in assessing average model performance. Climate Res. 30(1), 79-82. doi:10.3354/cr030079
[28] Azzouz,A.S., Krizek,R.J., Corotis,R.B. 1976. Regression analysis of soil compressibility. Soils Found. 16(2), 19-29. doi:10.3208/sandf1972.16.2_19
[29] Nagaraj,T.S., Murthy,B.R.S., Vatsala,A., Joshi,R.C.1990. Analysis of compressibility of sensitive soils. J. Geotech. Eng. 116(1), 105-118. doi:10.1061/(ASCE)0733-9410(1990)116:1(105)
[30] Park,H.I., Lee,S.R.2011. Evaluation of the compression index of soils using an artificial neural network. Comput. Geotech. 38(4), 472-481. doi:10.1016/j.compgeo.2011.02.011
[31] Koppula,S. 1981. Statistical estimation of compression index. Geotech. Test. J. 4(2), 68-73. doi:10.1520/GTJ10768J
[32] Al-Khafaji,A. W.N., Andersland,O.B. 1992. Equations for compression index approximation. J. Geotech. Eng. 118(1), 148-153. doi:10.1061/(ASCE)0733-9410(1992)118:1(148)
[33] Ahadiyan,J., Ebne,J.R., Bajestan,M.S.2008. Prediction determination of soil compression Index C_c in Ahwaz region. J. Faculty Eng. 35(3), 75-80.
[34] Terzaghi,K., Peck,R.B.,Mesri, G.1996. Soil mechanics in engineering practice. John Wiley & Sons, Third Edition,New York.
[35] Skempton,A.W., Jones,O.T.1944. Notes on the compressibility of clays. Q. J. Geol. Soc. 100(1944) 119-135. doi:10.1144/GSL.JGS.1944.100.01-04.08
[36] Thinh,P.H., Tuan,H.A., Bien,D.C., Ha,N.H. 2017. Research on correlation between compression index (C_c) and other properties of soil for geotechnical design in Coastal regions of Viet Nam and Cambodia. MOJ Civ. Eng. 2(3), 97-101. doi:10.15406/mojce.2017.02.00034
[37] Güllü,H., Canakci,H., Alhashemy,A.2016. Development of Correlations for Compression Index. AKU J. Sci. Eng. 16(2), 344-355.doi:10.5578/fmbd.26553
[38] Onyejekwe,S., Kang,X., Ge,L. 2015. Assessment of empirical equations for the compression index of fine-grained soils in Missouri. Bull. Eng. Geol. Environ. 74(3), 705-716. doi:10.1007/s10064-014-0659-8
[39] McCabe,B.A., Sheil,B.B., Long,M.M., Buggy,F.J., Farrell,E.R., Quigley,P. 2016. Discussion: Empirical correlations for the compression index of Irish soft soils. In: Proceedings of the Institution of Civil Engineers-Geotechnical Engineering. 169(1), 91-92. doi:10.1680/jgeen.15.00101
[40] Rendon-Herrero,O. 1983. Universal Compression Index Equation. J. Geotech. Eng. 109(5), 755-761. doi:10.1061/(ASCE)0733-9410(1983)109:5(755)
[41] Yoon,G.L., Kim,B.T., Jeon,S.S.2004. Empirical correlations of compression index for marine clay from regression analysis. Can. Geotech. J. 41(6), 1213-1221. doi:10.1139/t04-057
[42] Al-Khafaji, A. W. and Andersland, O. 1981. Compressibility and strength ofdecomposing fibre-

clay soils, Geotechnique. 31(4), 497-508.
[43] Hough, B. K. 1957. Basic Soils Engineering, 1st ed., The Ronald Press Company,New York.
[44] Bowles, J. E. 1989. Physical and Geotechnical Properties of Soils, McGraw-HillBook Co., Inc., New York, N.Y.
[45] Kootahi, K., and Moradi, G. 2017. Evaluation of Compression Index of MarineFine-Grained Soils by the Use of Index Tests. Marine Georesources&Geotechnology. 35(4), 548-570.
[46] Lambe, T. W. and Whitman, R. V. 1969. Soil Mechanics, John Wiley and Sons,Inc., New York, N.Y.
[47] Bouassida, M. 2015. Amélioration des sols en place, Université Tunis El Manar, Ecole Nationale d'Ingénieurs de Tunis, Tunisie.pp, 139-163.
[48] Mohamad, R. 2008.Precompression of soft soils by surcharge preloading—some common pitfalls and misunderstood fundamentals.pp, 1-4.
[49] Rujikiatkamjorn, C., Indraratna, B. and Chu, J. 2007. Numerical modelling of soft soil stabilized by vertical drains, combining surcharge and vacuum preloading for a storage yard, Canadian Geotechnical Journal, 44(2007), 326-342.
[50] Chu, J., and Yan, S.W. 2005. Application of vacuum preloading method in soil improvement project. Case Histories Book (Volume 3), Edited by Indraratna, B. and Chu, J., Elsevier, London, 91-118.
[51] Indraratna, B., Sathananthan, I., Rujikiatkamjorn C. and Balasubramaniam, A. S. 2005. Analytical and numerical modelling of soft soil stabilized by PVD incorporating vacuum preloading. International Journal of Geomechanics 5(2), 114-124.
[52] Indraratna,B. 2009.Recent advances in the application of vertical drains and vacuum preloading in soft soil stabilisation. Eh davis memorial lecture – australian geomechanics society.
[53] Nishida, Y.1956. A Brief Note on Compression Index of Soil. Journal of the Soil Mechanics and Foundation Engineering Proceedings of the American Society of Civil Engineers 82(3), 1-14.
[54] Ahadian, J., Bajestan,S.H.M., Abn, J. R. 2004. Estimate fourmula for compression index in ahvazsoil's. University of Tabriz Journal 35(2), 66-73.
[55] Chandra, B., Solanki,C.H., Vasanwala, S.A.2016. Influence of Fine Fraction on Shear Parameters and Consolidation Behavior of Tropical Residual Soil. Indian Journal of Science and Technology 9(41), 1-7.
[56] Abbasi, N. 2012. Prediction of Compression Behaviour of Normally Consolidated Fine-Grained Soils. World Applied Sciences Journal 18(1), 06-14.
[57] Bowles, J.W. 1979. Physical and Geotechnical Properties of Soil. New York: McGraw Hill. PMid:456581. pp 1-10.
[58] Sridharan, A., Nagaraj, H.B.2000. Compressibility behaviour of remoulded, fine-grained soils and correlation with index properties. Canadian Geotechnical Journal 37(3),712-22.
[59] Hough, B. 1957. Basic soil Engineering. New York: Ronald Press 12, 319-350.
[60] Koppula, S.D.1981. Statistical Estimation of compression Index. Geotechnical Testing Journal4(2), 68-73.
[61] Ozer, M. 2008. A statistical and neural network assessment of the compression index of clay-bearing soils. Bulletin Engineering Geology and the Environment 67(4), 537-45.
[62] Papke, M. 2011. Studying Consolidation Characteristics of Ohio Geo-Frontiers Conference Dallas: ASCE. p. 2838-46.
[63] RO,H.1983. Universal Compression Index Equation. Journal of Geotechnical Engineering 109(5), 755-61.
[64] Abdrabbo, F.M., Mahmud, M.A. 1990. Correaltionsbeetwen index test sand compressibility of egyptian clays. Soils and Foundations 30(2),128-32.
[65] Skempton, A. 1944. Notes of the compressibility of clays. Quarterly Journal 100(1944), 119-35.
[66] Azzouz, A. S., Krizek, J.R., Corotis, R.B.1976. Regression Analysis of Soil Compressibility. Quarterly Journal of the Soil and Foundations 16(2), 19-29.
[67] Terzaghi, K. 1967. John Wiley and Sons: Soil Mechanics in Engineering Practice (2nd Edition). New York.
[66] Cozzolino, V. M. 1961. Statistical forecasting of compression index, Proc. Int. conf. ofthe 5th international conference on soil mechanics and foundation engineering1, 51–53.
[67] Dway, S. M. M., and Thant, D. A. A. 2014. Soil Compression Index Prediction Model for Clayey Soils. Int. J. Scientific Eng. and Tech. Research 3(11), 2458-2462.
[68] Gunduz, Z., and Arman, H. 2007. Possible Relationships between Compression and Recompression Indices of a Low-Plasticity Clayey Soil. The Arabian J. for Science and Eng. 32(2B), 179-190.
[69] Kalantary, F., and Kordnaeij, A. 2012. Prediction of Compression Index UsingArtificial Neural Network. Scientific Research and Essays 7(31), 2835-2848.
[70] Koppula, S. D. 1981. Statistical Estimation of Compression Index, GeotechnicalTesting Journal, GTJODJ. 4(2), 68-73.DOI: 10.1520/GTJ10768J
[71] Gofar, N. and al. 2008. Performance of ground

improvement by pre-compression and vertical drain. Proc. Int. conf.Geotropika.
[72] Susanti,R. D., Waruwu, M. andWaruwu, A. 2017. Bearing capacity improvement of peat soil by preloading, Arpn Journal of Engineering and Applied Sciences 12(1), 121-124.
[73] Lopez-Caballero,F.,Modaresi-Farahmand-Razavi,A., Stamatopoulos,C.,Peridis,P.2012. Field test measuring the effect of preloading on soil properties affecting the seismic response and numerical simulation. Proc. Int. conf. 15 thWCEE,Lisbona.
[74] Mehrshahi,K.,Alielahi, H. 2017. Estimating Geotechnical Design Parameters of Improved Soil by the Preloading Method Using Instrumentation Results and Numerical Approach- a Case Study, Journal of Ferdowsi Civil Engineering. 30(1), 13-30. DOI: 10.22067/civil.v1i30.52137
[75] Zaman,W.,et al.2016. A study on correlation between consolidation properties of soil with liquid limit, in situ water content, void ratio and plasticity index, Geotechnics for Sustainable Infrastructure Development - Geotec Hanoi, Phung (edt). ISBN 978-604-82-1821-8.
[76] Zaman, W.,et al.2017. Correlation Studies between Consolidation Prop. & Some Index Prop. for Dhaka-Chi. Highway Soil. Proc. Int. conf. 1st International Conference on Engineering Research and PracticeDhaka, Bangladesh, pp 4-5.
[77] Sorensen, K.K. 2013. Correlation between drained shear strength and plasticity index of undisturbed overconsolidated clays, Proc. Int. conf. of the 18th International Conference on Soil Mechanics and Geotechnical Engineering 423-428.
[78] Lim,G.T., et al.2018. Predicted and measured behaviour of an embankment on PVD-improved Ballina clay, Computers and Geotechnics 93 (C), 204–221. DOI: 10.1016/j.compgeo.2017.05.024
[79] Zdravković, L., Jardine, R.J. 2001. The effect on anisotropy of rotating the principal stress axes during consolidation. Géotechnique51(1), 69–83.
[80] Onyejekwe, S., Kang, X., andGe, L. 2014.Assessment of empirical equations for the compression index of fine-grained soils in Missouri, Bull EngGeol Environ, Springer-Verlag Berlin Heidelberg. DOI 10.1007/s10064-014-0659-8
[81] Clemence, S.P., Finbarr, A.O. 1981. Design considerations for collapsible soils. Journal of the Geotechnical Engineering Division, ASCE, 107(GT3), 305-317.
[82] Gunduz,Z.,Arman,H. 2007.Possible relationships between compression and recompression indices of a low–plasticity clayey soil, The Arabian Journal for Science and Engineering 32 (2B), 179- 190.

EFFECTS OF GRAIN SHAPE ON THE STANDARD PENETRATION TEST AND PARTICLE PACKING

VPLIVI OBLIKE ZRN NA STANDARDNI PENETRACIJSKI PREIZKUS IN PAKIRANJE DELCEV

Ender Basari *(corresponding author)*
Manisa Celal Bayar university,
Department of civil engineering
Yunusemre / Manisa, Turkey
E-mail: ender.basari@cbu.edu.tr

Gurkan Ozden
Dokuz Eylul university,
Department of civil engineering
Buca / Izmir, Turkey
E-mail: gurkan.ozden@deu.edu.tr

DOI https://doi.org/10.18690/actageotechslov.17.2.65-75.2020

Keywords

mica, grain packing, delta deposit, sandy soil, standard penetration test

Ključne besede

sljuda, pakiranje zrn, rečna usedlina, peščena zemljina, standardni penetracijski preizkus

Abstract

Coarse soils can contain flaky grains in addition to rounded or angular grains, along with a varying fines content. Depending on the regional geology, however, the mica grain content can be remarkable, reaching 30 % or higher. Therefore, it is reasonable to expect that mica grains would affect the soil behaviour. In this study, soils of a delta deposit that are known to involve mica grains were examined. The river sand was considered as the host material and the mica grain contents were determined by means of the flotation technique. A correlation between the mica content as found using the flotation technique and XRD count numbers obtained using an X-ray diffraction test method for each soil sample was established. The standard penetration test (SPT) blow counts from various boreholes were interpreted from the mica content's influence point of view. The results showed that the mica grains would reduce the SPT resistance at certain fines-content, host-sand, mica-grain combinations. The reduction in the SPT resistance as a result of the presence of mica grains might reach eight units at depths close to the ground surface. This influence is expressed by means of a dimensionless parameter (MC_{ef}); however, it diminished with an increasing effective stress and fines content. The findings of the present study show that the influence of particle shape on the overall soil behaviour deserves further study.

Izvleček

Grobozrnate zemljine lahko poleg zaobljenih ali oglatih zrn vsebujejo tudi luskava zrna in različno vsebino drobnih delcev. Odvisno od regionalne geologije pa je vsebnost zrn sljude lahko izjemna in doseže 30 % ali več. Zato je smiselno pričakovati, da bi zrna sljude vplivala na obnašanje zemljin. V tej študiji so bile preučene zemljine rečnih usedlin, za katera je znano, da vsebujejo zrna sljude. Rečni pesek je bil gostiteljski material, vsebnost sljude pa je bila določena s flotacijsko tehniko. Za vsak vzorec zemljine je bila ugotovljena korelacija med vsebnostjo sljude, ugotovljena s flotacijsko tehniko, in številom XRD, dobljenim z rentgensko difrakcijsko preizkusno metodo. Število udarcev s standardnim penetracijskim preizkusom (SPT) iz različnih vrtin je bilo interpretirano z vidika vpliva vsebnosti sljude. Rezultati so pokazali, da bi zrna sljude zmanjšala odpornost na SPT pri določenih kombinacijah vsebnosti finih zrn, gostitelj-pesek in sljude. Zmanjšanje odpornosti pri SPT zaradi prisotnosti zrn sljude lahko doseže osem enot v globinah blizu površine tal. Ta vpliv je izražen s pomočjo brez dimenzionalnega parametra (MC_{ef}), ki se zmanjša z naraščajočo efektivno napetostjo in vsebnostjo finih delcev. Ugotovitve te študije kažejo, da si vpliv oblike delcev na splošno obnašanje zemljine zasluži nadaljnjo študijo.

1 INTRODUCTION

Soils are made of grains that reflect the mineralogical characteristics of the parent rocks from which they were formed by means of various weathering processes. It has long been recognized that grain shape has a considerable influence on soil behaviour. Mica grains are well known representatives of flaky grains. Soils involving 20 % or more mica grains were reported in Gidigasu (1976) [1], Bokhtair et al. (2000) [2]; Regmi et al. (2014) [3], Sun et al. (2017) [4], Tschernutter (2011) [5], Wang et al. (2015) [6], Chang et al. (2011) [7].

The mica grains are generally flaky shaped, and they can have a significant influence on the soil's response; Bokhtair et al. (1999) [8], Lee et al. (2007) [9], Santamarina and Cho (2004) [10], Cabalar and Cevik (2009) [11]. This remark especially holds for soils where sand-size mica grains are present in granular soils; Cabalar and Akbulut (2016) [12], Cerri et al. (2018) [13], Ghalehjough (2018) [14], Gilroy (1928) [15], Johnson et al. (1969) [16], Clayton et al. (2004) [17], Cabalar and Akbulut (2016) [18], Goktepe and Sezer (2010) [19], Cabalar and Mustafa (2015) [20], Cabalar and Demir (2019) [21]. It is a well-known fact that the compressibility of rigid particles such as grains composed of quartz, feldspar, or similar minerals are negligible, whereas the presence of platy grains can result in large volumetric deformations; Roberts and deSouza (1958) [22]. Similarly, some researchers reported that large-size mica flakes have a remarkable effect on the shear strength of the host sand; Harris et al. (1984a) [23], Harris et al. (1984b) [24], Hattamleh et al. (2010) [25]. Mica grains can also change the dynamic behaviour of sandy soils; Cabalar (2010) [26], Cabalar and Cevik (2011) [27], Cabalar et al. (2013) [28], Cabalar (2018) [29].

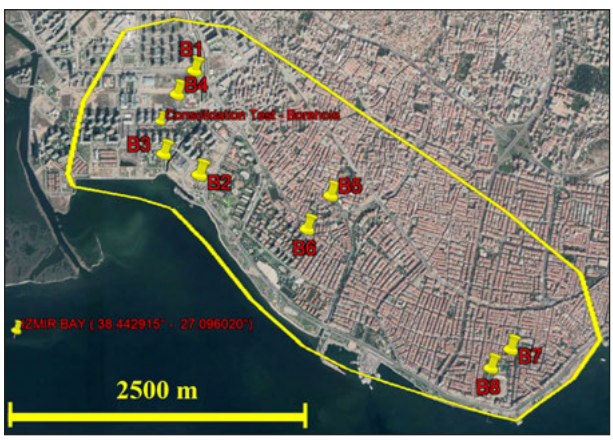

Figure 1. Borehole locations as shown on satellite view of the project area.

Past studies, as mentioned above, involved laboratory testing programs conducted using artificially prepared sand and mica mixtures. In this research, however, the mica grains' effect on the standard penetration test's resistance was studied using the data acquired from saturated alluvial deposits of Old Gediz River Delta (Fig. 1).

2 CHARACTERISTICS OF THE SOIL SAMPLES

The soil profile in the study area with a surface area of approximately 7.5 km^2 was formed by the sediments transported by the Gediz River. The riverbed was shifted towards the northwest in order to avoid the rapid deposition of the transport sediments into the İzmir Bay. The area was then open to settlement in late 1960s and locally called the Old Gediz River Delta. Although depth intervals for certain soil types do not vary abruptly in the region, the soil profile still exhibits considerable variations, even for the short distances typical of the alluvial soil deposits. Alternating, soft, cohesive and loose-to-medium-dense cohesionless soils along with frequent horizontally discontinuous clayey or sandy pockets are common in the region. The basic characteristics of the soil samples that were used in this study are given in Table 1. As we can see in this table, the majority of the sand samples are classified as silty sand (SM), whereas occasional clayey sands (SC) samples are encountered at certain depths. The fines portion of such samples, however, are classified as low plasticity clay.

As mentioned above, cohesive soils are in a very soft to soft consistency state and in general they can be considered as under consolidated, as illustrated by

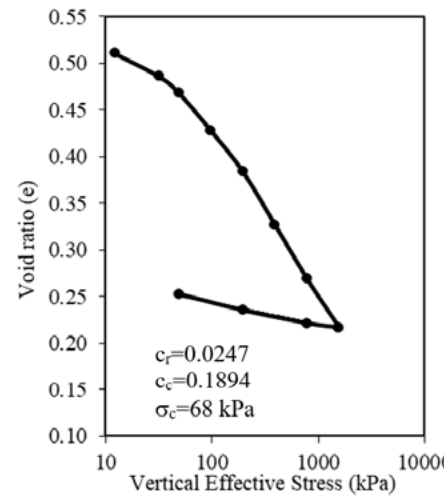

Figure 2. Consolidation test results for clayey layer in the study area.

the compression curve (Fig. 2) of a consolidation test performed on an undisturbed clay sample recovered at a depth of 22.25 m below the surface. The layers that are dominated by sandy soils, on the other hand, are assessed as normally consolidated due to their higher permeability and consequent faster compressibility characteristics.

3 EXPERIMENTAL STUDY

The soil samples from the cohesionless layers were recovered mostly by means of an SPT split-spoon sampler. The SPT tests were performed using a semi-automatic safety type hammer in all seven boreholes, according to ASTM D1586. The borehole diameters were less than or equal to 100 mm. Great care was taken so that the suction pressure did not take place during the lifting off the drilling set from the borehole and the SPT tests commenced after waiting for an appropriate amount of time, so that any possible excess pore pressure induced during the drilling operation could dissipate.

The presence of mica grains in the recovered soil samples could even be detected with the naked eye, due their shiny colour. The mineralogical structure of the flaky grains mainly consists of a muscovite mineral, according to the XRD test results. The percentage by weight of mica grains in the recovered samples was determined by evaluating the XRD data. Firstly, the reference samples with a certain amount of mica grains were established using the material (at about 150–200 grams of mica) already separated using the flotation technique, as described by Geredeli and Ozbayoglu (1995) [30]. In the flotation technique, the properties of mineral surfaces were altered to a hydrophobic or hydrophilic condition with chemical additive materials. That is, the surfaces of the mineral grains are either repelled or attracted by water. The condition of the created pulp (slurry) provides for the attachment of pre-determined mineral particles to air bubbles. The air bubbles carry the selected minerals to the surface of the pulp, pre-determined mineral, which is in the froth phase, is skimmed off and collected in a can. Other minerals remain submerged in the pulp. It was thought that the XRD count values of the reference samples would serve as the basis for determining the mica content of the field samples that were subject to an XRD test as well. The XRD test specimens for the reference and field samples were prepared by grinding 5 grams of material without changing the mineral content. The ambient temperature and humidity were kept constant throughout the XRD testing program. The experimental procedure and the sequence of the tests are described in Fig. 3.

4 TEST RESULTS

The mica contents of the reference samples were approximately set as 0 %, 5 %, 10 %, 20 %, 38 %, 56 % and 77 % for samples R1–7. It is important to note that "approximately" stands for the small amount of unseparated

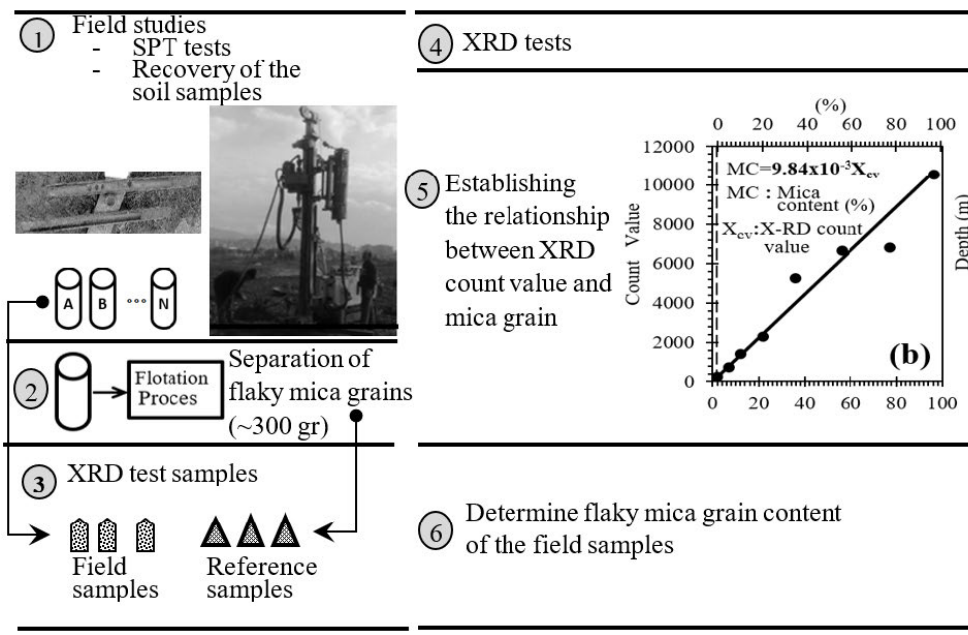

Figure 3. Sequence of mica grain content determination using the XRD technique.

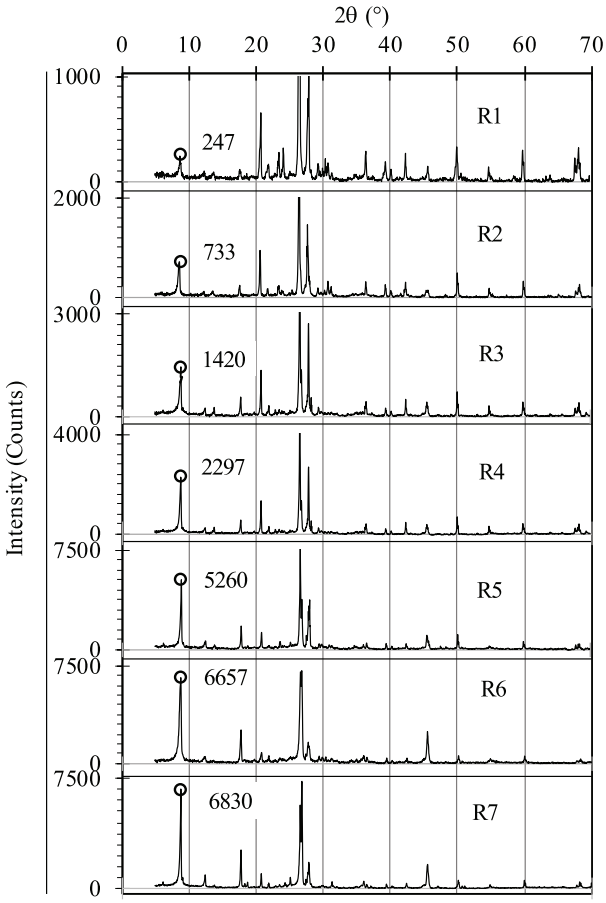

Figure 4. XRD test results for the reference samples.

mica and sand grains that would be left in the so-called pure mica or sand grains. The XRD test results of the reference samples are given in Fig. 4. The relationship between the XRD count values and the mica contents were established by Basari and Ozden (2013) [31] using the methodology proposed by Aydal (1990) [32]. In this respect, the characteristic patterns of the mica and quartz minerals were taken into consideration as a priority. It can be seen in Fig. 5 that certain peaks that are present in both patterns coincide, making it difficult to distinguish the mica at larger diffraction angles. Therefore, the peak

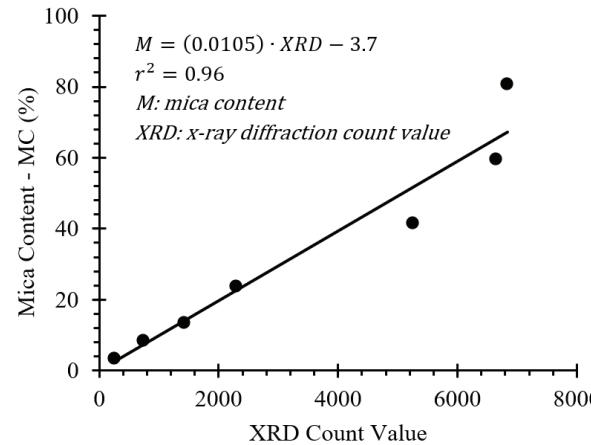

Figure 6. Relationship between the XRD count and the mica content.

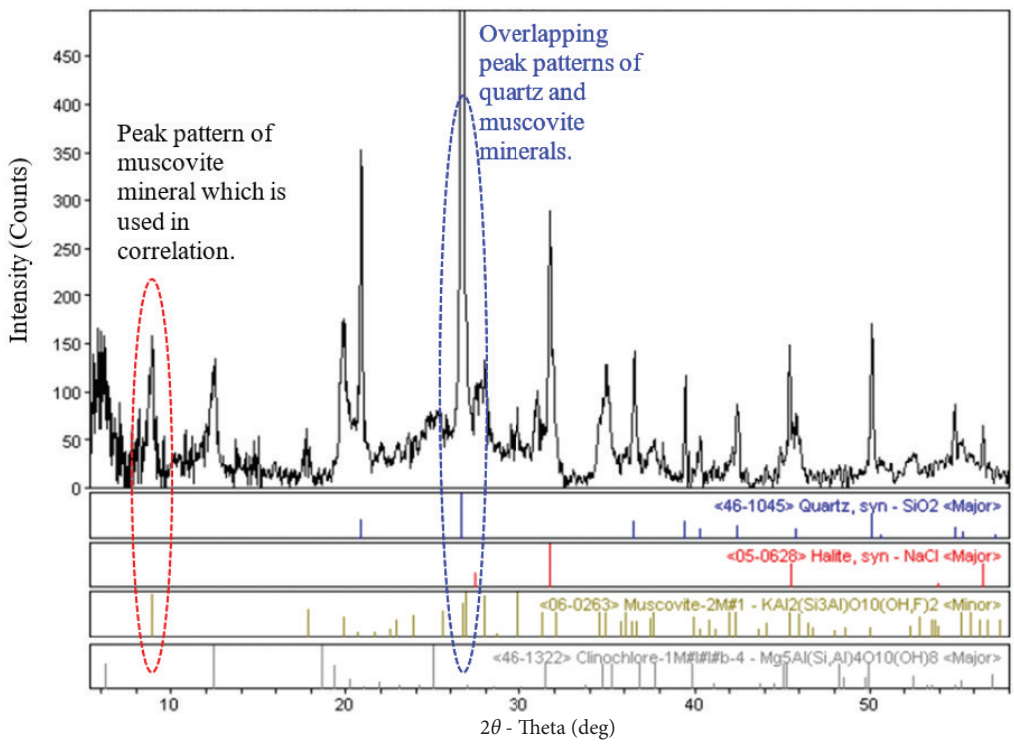

Figure 5. Peak patterns of the muscovite, quartz and some other minerals.

count value at 2θ=8.8° for the mica mineral (see Fig. 4) was used while establishing the correlation, as shown in Fig. 6.

The variations of the SPT blow counts for the silty sand samples recovered from various boreholes are given in Table 1. The coarse, fine and mica fractions of the samples are also provided in the same table. The groundwater table is 2 m below the grade, on average. The mica content of the field samples, as given in Table 1, were determined using the above-described methodology.

It is well known that overburden stress, fines content, excess pore pressure, rod length and the energy

Table 1. SPT resistance and properties of SPT samples.

Sample No	Bore Hole (*)	Depth (m)	-No.4 (%)	-No.200 (%)	Liquid limit w_{LL}	Plasticity index I_p	USCS (**)	SPT resistance	XRD Count Value (Intensity) for 2θ=8.88°	Flaky grain (mica) content(%)
S1	B1	8.3	100.0	42.5	37	NP	SM	13	1676	13.9
S2	B2	7.7	99.6	22.9	40	23	SC	20	3048	28.3
S3	B2	20.3	70.1	19.2	60	27	SM	22	2686	24.5
S4	B3	4.7	99.7	16.7		NP	SM	22	581	2.4
S5	B3	6.3	98.2	11.8	57	32	SP-SC	21	543	2.0
S6	B3	18.3	93.9	24.0		NP	SM	16	1667	13.8
S7	B3	21.3	95.6	35.0	32	17	SC	12	2267	20.1
S8	B4	4.7	98.6	17.0		NP	SM	17	3000	27.8
S9	B4	6.3	94.1	9.0		NP	SP-SM	13	1514	12.2
S10	B4	9.3	98.1	6.8		NP	SP-SM	23	1362	10.6
S11	B5	7.8	100.0	33.3		NP	SM	20	2429	21.8
S12	B5	10.8	100.0	34.7		NP	SM	22	495	1.5
S13	B5	13.8	97.3	40.1		NP	SM	12	1476	11.8
S14	B6	9.3	100.0	41.2	42	17	SC	13	1295	9.9
S15	B6	10.7	100.0	47.6	41	NP	SM	13	667	3.3
S16	B7	2.0	81.3	22.4	30	12	SC	15	1150	8.4
S17	B7	3.3	92.2	10.6		NP	SP-SM	13	1895	16.2
S18	B7	4.8	90.0	15.2	30	NP	SM	18	2162	19.0
S19	B7	6.3	99.3	15.0	29	NP	SM	16	1152	8.4
S20	B7	7.8	98.2	38.6	31	NP	SM	14	2371	21.2
S21	B7	9.3	89.4	8.8		NP	SP-SM	20	2505	22.6
S22	B7	10.8	98.0	10.0		NP	SP-SM	18	3095	28.8
S23	B7	15.4	97.1	47.2				12	2514	22.7
S24	B7	19.8	99.8	31.3				8	1429	11.3
S25	B7	21.3	98.0	30.0	33	NP	SM	11	1095	7.8
S26	B7	23.3	100.0	48.0	60	41	SC	19	2238	19.8
S27	B7	24.3	99.7	48.5				21	990	6.7
S28	B7	25.8	97.0	42.0	60	41	SC	14	1010	6.9
S29	B7	27.3	96.6	37.0				18	1810	15.3
S30	B8	6.3	100.0	43.6	35	NP	SM	20	1419	11.2
S31	B8	9.3	100.0	42.9	36	NP	SM	12	905	5.8
S32	B8	20.3	78.0	18.2	31	14	SC	24	1705	14.2

* Borehole depths: B1: 300m; B2-B4-B6-B8: 21m; B3: 150m; B5: 60m; B7: 144m
** USCS: Unified Soil Classification System

efficiency of the SPT equipment and some other factors such as borehole diameter and split-spoon liner have significant effects on the SPT resistance. Several researchers, Gibbs and Holtz (1957) [33], Riggs (1986) [34], Schmertmann (1979) [35], Seed (1985) [36], Skempton (1986) [37], proposed corrections to be applied to the SPT resistance so that the data could be standardized.

The SPT blow counts should be isolated from aforementioned effects in order to make the influence of the mica grains on the SPT resistance visible (Fig. 7). For this purpose, the SPT data with fine contents vary in a range for certain depth intervals are grouped in a matrix where the groups are tagged from A to J and the SPT blow counts are plotted with respect to the mica contents, as shown in Fig. 8. The graphs given in groups A to D reveal that the SPT resistance decreases as the mica content increases. Variations in the SPT and mica content data are denoted with the symbols ΔSPT and ΔMC in the graph of Group A. A new parameter to define the influence of a unit increase in the mica content on the SPT blow count variation is proposed as MC_{ef}=ΔSPT/ΔMC. ΔSPT represents the maximum variation in the SPT resistance for a group and ΔMC stands for the maximum variation in the mica content for a group as well. The suppressing effect of the effective stress on the influence of the mica content on the SPT blow count, however, can be noticed by comparing the graphs of Group A and B, as well as the Groups C and D. On the other hand, similar effects are not visible in Groups E, F, G, H, I and J.

It can be seen that the effect of the mica grains on the SPT resistance depends on the fines content upon

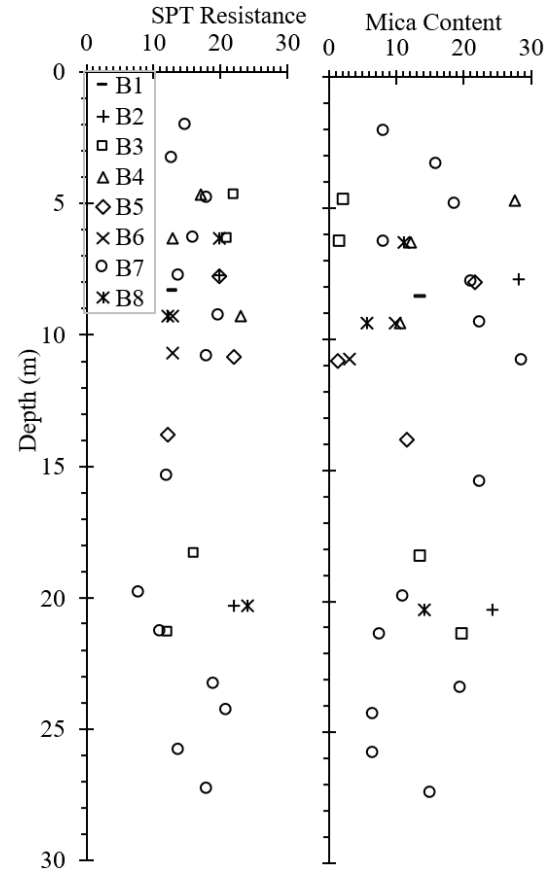

Figure 7. Variation of SPT resistances and mica grain contents.

examining the graphs of Group A, B, C and D. When comparing Group A with Group C, for instance, it is clear that the effect of the mica grains (MC_{ef}) on the SPT resistance is more visible in Group A than in Group C.

Table 2. Depth and fine material properties of the groups as illustrated in Fig. 8.

Group	Depth (m)		Fine Material Content (FC) % (-No.200)		ΔSPT	ΔMC	$MC_{ef} = \Delta SPT/\Delta MC$
	Depth interval	Average depth	Minimum and Maximum FC	Average FC			
A	2.0~7.0	~4.5	5.0 ~15.0	~10	8	14.2	$MC_{ef(A)} = 0.563$
B	7.0~12.0	~9.5	5.0 ~15.0	~10	5	18.2	$MC_{ef(B)} = 0.275$
C	2.0~7.0	~4.5	15.0 ~35.0	~25	7	25.4	$MC_{ef(C)} = 0.276$
D	7.0~12.0	~9.5	15.0 ~35.0	~25	2	26.8	$MC_{ef(D)} = 0.075$
E	12.0~20.0	~16.0	15.0 ~35.0	~25	Mica grain effect could not be observed		
F	20.0~28.0	~24.0	15.0 ~35.0	~25	Mica grain effect could not be observed		
G	2.0~7.0	~4.5	35.0 ~50.0	~42	Mica grain effect could not be observed		
H	7.0~12.0	~9.5	35.0 ~50.0	~42	Mica grain effect could not be observed		
I	22.0~20.0	~16.0	35.0 ~50.0	~42	Mica grain effect could not be observed		
J	20.0~28.0	~24.0	35.0 ~50.0	~42	Mica grain effect could not be observed		

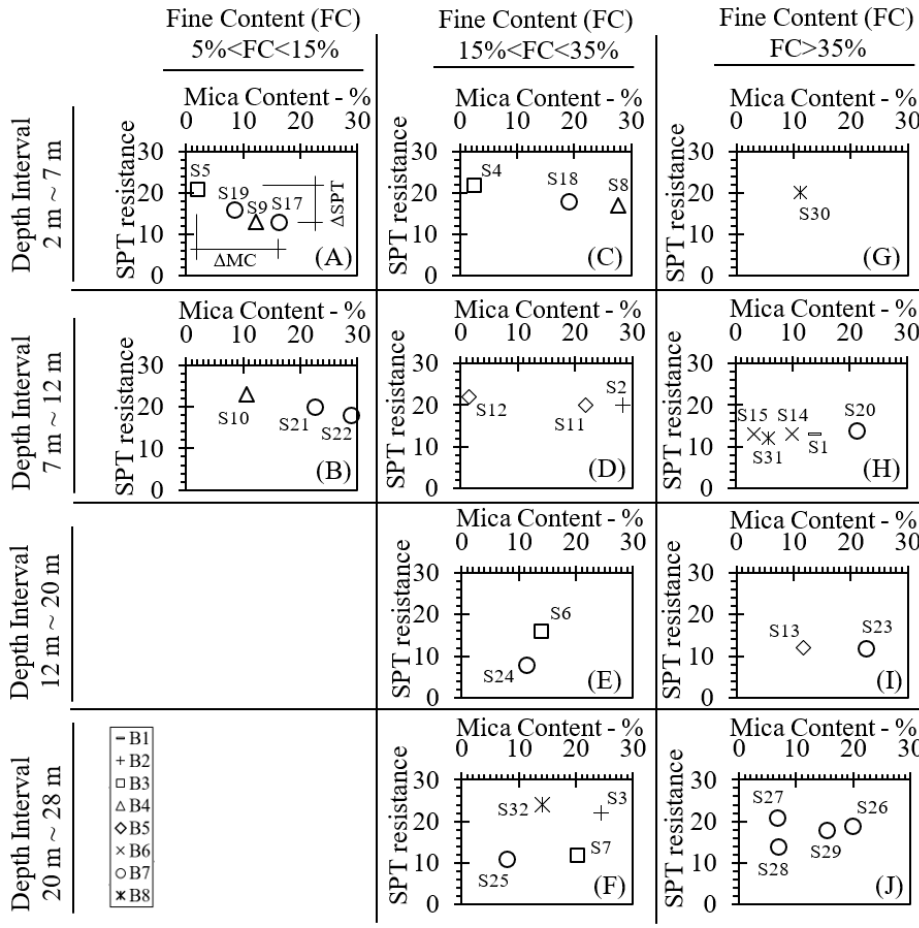

Figure 8. Grouped SPT resistances and mica grain contents.

A similar trend is also pronounced for Groups B and D. These comparisons show that the influence of the mica grains on the SPT resistance decreases with increasing fines content. This trend is especially obvious in the graph of Group H, where the fines content exceeds 35 %. The SPT blow counts of the E, F, I, and J groups, on the other hand, do not yield a meaningful relationship with the mica content variation. This can be attributed to the higher effective stresses beyond 12 m depth. The average depth, mica content and fine content values pertaining to each group are given in Table 2.

The effect of mica grains (MC_{ef}) on the SPT resistance, as determined from graphics A, B, C and D, are plotted in

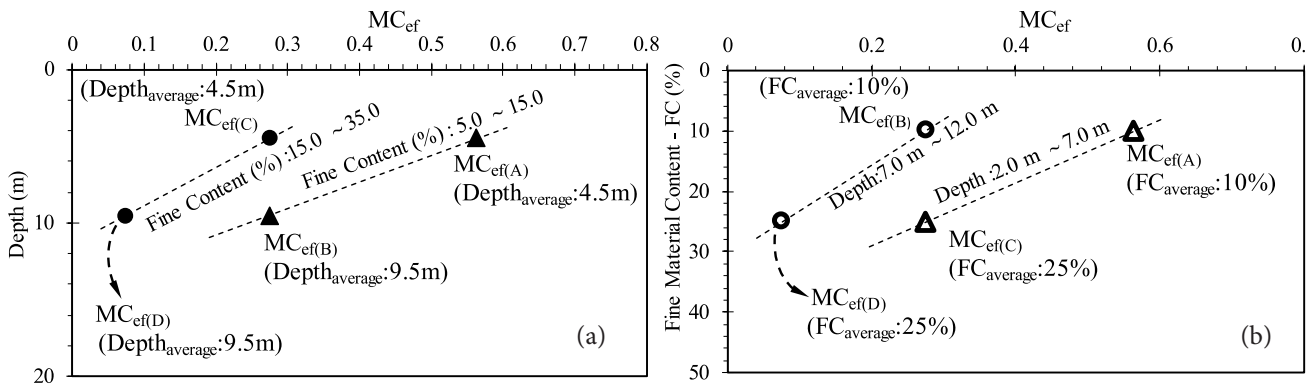

Figure 9. Variation of mica grain effect on SPT resistance (MC_{ef}) with depth (a), and fine material content (b).

Fig. 9. The variation of MC_{ef} with depth for different fine contents is plotted in Fig. 9a. The variation of MC_{ef} with the fine material content for different depth intervals, on the other hand, is plotted in Fig. 9b. Fig. 9a and Fig. 9b clearly show that the effect of mica grains (MC_{ef}) on the SPT resistance depends on the depth and the fine material content.

5 INFLUENCE MECHANISM OF THE MICA GRAINS ON THE SPT RESISTANCE

The effects of grain shape can be taken into consideration on a global (i.e., macro level) scale where the stress-strain response of the soil mixture is observed, and in the grain (i.e., micro level) scale such as grain angularity and roughness. The grain level soil characteristics govern the particle packing and mechanical response of the soil mass, Thevanayagam (2007a) [38], Thevanayagam (2007b) [39], Cho et al. (2006) [40], Cavarretta and Sullivan C. (2012) [41], Cabalar et al. (2019) [42], Cavarretta et al. (2010) [43]. The particle shape of the soil grains plays a major role in the packing of the soil grains via the ordering and orientation of the particles, especially for coarse–grained soils.

The mica effect on sand behaviour can be explained with the bridging concept, as shown in Fig. 10.a. According to this concept, mica grains create bridges among the sand grains, and increase the global void ratio. When the global void ratio increases, the shear strength of the sand decreases, while the compressibility of the sand increases. Similar concepts and mechanisms have been accepted for decades and they are supported by experimental studies such as the triaxial compression test, Bokhtair et al. (1999) [8], one-dimensional compression test, Lee et al. (2007) [9], and compaction test, Harris et al. (1984a) [23]. As mentioned in this paper, the mica grain effect was also observed in standard penetration test data. However, it was found that the macro scale effect of mica grains was restricted or suppressed by the fine material content and an increasing effective stress.

The macro scale effect of mica grains was more visible in sandy soils containing less than 30–35 % fine material and/or in shallow depths (to a depth of 10–12 m). This can be explained by the fact that the fine material is located in gaps, which are created by bridging mica grains and they cause a decrease in the mica ordering and orientation effects, as shown in Fig. 10c. and Fig. 10d. The effective stress causes a decrease in the mica ordering and orientation as well. The effective confining stress around the grains increases with depth and the bridges formed by the mica grains collapse, leading to a major reduction in both the number of the gaps and the global void ratio of the soil mass, as shown in Fig. 10b and Fig. 10d. Decreasing the gap and the void ratio reduces the influence of mica ordering and mica

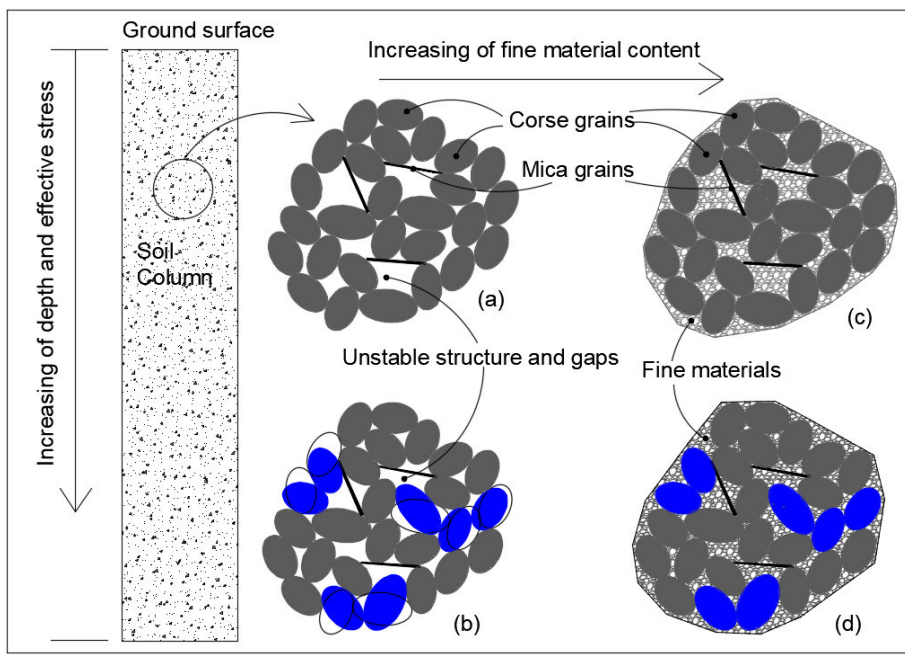

Figure 10. Interactions of mica grains, coarse grains and fine materials under the influence of the effective stress.

orientation. It seems that beyond certain combinations of effective stress and fine material content, the soil response, as reflected by SPT resistance, is not governed by the presence of mica grains.

6 CONCLUSIONS AND RECOMMENDATIONS

In this study it was understood that mica grains might have a significant effect on the standard penetration test blow counts, provided that the effective stress and fine material content are less than 100 kPa and 15 %, respectively. On the other hand, beyond certain combinations of fine material contents and effective stresses, the macro scale effect of the mica grains was either suppressed or restricted. This is best illustrated by Fig. 9, where the MC_{ef} parameter defining the shift in SPT resistance is plotted with respect to the mica content and the depth. It should be noted that Fig. 9 is produced using the data given in Table 2. This finding is interesting in the sense that the SPT resistance is not only a function of the fines content, but the grain shape may also have a marked influence on the blow counts for certain effective-stress, fines-content pairs. It is known that flaky mica grains constitute bridges across the host sand grains, resulting in the formation of soil layers with larger void ratios. This mechanism, however, is suppressed by increasing the effective stress, since the mica bridges become compressed, causing a reduction in the global void ratio.

It would be worthwhile to enhance the data set to further examine the interactions among the host sand, the mica grains and the fines content under varying confining stress conditions. The influence of cementation and over the consolidation ratio were not studied in this context.

Acknowledgment

The authors would like to acknowledge the financial support provided by T.R. Prime Ministry State Planning Organization and The Scientific & Technological Research Council of Turkey and the TÜBİTAK BİDEB program.

REFERENCES

[1] Gidigasu, M.D. 1976. Laterite soil engineering. Elsevier, Amsterdam, The Netherlands.

[2] Bokhtair M., Muqtadir, A. and Ali, M.H. 2000. Effect of mica content on stress - deformation behaviour of micaceous sand. Journal of Civil Engineering The Institution of Engineers Bangladesh 28(2):155-167.

[3] Regmi, A.D., Yoshida, K., Dhital, M.R. and Pradhan, B. 2014. Weathering and mineralogical variation in gneissic rocks and their effect in Sangrumba Landslide, East Nepal. Environ Earth Sci 71: 2711. https://doi.org/10.1007/s12665-013-2649-8

[4] Sun, W., Wang, L., Wang, Y. 2017. Mechanical properties of rock materials with related to mineralogical characteristics and grain size through experimental investigation: a comprehensive review, Front. Archit. Civ. Eng. 11(3):322-328.

[5] Tschernutter, P. 2011. Influence of soft rock-fill material as dam embankment with central bituminous concrete membrane, Front. Archit. Civ. Eng. 5(1):63-70.

[6] Wang, A., Li, X., Huang, Z., Huang, X., Wang, Z., Wu, Q., Cui, J. and Lu, X. 2015. Laboratory study on engineering geological characteristics and formation mechanism of altered rocks of Henan Tianchi pumped storage power station, China. Environ Earth Sci 74: 5063. https://doi.org/10.1007/s12665-015-4520-6

[7] Chang, N., Heymann, G. and Clayton, C. 2011. The effect of fabric on the behaviour of gold tailings. Géotechnique, 61(3), 187-197. DOI: 10.1680/geot.9.P.066

[8] Bokhtair, M., Muqtadir, A. and Ali, M.H. 1999. Stress-path dependent behaviour of micaceous sand. Journal of Civil Engineering The Institution of Engineers Bangladesh 27(2):129-141.

[9] Lee, J.S., Guimaraes, M. and Santamarina, J.C. 2007. Micaceous sands: Microscale mechanisms and macroscale response. Journal of Geotechnical and Geoenvironmental Engineering 133(9):1136-1143.

[10] Santamarina, J.C. and Cho, G.C. 2004. Soil Behavior: The Role of Particle Shape. Proc. Skempton Conf., March, London.

[11] Cabalar, A.F. and Cevik, A. 2009. Modelling damping ratio and shear modulus of sand-mica mixtures using neural networks. Engineering Geology 104:31-40.

[12] Cabalar, A.F. and Akbulut, N. 2016. Effects of the particle shape and size of sands on the hydraulic conductivity. Acta Geotechnica Slovenica, 13(2):83-93.

[13] Cerri, R.I., Reis, F.A.G.V., Gramani, M.F., Rosolen, V., Luvizotto, G.L., Giordano, L.C. and Gabelini, B.M. 2018. Assessment of landslide occurences in Serra do Mar mountain range using kinematic analyses. Environ Earth Sci 77: 325. https://doi.org/10.1007/s12665-018-7508-1

[14] Ghalehjough, B.K., Akbulut, S. and Celik, S. 2018.

Effect of particle roundness and morphology on the shear failure mechanism of granular soil under strip footing. Acta Geotechnica Slovenica, 15(1):43-53.
[15] Gilroy, G. 1928. The compressibility of sand-mica mixtures. Proc. Am. Soc.Civ. Eng. 54:555-568.
[16] Jhonson deGraft, J.W.S., Bhatia, H.S. and Gidigasu, D.M. 1969. The strength characteristics of residual micaceous soil and their application to stability problems. Proc. 7th Int. Conf. Soil Mech. Found. Eng. Mexico. 1:165-172.
[17] Clayton, C.R.I., Theron, M. and Best, A.I. 2004. The measurement of vertical shear-wave velocity using side-mounted bender elements in the triaxial apparatus. Géotechnique, 54(7), 495-498.
[18] Cabalar, A.F. and Akbulut, N. 2016. Evaluation of actual and estimated hydraulic conductivity of sands with different gradation and shape. SpringerPlus, 5:820, 1-16, doi:10.1186/s40064-016-2472-2
[19] Goktepe, A.B. and Sezer, A. 2010. Effect of particle shape on density and permeability of sands. Proc Inst Civil Eng. Geotech Eng. 163(6):307–320, doi: 10.1680/geng.2010.163.6.307
[20] Cabalar, A.F., and Mustafa, W S. 2015. Fall cone tests on clay–sand mixtures. Eng. Geology 192, 154-165, http://dx.doi.org/10.1016/j.enggeo.2015.04.009
[21] Cabalar, A.F. and Demir, S. 2019. Fall-cone testing of unsaturated sand–clay mixtures, Proceedings of the Institution of Civil Engineers-Geotechnical Engineering (in press), doi:10.1680/jgeen.18.00155
[22] Roberts, J.E. and deSouza, J.M. 1958. The compressibility of sands. Am. Soc. Test. and Meter. Proc. 58:1269-1277.
[23] Harris, W.G., Parker, J.C. and Zelazny, L.W. 1984a. Effects of mica content on engineering properties of sand. Soil Science Society of America Journal 48:501-505.
[24] Harris, W.G., Zelazny, L.W., Parker, J.C., Baker, J.C., Weber, R.S. and Elder, J.H. 1984b. Engineering properties of soils as related to mineralogy and particle-size distribution. Soil Science Society of America Journal 48:978-982.
[25] Hattamleh, O.A., AlShalabi, F., Qablan, H.A. and Al-Rousan, T. 2010. Effect of grain crushing and bedding plane inclination on Aqaba sand behavior. Bull Eng Geol Environ 69:41-49.
[26] Cabalar, A.F. 2010. Applications of the oedometer, triaxial and resonant column tests to the study of micaceous sands. Engineering Geology, 112, 21-28.
[27] Cabalar, A.F. and Cevik, A. 2011. Triaxial behavior of sand–mica mixtures using genetic programming. Expert Systems with Applications, 38, 10358-10367.
[28] Cabalar, A.F., Dulundu, K., and Tuncay, K. 2013. Strength of various sands in triaxial and cyclic direct shear tests. Engineering Geology. 156(1) 92-102. https://doi.org/10.1016/j.enggeo.2013.01.011
[29] Cabalar, A.F. 2018. Influence of grain shape and gradation on the shear behavior of sand mixtures. Scientia Iranica. Transaction A, Civil Engineering; 25(6): 3101-3109.
[30] Geredeli, A. and Ozbayoglu, G. 1995. Simav feldspatının flotasyonu. Endüstriyel Hammaddeler Sempozyumu:71-81, Izmir, Turkey.
[31] Basari, E. and Ozden, G. 2013. Post-liquefaction volume change in micaceous sandy soils of Old Gediz River Delta. Acta Geotechnica Slovenica, 13(1):33-40.
[32] Aydal, D. 1990. Cevherdeki toplam demir yuzdesinin XRD-floresans radyasyon siddeti yardimiyla kantitatif olarak bulunmasi. Maden Tetkik ve Arama Dergisi, 111: 133-152.
[33] Gibbs, H.J. and Holtz, W.G. 957. Research on Determining the Density of Sands by Spoon Penetration Testing. 4th ICSMFE 1:35-3.
[34] Riggs, C.O. 1986. American Standard Penetration Test Practice. 14thPSC, ASCE:949-967.
[35] Schmertmann, J.H. 1979. Statics of SPT. JGED, ASCE 105(GT5):655-670
[36] Seed, H.G. 1985. Influence of SPT Procedures in Soil Liquefaction Resistance Evaluations. JGED, ASCE 111(12):1425-1445
[37] Skempton, A.W. 1986. Standard Penetration Test Procedures. Géotechnique 36(3): 425-447
[38] Thevanayagam, S. 2007a. Intergrain contact density indices for granular mixes - I: Framework. Earthquake, Engineering And Engineering Vibration 6(2):123-134
[39] Thevanayagam, S. 2007b. Intergrain contact density indices for granular mixes - II: Framework. Earthquake, Engineering And Engineering Vibration 6(2):135-146
[40] Cho, G.C., Dodds, J. and Santamarina, C. 2006. Particle Shape Effects on Packing Density, Stiffness, and Strength: Natural and Crushed Sands. Journal of Geotechnical and Geoenvironmental Engineering, 132(5), 591-602, doi:10.1061/(ASCE)1090-0241(2006)132:5(591)
[41] Cavarretta, I. and O'Sullivan, C. 2012. The mechanics of rigid irregular particles subject to uniaxial compression. Géotechnique, 62(8), 681-692. http://dx.doi.org/10.1680/ geot.10.P.102
[42] Cabalar, A.F., Demir, S., and Khalaf, M.M. 2019. Liquefaction Resistance of Different Size/Shape Sand-Clay Mixtures Using a Pair of Bender Element–Mounted Molds. Journal of Testing and

Evaluation, 49 (in press). https://doi.org/10.1520/JTE20180677
[43] Cavarretta, I., Coop, M., and O'Sullivan, C. 2010. The influence of particle characteristics on the behavior of coarse grained soils. Géotechnique, 60(6):413-423. doi: 10.1680/geot.2010.60.6.413

NAVODILA AVTORJEM

Vsebina članka

Članek naj bo napisan v naslednji obliki:

- Naslov, ki primerno opisuje vsebino članka in ne presega 80 znakov.
- Izvleček, ki naj bo skrajšana oblika članka in naj ne presega 250 besed. Izvleček mora vsebovati osnove, jedro in cilje raziskave, uporabljeno metodologijo dela, povzetek izidov in osnovne sklepe.
- Največ 6 ključnih besed, ki bi morale biti napisane takoj po izvlečku.
- Uvod, v katerem naj bo pregled novejšega stanja in zadostne informacije za razumevanje ter pregled izidov dela, predstavljenih v članku.
- Teorija.
- Eksperimentalni del, ki naj vsebuje podatke o postavitvi preiskusa in metode, uporabljene pri pridobitvi izidov.
- Izidi, ki naj bodo jasno prikazani, po potrebi v obliki slik in preglednic.
- Razprava, v kateri naj bodo prikazane povezave in posplošitve, uporabljene za pridobitev izidov. Prikazana naj bo tudi pomembnost izidov in primerjava s poprej objavljenimi deli.
- Sklepi, v katerih naj bo prikazan en ali več sklepov, ki izhajajo iz izidov in razprave.
- Vse navedbe v besedilu morajo biti na koncu zbrane v seznamu literature, in obratno.

Dodatne zahteve

- Vrstice morajo biti zaporedno oštevilčene.
- Predložen članek ne sme imeti več kot 18 strani (brez tabel, legend in literature); velikost črk 12, dvojni razmik med vrsticami. V članek je lahko vključenih največ 10 slik. Isti rezultati so lahko prikazani v tabelah ali na slikah, ne pa na oba načina.
- Potrebno je priložiti imena, naslove in elektronske naslove štirih potencialnih recenzentov članka. Urednik ima izključno pravico do odločitve, ali bo te predloge upošteval.

Enote in okrajšave

V besedilu, preglednicah in slikah uporabljajte le standardne označbe in okrajšave SI. Simbole fizikalnih veličin v besedilu pišite poševno (npr. *v*, *T* itn.). Simbole enot, ki so sestavljene iz črk, pa pokončno (npr. Pa, m itn.). Vse okrajšave naj bodo, ko se prvič pojavijo, izpisane v celoti.

Slike

Slike morajo biti zaporedno oštevilčene in označene, v besedilu in podnaslovu, kot sl. 1, sl. 2 itn. Posnete naj bodo v katerem koli od razširjenih formatov, npr. BMP, JPG, GIF. Za pripravo diagramov in risb priporočamo CDR format (CorelDraw), saj so slike v njem vektorske in jih lahko pri končni obdelavi preprosto povečujemo ali pomanjšujemo.

Pri označevanju osi v diagramih, kadar je le mogoče, uporabite označbe veličin (npr. *v*, *T* itn.). V diagramih z več krivuljami mora biti vsaka krivulja označena. Pomen oznake mora biti razložen v podnapisu slike.

Za vse slike po fotografskih posnetkih je treba priložiti izvirne fotografije ali kakovostno narejen posnetek.

Preglednice

Preglednice morajo biti zaporedno oštevilčene in označene, v besedilu in podnaslovu, kot preglednica 1, preglednica 2 itn. V preglednicah ne uporabljajte izpisanih imen veličin, ampak samo ustrezne simbole. K fizikalnim količinam, npr. *t* (pisano poševno), pripišite enote (pisano pokončno) v novo vrsto brez oklepajev. Vse opombe naj bodo označene z uporabo dvignjene številke[1].

Seznam literature

Navedba v besedilu

Vsaka navedba, na katero se sklicujete v besedilu, mora biti v seznamu literature (in obratno). Neobjavljeni rezultati in osebne komunikacije se ne priporočajo v seznamu literature, navedejo pa se lahko v besedilu, če je nujno potrebno.

Oblika navajanja literature

V besedilu: Navedite reference zaporedno po številkah v oglatih oklepajih v skladu z besedilom. Dejanski avtorji so lahko navedeni, vendar mora obvezno biti podana referenčna številka.

Primer: »..... kot je razvidno [1,2]. Brandl and Blovsky [4], sta pridobila drugačen rezultat…«

V seznamu: Literaturni viri so oštevilčeni po vrstnem redu, kakor se pojavijo v članku. Označimo jih s številkami v oglatih oklepajih.

Sklicevanje na objave v revijah:

[1] Jelušič, P., Žlender, B. 2013. Soil-nail wall stability analysis using ANFIS. Acta Geotechnica Slovenica 10(1), 61-73.

Sklicevanje na knjigo:

[2] Šuklje, L. 1969. Rheological aspects of soil mechanics. Wiley-Interscience, London

Sklicevanje na poglavje v monografiji:

[3] Mitchel, J.K. 1992. Characteristics and mechanisms of clay creep and creep rupture, in N. Guven, R.M. Pollastro (eds.), Clay-Water Interface and Its Rheological Implications, CMS Workshop Lectures, Vol. 4, The clay minerals Society, USA, pp. 212-244..

Sklicevanje na objave v zbornikih konferenc:

[4] Brandl, H., Blovsky, S. 2005. Slope stabilization with socket walls using the observational method. Proc. Int. conf. on Soil Mechanics and Geotechnical Engineering, Bratislava, pp. 2485-2488.

Sklicevanje na spletne objave:

[5] Kot najmanj, je potrebno podati celoten URL. Če so poznani drugi podatki (DOI, imena avtorjev, datumi, sklicevanje na izvorno literaturo), se naj prav tako dodajo.

Podatki o avtorjih

Članku priložite tudi podatke o avtorjih: imena, nazive, popolne poštne naslove, številke telefona in faksa, naslove elektronske pošte. Navedite kontaktno osebo.

Sprejem člankov in avtorske pravlce

Uredništvo si pridržuje pravico do odločanja o sprejemu članka za objavo, strokovno oceno mednarodnih recenzentov in morebitnem predlogu za krajšanje ali izpopolnitev ter terminološke in jezikovne korekture. Z objavo preidejo avtorske pravice na revijo ACTA GEOTECHNICA SLOVENICA. Pri morebitnih kasnejših objavah mora biti AGS navedena kot vir.

Vsa nadaljnja pojasnila daje:

Uredništvo
ACTA GEOTECHNICA SLOVENICA
Univerza v Mariboru,
Fakulteta za gradbeništvo, prometno inženirstvo in arhitekturo
Smetanova ulica 17, 2000 Maribor, Slovenija
E-pošta: ags@um.si

INSTRUCTIONS FOR AUTHORS

Format of the paper

The paper should have the following structure:

- A Title, which adequately describes the content of the paper and should not exceed 80 characters;
- An Abstract, which should be viewed as a mini version of the paper and should not exceed 250 words. The Abstract should state the principal objectives and the scope of the investigation and the methodology employed; it should also summarise the results and state the principal conclusions;
- Immediately after the abstract, provide a maximum of 6 keywords;
- An Introduction, which should provide a review of recent literature and sufficient background information to allow the results of the paper to be understood and evaluated;
- A Theoretical section;
- An Experimental section, which should provide details of the experimental set-up and the methods used to obtain the results;
- A Results section, which should clearly and concisely present the data, using figures and tables where appropriate;
- A Discussion section, which should describe the relationships shown and the generalisations made possible by the results and discuss the significance of the results, making comparisons with previously published work;
- Conclusions, which should present one or more conclusions that have been drawn from the results and subsequent discussion;
- A list of References, which comprises all the references cited in the text, and vice versa.

Additional Requirements for Manuscripts

- Use double line-spacing.
- Insert continuous line numbering.
- The submitted text of Research Papers should cover no more than 18 pages (without Tables, Legends, and References, style: font size 12, double line spacing). The number of illustrations should not exceed 10. Results may be shown in tables or figures, but not in both of them.
- Please submit, with the manuscript, the names, addresses and e-mail addresses of four potential referees. Note that the editor retains the sole right to decide whether or not the suggested reviewers are used.

Units and abbreviations

Only standard SI symbols and abbreviations should be used in the text, tables and figures. Symbols for physical quantities in the text should be written in Italics (e.g. v, T, etc.). Symbols for units that consist of letters should

be in plain text (e.g. Pa, m, etc.).
All abbreviations should be spelt out in full on first appearance.

Figures

Figures must be cited in consecutive numerical order in the text and referred to in both the text and the caption as Fig. 1, Fig. 2, etc. Figures may be saved in any common format, e.g. BMP, JPG, GIF. However, the use of CDR format (CorelDraw) is recommended for graphs and line drawings, since vector images can be easily reduced or enlarged during final processing of the paper.

When labelling axes, physical quantities (e.g. *v*, *T*, etc.) should be used whenever possible. Multi-curve graphs should have individual curves marked with a symbol; the meaning of the symbol should be explained in the figure caption. Good quality black-and-white photographs or scanned images should be supplied for the illustrations.

Tables

Tables must be cited in consecutive numerical order in the text and referred to in both the text and the caption as Table 1, Table 2, etc. The use of names for quantities in tables should be avoided if possible: corresponding symbols are preferred. In addition to the physical quantity, e.g. *t* (in Italics), units (normal text), should be added on a new line without brackets.
Any footnotes should be indicated by the use of the superscript[1].

LIST OF references

Citation in text

Please ensure that every reference cited in the text is also present in the reference list (and vice versa). Any references cited in the abstract must be given in full. Unpublished results and personal communications are not recommended in the reference list, but may be mentioned in the text, if necessary.

Reference style

Text: Indicate references by number(s) in square brackets consecutively in line with the text. The actual authors can be referred to, but the reference number(s) must always be given:

Example: "... as demonstrated [1,2]. Brandl and Blovsky [4] obtained a different result ..."

List: Number the references (numbers in square brackets) in the list in the order in which they appear in the text.

Reference to a journal publication:

[1] Jelušič, P., Žlender, B. 2013. Soil-nail wall stability analysis using ANFIS. Acta Geotechnica Slovenica 10(1), 61-73.

Reference to a book:

[2] Šuklje, L. 1969. Rheological aspects of soil mechanics. Wiley-Interscience, London

Reference to a chapter in an edited book:

[3] Mitchel, J.K. 1992. Characteristics and mechanisms of clay creep and creep rupture, in N. Guven, R.M. Pollastro (eds.), Clay-Water Interface and Its Rheological Implications, CMS Workshop Lectures, Vol. 4, The clay minerals Society, USA, pp. 212-244.

Conference proceedings:

[4] Brandl, H., Blovsky, S. 2005. Slope stabilization with socket walls using the observational method. Proc. Int. conf. on Soil Mechanics and Geotechnical Engineering, Bratislava, pp. 2485-2488.

Web references:

[5] As a minimum, the full URL should be given and the date when the reference was last accessed. Any further information, if known (DOI, author names, dates, reference to a source publication, etc.), should also be given.

Author information

The following information about the authors should be enclosed with the paper: names, complete postal addresses, telephone and fax numbers and E-mail addresses. Indicate the name of the corresponding author.

Acceptance of papers and copyright

The Editorial Committee of the Slovenian Geotechnical Review reserves the right to decide whether a paper is acceptable for publication, to obtain peer reviews for the submitted papers, and if necessary, to require changes in the content, length or language.
On publication, copyright for the paper shall pass to the ACTA GEOTECHNICA SLOVENICA. The AGS must be stated as a source in all later publication.

For further information contact:

Editorial Board
ACTA GEOTECHNICA SLOVENICA
University of Maribor,
Faculty of Civil Engineering, Transportation Engineering and Architecture
Smetanova ulica 17, 2000 Maribor, Slovenia
E-mail: ags@um.si

NAMEN REVIJE

Namen revije ACTA GEOTECHNICA SLOVENICA je objavljanje kakovostnih teoretičnih člankov z novih pomembnih področij geomehanike in geotehnike, ki bodo dolgoročno vplivali na temeljne in praktične vidike teh področij.

ACTA GEOTECHNICA SLOVENICA objavlja članke s področij: mehanika zemljin in kamnin, inženirska geologija, okoljska geotehnika, geosintetika, geotehnične konstrukcije, numerične in analitične metode, računalniško modeliranje, optimizacija geotehničnih konstrukcij, terenske in laboratorijske preiskave.

Revija redno izhaja dvakrat letno.

AIMS AND SCOPE

ACTA GEOTECHNICA SLOVENICA aims to play an important role in publishing high-quality, theoretical papers from important and emerging areas that will have a lasting impact on fundamental and practical aspects of geomechanics and geotechnical engineering.

ACTA GEOTECHNICA SLOVENICA publishes papers from the following areas: soil and rock mechanics, engineering geology, environmental geotechnics, geosynthetic, geotechnical structures, numerical and analytical methods, computer modelling, optimization of geotechnical structures, field and laboratory testing.

The journal is published twice a year.

AVTORSKE PRAVICE

Ko uredništvo prejme članek v objavo, prosi avtorja(je), da prenese(jo) avtorske pravice za članek na izdajatelja, da bi zagotovili kar se da obsežno razširjanje informacij. Naša revija in posamezni prispevki so zaščiteni z avtorskimi pravicami izdajatelja in zanje veljajo naslednji pogoji:

Fotokopiranje

V skladu z našimi zakoni o zaščiti avtorskih pravic je dovoljeno narediti eno kopijo posameznega članka za osebno uporabo. Za naslednje fotokopije, vključno z večkratnim fotokopiranjem, sistematičnim fotokopiranjem, kopiranjem za reklamne ali predstavitvene namene, nadaljnjo prodajo in vsemi oblikami nedobičkonosne uporabe je treba pridobiti dovoljenje izdajatelja in plačati določen znesek.

Naročniki revije smejo kopirati kazalo z vsebino revije ali pripraviti seznam člankov z izvlečki za rabo v svojih ustanovah.

Elektronsko shranjevanje

Za elektronsko shranjevanje vsakršnega gradiva iz revije, vključno z vsemi članki ali deli članka, je potrebno dovoljenje izdajatelja.

COPYRIGHT

Upon acceptance of an article by the Editorial Board, the author(s) will be asked to transfer copyright for the article to the publisher. This transfer will ensure the widest possible dissemination of information. This review and the individual contributions contained in it are protected by publisher's copyright, and the following terms and conditions apply to their use:

Photocopying

Single photocopies of single articles may be made for personal use, as allowed by national copyright laws. Permission of the publisher and payment of a fee are required for all other photocopying, including multiple or systematic copying, copying for advertising or promotional purposes, resale, and all forms of document delivery.

Subscribers may reproduce tables of contents or prepare lists of papers, including abstracts for internal circulation, within their institutions.

Electronic Storage

Permission of the publisher is required to store electronically any material contained in this review, including any paper or part of the paper.

ODGOVORNOST

Revija ne prevzame nobene odgovornosti za poškodbe in/ali škodo na osebah in na lastnini na podlagi odgovornosti za izdelke, zaradi malomarnosti ali drugače, ali zaradi uporabe kakršnekoli metode, izdelka, navodil ali zamisli, ki so opisani v njej.

RESPONSIBILITY

No responsibility is assumed by the publisher for any injury and/or damage to persons or property as a matter of product liability, negligence or otherwise, or from any use or operation of any methods, products, instructions or ideas contained in the material herein.

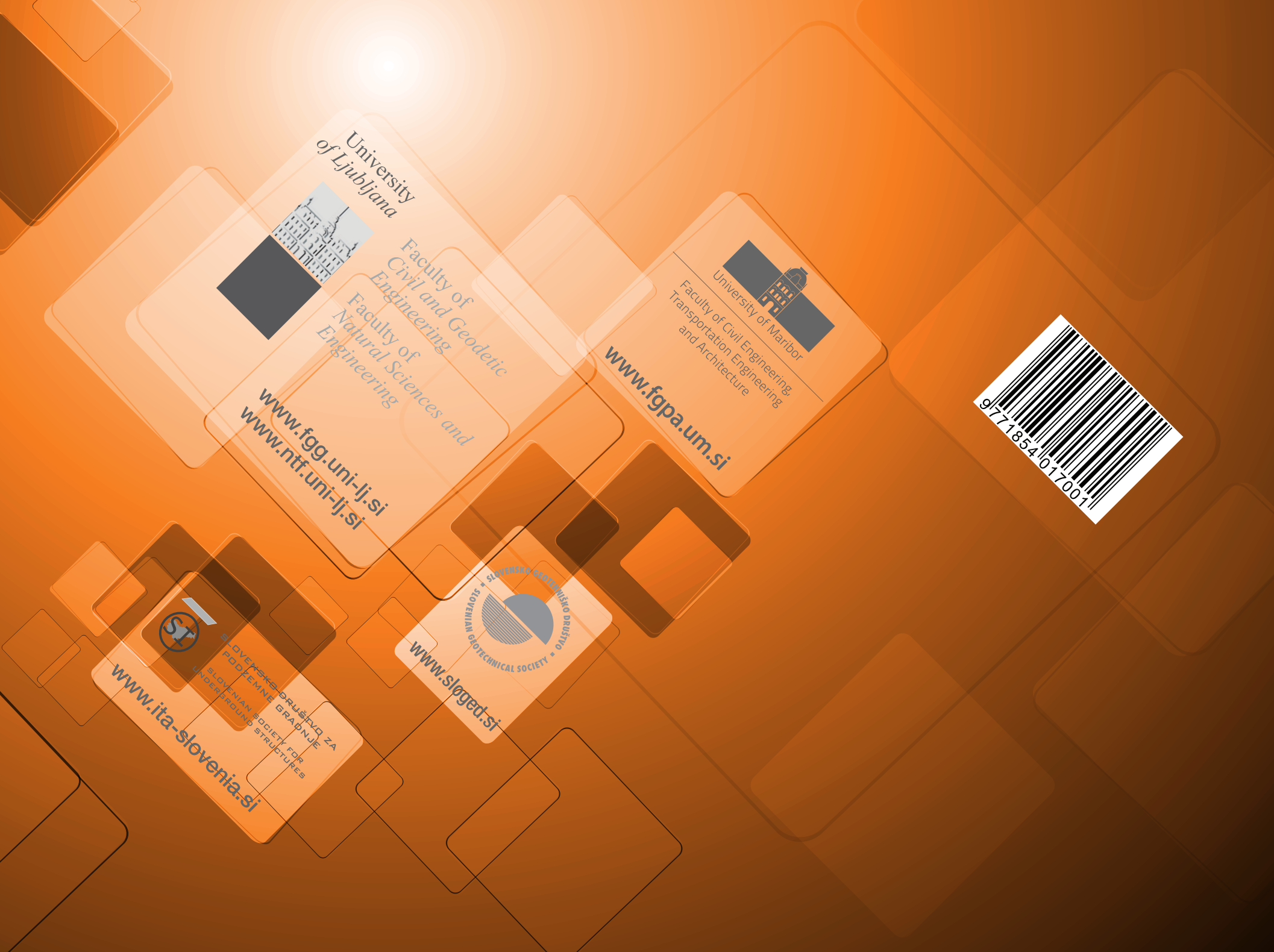
University of Ljubljana
Faculty of Civil and Geodetic Engineering
Faculty of Natural Sciences and Engineering
www.fgg.uni-lj.si
www.ntf.uni-lj.si
University of Maribor
Faculty of Civil Engineering, Transportation Engineering and Architecture
www.fgpa.um.si
9 771854 017001
SLOVENSKO DRUŠTVO ZA PODZEMNE GRADNJE
SLOVENIAN SOCIETY FOR UNDERGROUND STRUCTURES
www.ita-slovenia.si
SLOVENSKO GEOTEHNIŠKO DRUŠTVO
SLOVENIAN GEOTECHNICAL SOCIETY
www.sloged.si